LONDON'S GLOBAL UNIVERSITY

UCL

Digital Linearization of High Capacity and Spectrally Efficient Direct Detection Optical Transceivers

Zhe Li

A thesis submitted to University College London for the degree of Doctor of Philosophy (Ph.D)

Optical Networks Group

Department of Electronic and Electrical Engineering

University College London (UCL)

September 2017

I, Zhe Li, confirm that the work presented in this thesis is my own. Where information has been derived from other sources, I confirm that this has been indicated in the thesis.

ACKNOWLEDGEMENTS

It is amazing to me when I start to write this section, just how many people have contributed to the success of this Ph.D work. Firstly, with my utmost sincerity, I wish to thank my primary supervisor Dr. Robert Killey for his faith in my capability, giving me the opportunity to pursue a Ph.D degree with the Optical Networks Group (ONG) at UCL. I could not have done this without his calm, patient, positive guidance and deep understanding. At the same time, I would like to express my gratitude to my second supervisor, Prof. Polina Bayvel, who founded and built up the ONG group and its impressive laboratory, creating an excellent environment for world class research. I am absolutely proud to have done my research and study in such a group.

Besides my supervisors, my sincere thanks go to Dr. Benn Thomsen for sharing his valuable ideas and suggestions which helped me to improve my problem solving and experimental skills.

I would like to express my deep appreciation to my colleagues in ONG, who have made my Ph.D experience a happy and stimulating one. I have received a great amount of help from Dr. M. Sezer Erkılınç, Dr. Kai Shi, Dr. Rachid Bouziane, Dr. Lidia Galdino, Dr. Tianhua Xu and Dr. Domaniç Lavery for everything from research advice, reading numerous drafts, to everyday discussion of any topic that we could think of.

Additionally, I would like to acknowledge the financial support from Semtech Corp., USA, the European Commission (EU FP7 ASTRON project), the Technology Strategy Board (ERANET+ project IMPACT), the UK Engineering and Physical Sciences Research Council (EPSRC), SPIE (the International Society of Optics and Photonics) Optics and Photonics Education Scholarship, the IEEE Photonics Society Postgraduate Fellowship and the IET (the Institution of Engineering and Technology) Postgraduate Scholarship.

Finally, but most importantly, I would like to thank my parents, Jiajun Li and Limei Wang and my wife, Nannan Wang. They have given me their constant support and love throughout the whole Ph.D process. None of this would have been possible without them.

Zhe Li

ABSTRACT

Metropolitan area networks are experiencing unprecedented traffic growth. The provision of information and entertainment supported by cloud services, broadband video and mobile technologies such as long-term evolution (LTE) and 5G are creating a rapidly increasing demand for bandwidth. Although wavelength division multiplexing (WDM) architectures have been introduced into metro transport networks to provide significant savings over single-channel systems, to cope with the ever-increasing traffic growth, it is urgently required to deploy higher data rates (100 Gb/s and beyond) for each WDM channel.

In comparison to dual-polarization digital coherent transceivers, single-polarization and single photodiode-based direct-detection (DD) transceivers may be favourable for metropolitan, inter-data centre and access applications due to their use of a simple and low-cost optical hardware structure. Single sideband (SSB) quadrature amplitude modulation (QAM) subcarrier modulation (SCM) is a promising signal format to achieve high information spectral density (ISD). However, due to the nonlinear effect termed signal-signal beat interference (SSBI) caused by the square-law detection, the performance of such SSB SCM DD systems is severely degraded. Therefore, it is essential to develop effective and low-complexity linearization techniques to eliminate the SSBI penalty and improve the performance of such transceivers.

Extensive studies on SSB SCM DD transceivers employing a number of novel digital linearization techniques to support high capacity ($\geq$ 100 Gb/s per channel) and spectrally-efficient (net ISD > 2 b/s/Hz) WDM transmission covering metropolitan reach scenarios (up to 240 km) are described in detail in this thesis. Digital modulation formats that can be used in DD links and the corresponding transceiver configurations are firstly reviewed, from which the SSB SCM signalling format is identified as the most promising format to achieve high data rates and ISDs. Following this, technical details of the digital linearization approaches (iterative SSBI cancellation, single-stage linearization filter and simplified non-iterative SSBI cancellation, two-stage linearization filter, Kramers-Kronig scheme) considered in the thesis are presented. Their compensation performance in a dispersion pre-compensated (Tx-EDC) 112 Gb/s per channel 35 GHz-spaced WDM SSB 16-QAM Nyquist-SCM DD system transmitting over up to 240 km standard single-mode fibre (SSMF) is assessed. Net ISDs of up to 3.18 b/s/Hz are achieved. Moreover, we also show that, with the use of effective digital linearization techniques, further simplification of the DD transceivers can be realized by moving electronic dispersion compensation from the transmitter to the receiver without sacrificing performance. The optical ISD limit of SSB SCM DD system finally explored through experiments with higher-order modulation formats combined with effective digital linearization techniques. 168 Gb/s per channel WDM 64-QAM signals were successfully transmitted over 80 km, achieving a record net optical ISD of 4.54 b/s/Hz. Finally, areas for further research are identified.

IMPACT STATEMENT

The goal of the research work presented in this thesis is to explore the performance limits of spectrally-efficient and low-cost direct-detection transceiver technologies for optical fibre communications to cope with the ongoing rapid growth in network traffic due to increasing use of internet services. The knowledge, analysis, and results presented in this thesis could be of interest to readers in the areas of direct-detection optical communication systems and spectrally-efficient, low-cost metro, inter-data centre, back-haul and access networks.

In this research work, a number of simple and effective digital signal processing (DSP) techniques (*e.g.* non-iterative beating interference estimation and cancellation, two-stage linearization filter and the Kramers-Kronig algorithm) to mitigate the nonlinearities introduced by direct photodetection have been demonstrated experimentally for the first time. The first two of these techniques were proposed by the author. 112 Gb/s/λ wavelength division multiplexing (WDM) transmission over a 240 km link at a net information spectral density (ISD) of 3.1 b/s/Hz and 168 Gb/s/λ WDM transmission over a 80 km link at a net ISD of 4.5 b/s/Hz were both experimentally achieved, which were both the capacity records for single photodiode, single-polarization direct-detection transceivers at the time of publication.

This research work has led to fifteen first authored research papers in high impact journals and leading international conferences. Two journal papers are invited papers by IEEE/OSA Journal of Lightwave Technology and two conference papers are top scoring papers in the Optical Fiber Communication Conference (OFC) and European Conference on Optical Communications (ECOC) respectively.

A variety of prestigious international awards have also been received during the production of this thesis, including the best paper awards in OFC 2017 (Grand Prize) and ECOC 2016 (Runner-Up), ECOC 2017 (Runner-Up), the 2017 IEEE Photonics Society Graduate Student Fellowship (1 of 10 worldwide), the 2017 IET Postgraduate Prize (1 of 5 worldwide), and the 2016 SPIE Optics and Photonics Education Scholarship.

The demonstrated transceiver designs employ low complexity digital signal processing algorithms, which are expected to require low chip area and operate with low power consumption, and consequently has generated significant attention and research interest, both across academia and industry internationally.

CONTENTS

LIST OF FIGURES

CHAPTER 1

INTRODUCTION

Optical fibre communication is a method of transmitting information from one position to another by sending modulated optical signals through optical fibres. The implementation of optical fibre communication systems is one of the greatest engineering achievements of the past century. Advances made in fibre technology have revolutionised society, allowing, initially, low-cost, high-quality voice communications, and, more recently, the development of the internet. Generally, modern optical fibre communication systems include an optical transmitter, which converts the electrical signal into optical form, an optical channel, which carries the signal to its destination, and an optical receiver, which converts the optical signal at the output end of the optical channel back into electrical form. Optical fibre communication offers a number of attractive merits and special features over conventional copper cable-based communications, such as enormous potential bandwidth, small size and weight, electrical isolation, immunity to interference and crosstalk, signal security, low transmission loss, ruggedness and flexibility, system reliability and ease of maintenance, and potentially low cost. Because of its advantages over copper cable-based transmission, optical fibres have largely replaced copper wires in core networks around the world.

The development of optical fibre communication systems can be grouped into several distinct generations: the first generation, which became available commercially in 1980, operated at wavelengths near 0.8 μm and used GaAs semiconductor lasers and multi-mode fibre. They operated at a bit rate of up to 100 Mb/s and allowed repeater spacing of up to 10 km [1]. Towards the end of the decade, the second-generation systems, operating near 1.3 μm and using single-mode fibres increased the bit rates up to 1.7 Gb/s with a repeater spacing of about 50 km. The main limitation of the repeater spacing of these systems was the silica fibre losses at 1.3 μm (typically 0.5 dB/km). In the third generation, introduced from around 1990, the systems operated near 1.55 μm with the minimum fibre loss of 0.2 dB/km, and were capable of achieving bit rates of up to 10 Gb/s with electronic repeaters (3R repeaters performing re-amplification, re-shaping and re-timing) spaced apart typically by 60-70 km by using dispersion-shifted fibres (DSF) or dispersion compensation. In the mid-1990s, the fourth-generation systems made use of two techniques, optical amplification, particularly the erbium-doped fibre amplifier (EDFA) to enhance the repeater spacing and wavelength-division multiplexing (WDM) to increase the bit rate, leading to doubling of the system capacity every 6 months or so [1].

The current research interest of the fifth-generation systems is concerned with extending the WDM simultaneous operating wavelength range from conventional wavelength window (C-band) to both the long- and short-wavelength sides (L- and S- band) using new amplification techniques (*e.g.* Raman amplification) and new fibres (*e. g.* dry fibre, where the fibre losses are low over the entire wavelength region extending from 1.30 to 1.65 μm) to enable optical fibre communication systems with thousands of WDM channels [2]. At the same time, digital signal processing (DSP), forward error correction (FEC) and coherent optical detection have been introduced in this generation of optical fibre communication systems. In DSP-based advanced modulation formats, both the amplitude and phase of the optical carrier are used to encode the information [3], thus enabling the more efficient use of the optical bandwidth and leading to increases in the information

spectral density (ISD) of WDM systems. The highest ISDs have increased from 0.8 (b/s)/Hz in the fourth-generation systems to more than 8 (b/s)/Hz in the current dual-polarisation systems [4].

The main motivation behind this series of innovations and developments is the commercial and consumer demand for high capacity communications, especially after the development of the Internet (email and World Wide Web) in the 1990s. Fig. 1.1 shows the trend in global Internet traffic between 2000 and 2020. During the past 30 years (1985 – 2015), total global Internet and IP traffic increased from 15 Gigabytes to 42.4 Exabytes (1 Exabyte = 10^{18} bytes) per month, an increase by a factor of 2.7 billion [5]. Furthermore, the forecasts of communication technology analysts suggest that annual global Internet and IP traffic will grow to 2.0 Zettabyte per year (1 Zettabyte = 10^{21} bytes) by 2019 [6]. The biggest contribution to Internet and IP traffic is made by video-centric network applications (video-on-demand (VOD)), which is increasing with mobile data usage, in particular with wireless fidelity (Wi-Fi) internet access and 4G/Long Term Evolution (LTE) cellular networks enabling the streaming/downloading of videos with smart phones or tablets at any time. Thus, further increases in the capacity of optical fibre communication systems are needed to continue to meet this demand.

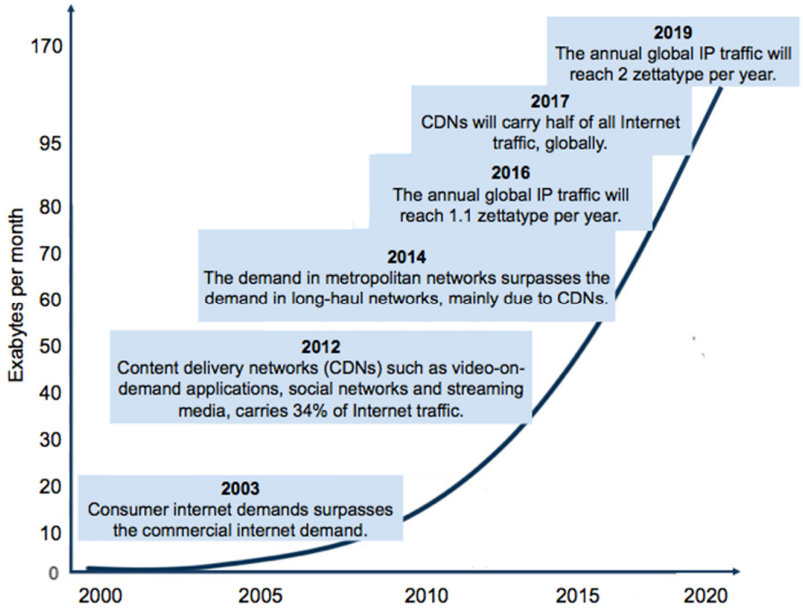

Fig. 1.1: The trend in Internet (IP and mobile) traffic [6]

1.1 Architectural Overview of an Optical Network Structure

Fig. 1.2 depicts an overview of a fibre-optic network structure. It is worth noting that a public optical network in a real scenario is very extensive with a very complex structure because it is run by different service providers and network operators at different parts of the network. The network nodes are central offices or other locations where the respective carrier has a point of presence (POP) and can create a hub where fibres can be interconnected. The links between the nodes can be single optical fibres, fibre pairs, or multiple fibre pairs, typically deployed in underground ducts [7]. Generally, optical networks can be classified within three different categories, namely the long-haul (or core) part, a metropolitan (metro or regional) part and an access part, as shown in Fig. 1.2.

Each network has different technical and operational requirements, such as transmission reach (distance), capacity, and cost.

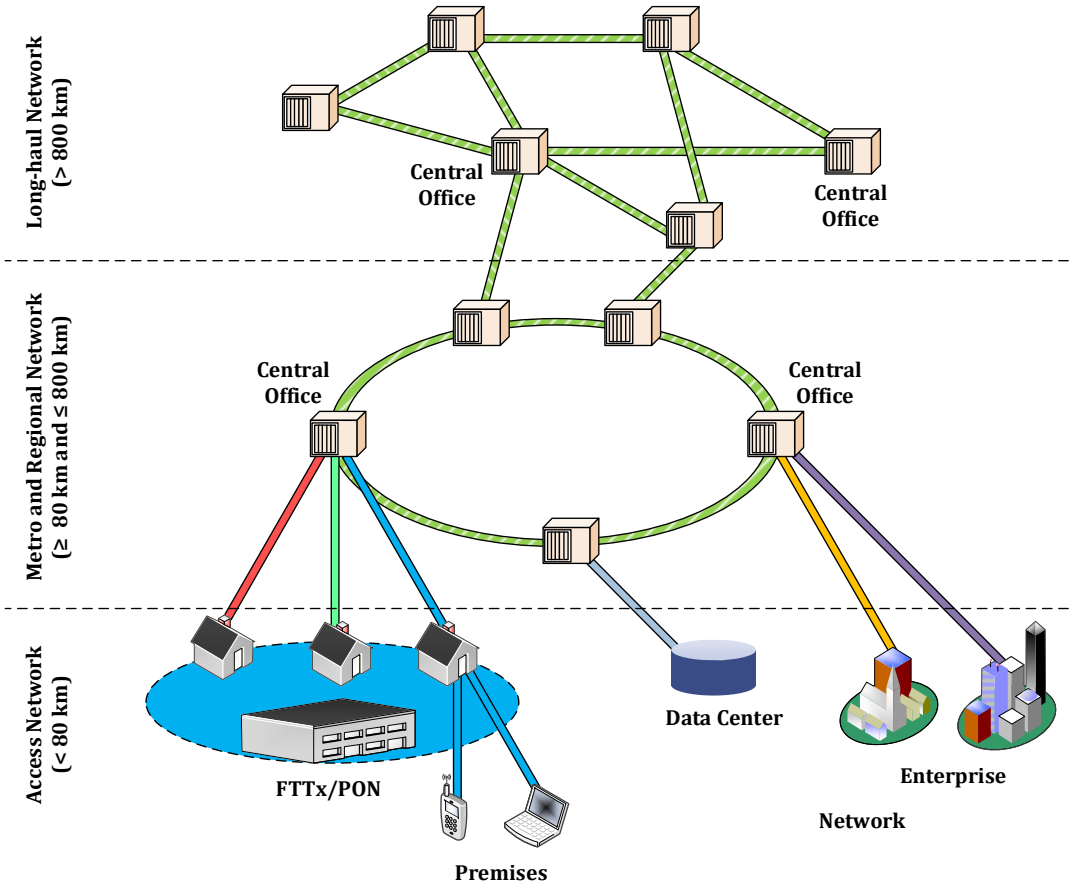

Fig. 1.2: Overview of an optical fibre network structure [7].

The long-haul links/networks interconnect different regions and countries, often covering transoceanic distances (> 800 km). Amplification and regeneration of the transmitted optical signals at intermediate points are required for such long distances. The most important factors in such applications are achieving long transmission reach, high capacity and high ISD. In long-haul optical networks, multi-level and multi-dimensional modulation techniques, such as polarization division multiplexed quadrature amplitude modulation (QAM) in which the data is modulated on amplitude, phase and polarization dimensions, and detected using coherent receivers [8] have been used to enhance the system capacity. Thus, the system capacity has been already upgraded from a bit rate of 10 Gb/s to ≥ 100 Gb/s per wavelength. This is mainly because coherent detection gives the ability to capture all the dimensions of the transmitted light information, namely the amplitude, phase and state of polarization (SoP), and subsequently to recover the full optical field which allows high spectral efficiency and the capability to mitigate transmission impairments by utilizing advanced DSP implemented on high-speed complementary metal oxide silicon (CMOS) digital circuits [9]. Therefore, currently, polarization- and phase-diverse coherent receivers have become the standard in long-haul communication links.

Metro, inter-data centre networks comprise interconnections between the central offices or data centres in a large city or cities in a region, the typical transmission distances being around 80-100

km up to 500-800 km. It has been reported that the data traffic in metropolitan (metro) and inter-data centre networks surpassed the traffic of the long-haul (> 800 km) networks in 2014, and will comprise 62% of total data traffic by 2019 since it is currently growing almost two times faster than long-haul traffic [6]. This rapid increase is mainly due to the important role of caching and content delivery networks (34% in 2014 and predicted to be 62% by 2019) which constitute a large portion of the Internet content accessing today, including web and downloadable objects (files, software, applications, *etc*.), scientific and cloud computing, and social networks. Therefore, metro and inter-data centre application scenarios in which link lengths of between 80 km and 800 km are becoming more and more essential and have attracted much attention by the optical communications research community.

Access networks, finally, contain the links from nodes in the metro networks out to the subscriber premises, such as data-centres, large enterprises or campuses, or individual users of a telecom service, referred to as Fibre to the Node, Curb, Building or Home (FTTx). Typically, the access links are a few tens of kilometres (< 80 km). Typical classification of different WDM systems based on transmission distances are listed in Table. 1.1.

Table 1.1: Classification of WDM systems based on transmission distances [27]

Class	System	Distance (km)
Short-haul	Interconnects	< 10 km
Short-haul	Data centres	< 40 km
Medium-haul	Access	< 80 km
Medium-haul	Metro & Inter-data centre	80 – 300 km
Medium-haul	Regional	300 – 800 km
Long-haul	Terrestrial	800 – 3000 km
Ultra long-haul	Submarine & Transoceanic	> 3000 km

Unlike long-haul applications, the primary requirement for short- and medium- haul links is cost-effectiveness, a requirement that can be met using direct-detection transceiver technology. In contrast to the coherent detection scheme which requires complex transceiver hardware, including local oscillator, polarization beam splitters, 90^{o} optical hybrids, balanced detectors and multiple analogue-to-digital converters (ADCs), the single polarization direct-detection (DD) scheme utilizes a simpler receiver structure consisting of a single photodiode and a single ADC. DD also relaxes the laser linewidth requirements, and simplifies the receiver DSP complexity. Recently, in order to fulfil the unprecedented traffic growth in short- and medium-haul applications, service providers have started to build 100 Gb/s (4 × 28 Gb/s optical duobinary) metro optical solutions

using DD technology [10], mainly due to these advantages provided by the use of single-polarization direct-detection WDM systems.

1.2 Thesis Motivation

In long-haul applications, multi-level and multi-dimensional modulation techniques, combined with phase- and polarization-diverse coherent receivers have been well established and are able to achieve the high capacity and high net ISDs [11-15]. On the other hand, due to the constraints of tight budget and footprint, intensity modulation direct detection (IM-DD) systems, in which a double-sideband signal is generated by a directly modulated laser (DML) and detected by a single photodiode, have been extensively used for short- haul links [16-18]. In medium-haul applications such as metro, back-haul and inter-data centre networks, since a massive number of transceivers are utilized, cost-effectiveness is still the primary requirement. In contrast to the polarization multiplexed coherent transceivers with high cost optical components, the DD transceivers are still more favourable. At the same time, due to the unprecedented traffic growth within such applications, the transceivers implemented are expected to offer high data rate ($\geq$ 100 Gb/s per channel), spectral efficiency (> 2 b/s/Hz) and tolerance to noise and fibre impairments over metro transmission reaches (80 – 300 km). However, because of the severe power fading introduced following the transmission and direct photodetection, the IM-DD systems' performance is seriously impaired, and the achievable system capacity is limited [19, 20].

In order to avoid the power fading impairment and therefore improve the performance of DD systems, single-sideband (SSB) DD systems have been demonstrated [21]. A digital SSB signal is initially generated and an optical carrier is added using an externally modulated transmitter (the optical carrier is obtained by biasing the modulator above the null point). Following transmission and photodetection, the amplitude and phase of the SSB signal can be recovered through the carrier-signal beating terms. The achievable ISD can be further increased by implementing the subcarrier modulation (SCM) technologies, including orthogonal frequency division multiplexing (OFDM) [21, 22] and Nyquist-pulse shaped subcarrier modulation (Nyquist-SCM) [23, 24]. A drawback of the SSB SCM DD technique (both OFDM and Nyquist-SCM) is that, in addition to the wanted carrier-signal beating terms, signal-signal beating products are also generated during the square-law detection, which interfere with the desired carrier-signal beating terms. This nonlinear effect is known as signal-signal beat interference (SSBI) and causes a significant degradation in the receiver sensitivity [25]. Since the SSBI level is at a maximum at low frequencies and falls to zero at a point equal to the bandwidth of the subcarrier, placing a spectral guard band ($\geq$ signal baudrate) between the optical carrier and the subcarrier signal [26] is the simplest method to avoid the SSBI penalty. However, this method is not suitable for spectrally-efficient WDM system since the spectral efficiency is halved and approximately 50% of the electrical and optical components' bandwidth is wasted. We wish to reduce the guard band, and at the same time minimize the penalty due to SSBI. Consequently, it is desirable to develop effective compensation/linearization techniques to cancel or mitigate the nonlinearities caused by square-law detection.

Therefore, the key aim of the research described in this thesis is to study whether the SSB SCM DD system are capable to support high data rate ($\geq$ 100 Gb/s per channel) and spectrally-efficient (net ISD > 2 b/s/Hz) WDM transmissions covering the metropolitan reach (up to 300 km) through

employing effective linearization technologies. Moreover, the development of novel linearization schemes, with either reduced DSP complexity or improved compensation performance, was also an important aim.

1.3 Thesis Outline

The remainder of this thesis is organized as follows: Chapter 2 focuses on the requisite theory for the work discussed in this thesis including optical fibre transmission impairments (fibre attenuation, chromatic dispersion, amplified spontaneous emission noise and fibre nonlinearities) and SSB SCM DD techniques (including the theory of the noise and its management in such systems). In addition, digital subsystems employed at the transceiver including digital sideband filtering for SSB signal generation, electronic dispersion compensation (EDC) and digital equalization are also described.

Chapter 3 gives an overview of the techniques applied for DD systems. Digital modulation formats that can be used for DD links are first described. Their corresponding transceiver configurations, achieved ISDs, and capacity versus transmission distance performance are also presented. Following this, the characteristics of a number of previously proposed optical and digital linearization techniques to eliminate the SSBI penalty within SSB SCM DD systems are also described.

Chapters 4, 5, 6 and 7 present the technical details of the proposed and demonstrated digital linearization techniques in this study (namely, iterative SSBI cancellation, the single-stage linearization filter and simplified non-iterative SSBI cancellation, the two-stage linearization filter, and the Kramers-Kronig scheme). Their experimental performance in a dispersion pre-compensated (Tx-EDC) 112 Gb/s per channel 35 GHz-spaced WDM SSB 16-QAM Nyquist-SCM DD system transmitting over distances of up to 240 km of standard single-mode fibre (SSMF) is presented.

Chapter 8 presents experimental evaluations of electronic dispersion post-compensation (Rx-EDC) in SSB SCM DD systems for the cases without and with digital linearization. The experimental assessments were carried out on a 112 Gb/s per channel 37.5 GHz-spaced WDM SSB 16-QAM Nyquist-SCM DD system with transmission over up to 240 km SSMF.

Chapter 9 covers a simulation-based study on the fundamental performance of different 100 G transceiver structures studied in the previous chapters, comparing them with that of direct detection systems with optical linearization, and coherent systems (both homodyne and heterodyne) and recently obtained experimental results for beyond 100 G (168 Gb/s per channel) SSB 64-QAM SCM DD transceivers operating over a typical metro link length (80 km) are presented

Finally, Chapter 10 draws conclusions based on the results described in this study and some possible future directions of this work are proposed.

1.4 Papers Published in the Production of this Thesis

The following list cites the publications arising from the work presented in this thesis:

1. **Z. Li**, M.S. Erkılınç, K. Shi, E. Sillekens, L. Galdino, T.Xu, B.C. Thomsen, P. Bayvel, and R.I. Killey, "Spectrally-efficient 168 Gb/s WDM 64-QAM single-sideband Nyquist-subcarrier modulation with Kramers-Kronig direct-detection receivers", **IEEE/OSA Journal of Lightwave Technology**, to be published, 2018 (**invited paper**).

2. **Z. Li**, M.S. Erkılınç, K. Shi, E. Sillekens, L. Galdino, B.C. Thomsen, P. Bayvel, and R.I. Killey, "168 Gb/s/λ direct-detection 64-QAM SSB Nyquist-SCM transmission over 80 km uncompensated SSMF at 4.54 b/s/Hz net ISD using a Kramers-Kronig receiver", in European Conference on Optical Communications (**ECOC**), paper Tu.2.E.1, 2017. **(top-scored paper)**

3. **Z. Li**, M.S. Erkılınç, K. Shi, E. Sillekens, L. Galdino, B.C. Thomsen, P. Bayvel, and R.I. Killey, "Joint optimisation of resampling rate and carrier-to-signal power ratio in direct-detection Kramers-Kronig receivers", in European Conference on Optical Communications (**ECOC**), paper W.2.D.3, 2017. **(top-scored student paper)**

4. **Z. Li**, M.S. Erkılınç, K. Shi, E. Sillekens, Tianhua Xu, L. Galdino, B.C. Thomsen, P. Bayvel, and R.I. Killey, "Direct-detection transceiver designs for 100 Gb/s/λ spectrally-efficient WDM metro networking", **IEEE/OSA Journal of Lightwave Technology**, to be published, 2018 (**invited paper**).

5. **Z. Li**, M.S. Erkılınç, K. Shi, E. Sillekens, L. Galdino, B.C. Thomsen, P. Bayvel, and R.I. Killey, "SSBI mitigation and Kramers-Kronig scheme in single-sideband direct-detection transmission with receiver-based electronic dispersion compensation", **IEEE/OSA Journal of Lightwave Technology**, vol. 35, no. 10, pp.1887-1893, 2017.

6. **Z. Li**, M.S. Erkılınç, K. Shi, E. Sillekens, L. Galdino, B.C. Thomsen, P. Bayvel, and R.I. Killey, "Improvement of digital chromatic dispersion post-compensation by utilizing beating interference mitigation for direct-detection SSB Nyquist-SCM", in Optical Fiber Communication Conference (**OFC**), paper Th3D.2, 2017.

7. **Z. Li**, M.S. Erkılınç, K. Shi, E. Sillekens, L. Galdino, B.C. Thomsen, P. Bayvel, and R.I. Killey, "112 Gb/s/λ WDM direct-detection Nyquist-SCM transmission at 3.15 (b/s)/Hz over 240 km SSMF enabled by novel beating interference compensation", in Optical Fiber Communication Conference (**OFC**), paper Tu3I.4, 2017. **(top-scored paper)**

8. **Z. Li**, M. S. Erkilinc, L. Galdino, K. Shi, B. C. Thomsen, P. Bayvel, and R. I. Killey, " Comparison of Digital Signal-Signal Beat Interference Compensation Techniques in Direct-Detection Subcarrier Modulation Systems", **OSA Optics Express**, vol. 24, no. 25, pp. 29176-29189, 2016.

9. **Z. Li**, M. S. Erkilinc, R. Maher, L. Galdino, K. Shi, B. C. Thomsen, P. Bayvel, and R. I. Killey, "Two-stage linearization filter for direct-detection subcarrier modulation", **IEEE Photonics Technology Letters**, vol. 28, no. 24, 2016.

10. **Z. Li**, M. S. Erkilinc, R. Bouziane, B. C. Thomsen, P. Bayvel, and R. I. Killey, "Simplifed DSP-based signal-signal beat interference mitigation technique for direct

detection OFDM", **IEEE/OSA Journal of Lightwave Technology**, vol. 34, no. 3, pp.866-872, 2016.

11. **Z. Li**, M. S. Erkilinc, S. Pachnicke, H. Griesser, R. Bouziane, B. C. Thomsen, P. Bayvel, and R. I. Killey, "Signal-signal beat interference cancellation in spectrally-efficient WDM direct-detection Nyquist-pulse-shaped 16-QAM subcarrier modulation", **OSA Optics Express**, vol. 23, no. 18, pp. 23694-23709, 2015.
12. **Z. Li**, M. S. Erkilinc, R. Maher, L. Galdino, K. Shi, B. C. Thomsen, P. Bayvel, and R. I. Killey, "Reach enhancement for WDM direct-detection subcarrier modulation using low-complexity two-stage signal-signal beat interference cancellation", in European Conference on Optical Communications (**ECOC**), paper M.2.B.1, 2016. **(top-scored student paper)**
13. **Z. Li**, M. S. Erkilinc, R. Bouziane, R. Maher, L. Galdino, K. Shi, B. C. Thomsen, P. Bayvel, and R. I. Killey, "Simplifed DSP-based signal-signal beat interference mitigation for direct detection subcarrier modulation", in Optical Fiber Communication Conference (**OFC**), paper W1A.3, 2016.
14. **Z. Li**, M.S. Erkilinc, S. Pachnicke, H. Griesser, B.C. Thomsen, P. Bayvel, and R.I. Killey, "Direct-Detection 16-QAM Nyquist-Pulse-Shaped Subcarrier Modulation with SSBI Mitigation", in International Conference on Communications (**ICC**), pp. 5204-5209, 2015.
15. **Z. Li**, M.S. Erkilinc, S. Pachnicke, H. Griesser, R. Bouziane, B.C. Thomsen, P. Bayvel, and R.I. Killey, "Performance Limits of Spectrally-Efficient WDM Direct-Detection SSB Nyquist Subcarrier Modulation with Signal-Signal Beat Interference Cancellation", in European Conference on Network and Optical Communications (**NOC**), pp. 1-6, 2015.

1.5 Honours and Awards Received in the Production of this Thesis

The international honours and awards achieved as result of the work presented in this thesis are listed below:

1. The IEEE Photonics Society Graduate Student Fellowship, 2017.
2. Winner of the IET Postgraduate Prize, 2017.
3. Runner Up of the ADVA Best Student Paper Award in the European Conference and Exhibition on Optical Communication (ECOC), 2017.
4. Grand Prize Winner of the OSA Corning Paper Competition at the Optical Fiber Communication Conference (OFC), 2017.
5. Runner Up of the ADVA Best Student Paper Award in European Conference and Exhibition on Optical Communication (ECOC), 2016.
6. SPIE Optics and Photonics Education Scholarship, 2016.

References

[1] G.P. Agrawal, Fiber-optic Communication Systems. 3rd ed. (John Wiley & Sons, 2010).

[2] G.A. Thomas, B.L. Shraiman, P.F. Glodis, and M.J. Stephan, "Towards the clarity limit in optical fibre," in Nature 404, 262-264 (2000).

[3] P.J. Winzer and R.J. Essiambre, "Advanced modulation formats for high-capacity optical transport networks," in J. Lightw. Technol. 24(12), 4711-4728 (2006).

[4] X. Zhou, J. Yu, M.F. Huang, Y. Shao, T. Wang, L. Nelson, P. Magill, M. Birk, P.I. Borel, D.W. Peckham, and Robert Lingle, "64-Tb/s (640x107-Gb/s) PDM-36QAM transmission over 320km using both pre-and post-transmission digital equalization" in Optical Fiber Communication Conference, OSA Technical Digest Series (CD) (Optical Society of America, 2010), paper PDPB9.

[5] Cisco, "The history and future of Internet traffic," (2015).

[6] Cisco, "Cisco visual networking index: forecast and methodology, 2014-2019," White Paper (2015).

[7] Infinera, "WDM - the Transmode way, optics and communications" (2015).

[8] P.J. Winzer, "High-spectral-efficiency optical modulation formats," in J. Lightw. Technol. 30(24), 3824-3835 (2012).

[9] S.J. Savory, "Digital coherent optical receivers: algorithms and subsysstems," IEEE J. Sel. Topics Quantum Electron., 16(5), 1164-1179 (2010).

[10] ADVA, Efficient 100G Transport (2014).

[11] S. Chandrasekhar, X. Liu, B. Zhu, and D.W. Peckham, "Transmission of a 1.2-Tb/s 24-carrier no-guard-interval coherent OFDM superchannel over 7200-km of ultra-large-area fiber," in European Conference and Exhibition on Optical Communication (ECOC 2009), paper 1, 2.

[12] J.-X. Cai, Y. Sun, H.G. Batshon, M. Mazurczyk, H. Zhang, D.G. Foursa, and A.N. Pilipetskii , "54 Tb/s transmission over 9,150 km with optimized hybrid Raman-EDFA amplification and coded modulation," in European Conference and Exhibition on Optical Communication (ECOC 2014), paper PD.3.3.

[13] J. Zhang, J. Yu, Y. Fang, and N. Chi, "High speed all optical Nyquist signal generation and full-band coherent detection," Scientific Report 4, 6156 (2014).

[14] S. Beppu, M. Yoshida, K. Kasai, and M. Nakazawa, "2048 QAM (66 Gbit/s) single-carrier coherent optical transmission over 150 km with a potential SE of 15.3 bit/s/Hz," in Optical Fiber Communication Conference, OSA Technical Digest Series (CD) (Optical Society of America, 2014), paper W1A.6.

[15] T.J. Xia, S. Gringeri, and M. Tomizawa, "High- capacity optical transport networks," IEEE Commun. Mag. 50(11), 170-178 (2012).

[16] K. Zhong, X. Zhou, Y. Gao, Y. Yang, W. Chen, J. Man, L. Zeng, A.P. Lau, and C. Lu, "Transmission of 112Gbit/s single polarization half-cyle 16QAM Nyquist-SCM with 25Gbps EML and direct detection," in European Conference and Exhibition on Optical Communication (ECOC 2015), paper 0136.

[17] K. Zhong, X. Zhou, T. Gui, L. Tao, Y. Gao, W. Chen, J. Man, L. Zeng, A.P. Lau, and C. Lu, "Experimental study of PAM-4, CAP-16, and DMT for 100 Gb/s short reach optical transmission systems," Opt. Express 23(2), 1176-1189 (2015).

[18] J. Lee, N. Kaneda, T. Pfau, A. Konczykowska, F. Jorge, A-Y. Dupuy, and Y.K. Chen, in Optical Fiber Communication Conference, OSA Technical Digest Series (CD) (Optical Society of America, 2014), paper Th5A.5.

[19] Z. Liu, G. Hesketh, B. Kelly, J. O'Caroll, R. Phelan, D.J. Richardson, and R. Slavik, , "300-km transmission of dispersion pre-compensated PAM4 using direct modulation and direct detection," in Optical Fiber Communication Conference, OSA Technical Digest Series (CD) (Optical Society of America, 2017), paper Th3D.6.

[20] Z. Liu, M.S. Erkilinç, B. Kelly, J.O'Carroll, R. Phelan, B.C. Thomsen, R.I. Killey, D.J. Richardson, P. Bayvel, and R. Slavik, "49 Gbit/s direct-modulation and direct-detection transmission over 80 km SMF-28 without optical amplification or filtering," in European Conference and Exhibition on Optical Communication (ECOC 2016), 145-147.

[21] W.-R. Peng, X. Wu, V.R. Arbab, K.-M. Feng, B. Shamee, L.C. Christen, J.Y. Yang, A.E. Willner, and S. Chi, "Theoretical and experimental investigations of direct-detected RF-tone-assisted optical OFDM systems," J. Lightw. Technol., 27(10), 1332-1339 (2007).

[22] A.J. Lowery, L.B. Du, and J. Armstrong, “Performance of optical OFDM in ultralong-haul WDM lightwave systems,” J. Lightw. Technol., 25(1), 131-138 (2007).

[23] A.O. Wiberg, B.-E. Olsson, and P.A. Andrekson, “Single cycle subcarrier modulation,” in Optical Fiber Communication Conference, OSA Technical Digest Series (CD) (Optical Society of America, 2009), paper OTuE.1.

[24] J.C. Cartledge and A.S. Karar, “100 Gb/s intensity modulation and direct detection,” J. Lightw. Technol., 32(16), 2809-2814 (2014).

[25] A.J. Lowery, “Amplified-spontaneous noise limit of optical OFDM lightwave systems,” Opt. Express 16(2), 860-865 (2008).

[26] B.J.C. Schmidt, A.J. Lowery, and L.B. Du, “Low sample rate transmitter for direct-detection optical OFDM,” in Optical Fiber Communication Conference, OSA Technical Digest Series (CD) (Optical Society of America, 2009), paper OWM4.

[27] M.S. Erkilinç, “Cost-effective spectrally-efficient optical transceiver architectures for metropolitan and regional links,” PhD thesis, 2015.

CHAPTER 2

THEORY

This chapter focuses on the requisite theory for the work presented in this thesis. Section 2.1 describes the impairments suffered by signals in transmission through an optical fibre. It firstly covers the linear impairments: fibre attenuation, chromatic dispersion (CD) and amplified spontaneous emission (ASE)-noise. Following this, fibre nonlinear effects are described. In Section 2.2, direct-detection technology is discussed, and is compared with coherent detection techniques. Furthermore, since the single-sideband subcarrier modulation (SSB OFDM and SSB Nyquist-SCM) technique employing direct detection is the system studied throughout this thesis, the theory and management of optical noise in SSB SCM DD systems are explained. Section 2.3 covers the digital subsystems implemented within the transceiver, including the discrete Hilbert transform (HT) filter for single-sideband modulation, electronic dispersion compensation (EDC) and digital equalization for time recovery.

2.1 Optical Fibre Transmission Impairments

In the first part of this section, optical fibre impairments, namely fibre attenuation, CD and ASE-noise that exhibit linear behaviour during the transmission over fibre are explained. Following this, fibre nonlinear impairments, self-phase modulation (SPM), cross-phase modulation (XPM) and four-wave mixing (FWM), incurred by the Kerr effect are briefly described. Note that, since polarization mode dispersion (PMD) is generally low in short- and medium-haul links, a description of PMD is not included in this chapter.

2.1.1 Linear Optical Impairments

Fibre Attenuation

In optical fibre transmission, the fibre loss reduces the signal power reaching the optical receiver. Since the receivers require a certain minimum amount of optical power for accurate signal recovery, the fibre attenuation, which results from mainly material absorption and Rayleigh scattering, inherently limits the performance of optical communication systems. Changes in the amplitude, A, of a signal propagating through an optical fibre are governed by the equation [1]:

$$\frac{\partial A}{\partial z} + \frac{\alpha}{2} A = 0 \tag{2.1}$$

where α is the attenuation coefficient, and z represents the propagation direction. The solution of this first-order differential equation is:

$$P_{out} = P_{in} exp(-\alpha L) \tag{2.2}$$

where P_{in} is the optical launch power at the input of an optical fibre with length L, and P_{out} is the output power. It is customary to express the attenuation coefficient, α, in units of dB/km based on the relation:

$$\alpha(dB/km) = -\frac{10}{L} log_{10}\left(\frac{P_{out}}{P_{in}}\right) \approx 4.343\alpha \tag{2.3}$$

Fibre attenuation depends on the wavelength of the transmitted light and it reaches its minimum value of only about 0.2 dB/km between 1460 and 1625 nm for silica fibre. Therefore, today's optical fibre communication systems operate in the S-band (short-wavelength band) from 1460 to 1530nm, C- band (conventional wavelength band) from 1530 to 1565 nm and L- band (long wavelength band) from 1565 to 1625 nm, according to International Telecommunication Union (ITU) standards. Throughout the thesis, the optical fibre transmission studies consider only the C-band, with EDFAs employed for optical amplification.

Chromatic Dispersion

In medium- and long-haul optical fibre communication systems, fibre group-velocity dispersion (GVD) represents another limiting factor because it broadens optical pulses as they propagate along the fibre. This pulse broadening leads to a power reduction at the pulse peaks [2], and, as shown in Fig. 2.1, in the time domain, the broadened pulses start to interfere with pulses in the neighbouring symbol slots (shaded regions), an effect referred to as inter-symbol interference (ISI) which causes errors when using threshold-based symbol decisions at the receiver. Considering the effect of GVD in the frequency domain, different frequency components of a signal travel at different group velocities, thus making the GVD a wavelength/frequency-dependent shift (walk-off). Furthermore, if linear shift with frequency is assumed, the optical phase shift (φ) is quadratic with respect to the frequency. The impact of GVD scales quadratically with the symbol rate. For instance, the dispersion-limited distance of a 28 Gbaud signal is 16 times lower than that of a 7 Gbaud signal.

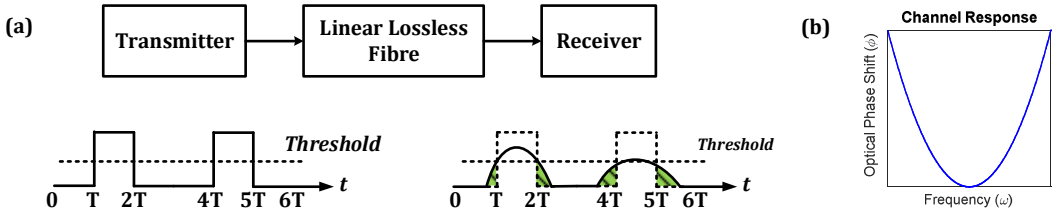

Fig. 2.1: Dispersion effect on a time (a) and frequency (b) domain signal.

If the frequency dependent pulse propagation term, $\beta(\omega)$, is included in Eq. 2.1, with this term expanded in a Taylor series around the carrier frequency and terms up to the third order retained, Eq. 2.1 is replaced by [3]:

$$\frac{\partial A}{\partial z} + \frac{\alpha}{2}A + \beta_1\frac{\partial A}{\partial t} + \frac{i\beta_2}{2}\frac{\partial^2 A}{\partial t^2} - \frac{\beta_3}{6}\frac{\partial^3 A}{\partial t^3} = 0 \tag{2.4}$$

where β_1 is inversely proportional to the group velocity v_g (β_1=1/ v_g), β_2 is the GVD coefficient and β_3 is the GVD slope coefficient. β_1 can be written as:

$$\beta_1 = \frac{1}{v_g} = \frac{1}{c}\left(n + \omega\frac{dn}{d\omega}\right) \tag{2.5}$$

where c is the speed of light in vacuum, n is the linear refractive index of the optical fibre and ω is the angular optical frequency. In order to simplify Eq. 2.4, the β_1 term can be eliminated under the

assumption of a frame of reference moving with the pulse at the group velocity, v_g. Moreover, if β_2 is sufficiently high, as is the case with SSMF at the wavelength of 1550 nm [4], the β_3 term can be neglected for a single channel. In such cases, the β_2 term is the main coefficient that leads to pulse broadening, and thus, Eq. 2.4 can be simplified as:

$$\frac{\partial A}{\partial z} + \frac{\alpha}{2}A + \frac{i\beta_2}{2}\frac{\partial^2 A}{\partial t^2} = 0 \tag{2.6}$$

where the β_2 term is defined as:

$$\beta_2 = \frac{d\beta_1}{d\omega} = \frac{d}{d\omega}\left[\frac{1}{c}\left(n + \omega\frac{dn}{d\omega}\right)\right] = \frac{1}{c}\left(2\frac{dn}{d\omega} + \omega\frac{d^2n}{d\omega^2}\right) \tag{2.7}$$

In addition, the dispersion parameter of SSMF, D_{SMF}, which is defined as the first derivative of the β_1 term with respect to the wavelength λ, can be denoted as:

$$D_{SMF} = \frac{d\beta_1}{d\lambda} = \frac{d(1/v_g)}{d\lambda} = \frac{d}{d\lambda}\left[\frac{1}{c}\left(n + \omega\frac{dn}{d\omega}\right)\right] = \frac{-2\pi c}{\lambda^2}\beta_2 \tag{2.8}$$

Therefore, for a linear and lossless fibre, the solution of Eq. 2.6, in the frequency domain, is given by:

$$H(\omega, L) = exp\left(-\frac{j}{2}\beta_2\omega^2 L\right) = \exp\left(-j\frac{D_{SMF}}{4\pi c}\lambda_0{}^2\omega^2 L\right) \tag{2.9}$$

where $H(\omega, L)$ is the channel response due to the chromatic dispersion, λ_0 is the carrier wavelength, D_{SMF} is the dispersion parameter at λ_0 and is expressed in units of ps/(km·nm).

There are two main contributions to the total chromatic dispersion of a SSMF, material dispersion and waveguide dispersion. Material dispersion occurs because the refractive index of silica changes with the optical wavelength, while waveguide dispersion results from the wavelength-dependence of the optical waveguide propagation coefficient. A general technique to compensate the dispersion optically is to design dispersion modified (*e.g.* dispersion-shifted, dispersion-flattened, dispersion-decreasing or dispersion-compensating) fibres [5-8]. This involves the use of multiple cladding layers and a tailoring of the refractive index profile of the fibres. On the other hand, the accumulated chromatic dispersion can also be compensated digitally with EDC either at the transmitter or at the receiver. A detailed discussion of EDC will be presented in Section 2.3.2 in this chapter.

Amplified Spontaneous Emission (ASE) Noise

It is necessary to compensate the fibre loss by using optical amplifiers to prevent the signal from becoming too weak to be detected. All optical amplifiers degrade the signal-to-noise ratio (SNR) of the amplified signal due to the amplified spontaneous emission that adds noise to the signal during the amplification [1]. Generally, the ASE-noise introduced by EDFAs is the ultimate limiting factor in amplified optical transmission systems. The Erbium ions are first excited so that higher-energy states become more populated than the lower-energy state, termed population inversion. While the excited ions are returning to a lower-energy state to reach the equilibrium state, they transfer their energy to the optical signal field in the form of additional photons with the

identical frequency, phase, polarization and direction, through the process of stimulated emission. Consequently, the incoming optical signal is amplified in this process. However, some erbium ions in the excited energy state release their energy to the optical signal field in the form of photons with random frequency, phase, polarization and direction, through spontaneous emission. These photons are emitted in all different phases and directions, with some captured by the fibre and interacting with the other dopant ions. Therefore, stimulated emission amplifies the other photons in the same manner as the signal [9]. Since the amplified spontaneous emission noise has random frequency and phase, the optical signal-to-noise power ratio (OSNR) value is reduced during amplification. The ASE-noise can be modelled as an independent and identically distributed Gaussian random process and its spectral density, $S_{ASE}(v)$ is nearly constant (white noise), which is given by:

$$S_{ASE}(v) = n_{sp} h v_0 (G - 1) \tag{2.10}$$

where n_{sp} is the spontaneous emission factor (or population-inversion factor), h is Planck's constant, v_0 is the frequency of the signal being amplified and G is the gain of the amplifier ($G = P_0 / P_i$, where P_0 and P_i are output and input powers of the signal being amplified). The ASE-noise is unpolarised, *i.e.*, equal power in both polarizations ($[P_{ASEX}, P_{ASEY}]$), and it affects both the in-phase (I) and quadrature (Q) components of the optical signal in both polarizations in the same way. Therefore, the ASE-noise tolerance of a given modulation format can be measured based on the closest Euclidean distance between the symbols, because it appears as a symmetrical spread around symbol points on the constellation in all degrees of freedom of an incoming light.

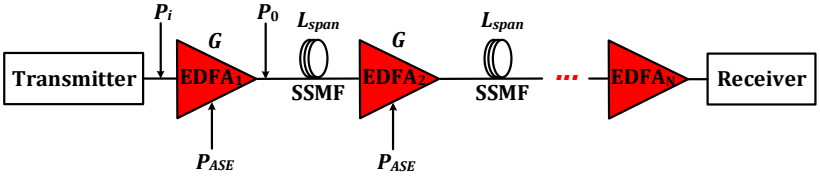

Fig. 2.2: Structure of a typical point-to-point optical transmission link using distributed amplification (cascaded EFDAs) scheme.

The structure of a typical point-to-point optical transmission link using cascaded EDFAs is shown in Fig. 2.2. ASE-noise accumulates from one amplifier to another and gradually reduces the OSNR. The OSNR is defined as the ratio of optical output signal power (P_0) to the ASE-noise power (P_{ASE}) resulted from an EDFA. For large amplifier gains ($G \gg 1$), OSNR can be given as follows:

$$OSNR = \frac{P_0}{P_{ASE}} = \frac{G P_i}{2 n_{sp} h v_0 (G-1) BW_{res}} \approx \frac{P_i}{2 n_{sp} h v_0 BW_{res}} \tag{2.11}$$

The ASE-noise power is defined for a given resolution bandwidth (BW_{res}) in the OSNR value (typically 0.1 nm). By including the values of hv_0 and BW_{res}, the OSNR in decibel can be written as:

$$OSNR(dB) \approx 58 + P_i(dBm) - NF(dB) \tag{2.12}$$

where NF is the noise figure of the amplifier. In a point-to-point optical transmission system as shown in Fig. 2.2, assuming each EDFA is identical and compensates exactly the loss of each

SSMF span, for the link with N EDFAs and N - 1 SSMF spans, the OSNR at the end of the whole link is:

$$OSNR(dB) \approx 58 + P_i(dBm) - NF(dB) - 10log_{10}(N) \quad (2.13)$$

2.1.2 Nonlinear Optical Impairments (Kerr Effect)

The refractive index of a silica optical fibre was assumed to be power independent in the discussion in Section 2.1.1. However, in reality, silica, like all materials, behaves nonlinearly at high intensities and its refractive index increases with intensity. This effect is called the Kerr effect, and its physical origin lies in the enharmonic response of electrons to optical fields, leading to a nonlinear susceptibility [10]. To account for the nonlinear refraction effect, the refractive index of an optical fibre can be described by:

$$n' = n + n_2(P/A_{eff}) \quad (2.14)$$

where n_2 is the nonlinear-index coefficient, P is the optical power propagating along the fibre, and A_{eff} is the effective mode area. The value of n_2 is approximately 2.6×10^{-20} m^2/W for silica optical fibres and varies with the dopants used inside the core. Although the nonlinear part of the refractive index is relatively small ($< 10^{-12}$ at a power level of 1 mW in SSMF), it affects optical fibre communication systems considerably over transmission distances of more than a few hundred kilometres, or where the launch power is particularly high (*e.g.* in extended reach repeaterless links). In particular, it results in the nonlinear phenomena of self- and cross- phase modulation and four wave mixing.

Self-Phase Modulation

The intensity dependence of the refractive index produces a time-dependent nonlinear phase shift. Since the resulting nonlinear phase modulation is self-induced, the phenomenon responsible for it is known as self-phase modulation (SPM). SPM leads to an instantaneous frequency chirping of optical pulses depending on the optical intensity, and causes additional signal bandwidth broadening, thus limiting the system performance.

Cross-Phase Modulation

The Kerr effect also leads to another nonlinear phenomenon termed cross-phase modulation (XPM). XPM occurs when two or more optical channels are transmitted simultaneously through the optical fibre utilizing the WDM technique. In WDM systems, the nonlinear phase shift for a specific channel not only depends on the optical intensity of the propagating channel of interest but also on the optical intensity of the signals propagating in the other channels.

Four-Wave Mixing

If three optical fields (A_1, A_2 and A_3) with carrier frequencies ω_{c1}, ω_{c2} and ω_{c3} co-propagate through the fibre simultaneously, the Kerr nonlinearity results in the generation of a fourth field (A_4) whose frequency ω_{c4} is related to other frequencies by a relation $\omega_{c4} = \omega_{c1} \pm \omega_{c2} \pm \omega_{c3}$. It is possible in principle for several frequencies to be generated, corresponding to different plus and minus sign combinations. In practice, most of these combinations do not build up because of a phase-matching

requirement [3]. These generated frequency components overlap with the channel of interest, thus impacting the system performance.

The nonlinear propagation of signals and noise are described by the nonlinear Schrödinger equation (NLSE), Eq. 2.6 extended to include the nonlinear effects [3]:

$$\frac{\partial A}{\partial z}+\frac{\alpha}{2}A+\frac{i}{2}\beta_2\frac{\partial^2 A}{\partial t^2}=i\gamma|A|^2A \tag{2.15}$$

where the nonlinear coefficient γ depends inversely on the effective mode area and can be written as:

$$\gamma=\frac{n_2\omega}{cA_{eff}} \tag{2.16}$$

If the optical field of each WDM channel is simulated as separate vectors, Eq. 2.15 can be extended as follows:

$$\frac{\partial A_1}{\partial z}+\frac{\alpha}{2}A_1+\frac{i}{2}\beta_2\frac{\partial^2 A_1}{\partial t^2}=\underbrace{i\gamma|A_1|^2A_1}_{SPM}+\underbrace{2i\gamma(|A_2|^2+|A_3|^2)A_1}_{XPM}+\underbrace{i\gamma A_2^2A_3^*}_{FWM} \tag{2.17}$$

However, the computational complexity of this operation is significantly increased in numerical simulations. Therefore, to simplify the simulations, Eq. 2.15 is utilized in simulations throughout the thesis.

2.2 Direct-detection Technology

An optical receiver converts the optical signal received at the output of the optical fibre into an electrical signal. Fundamentally, there are three types of optical detection technique, known as direct (square-law) detection, balanced detection and coherent detection. Since the single-sideband subcarrier modulation (SSB SCM) technique employing direct-detection is the main technique studied throughout the thesis, due to its relative simplicity compared with coherent and balanced detection, this section provides a detailed description of direct-detection receivers. The noise theory and noise management in SSB SCM DD systems are discussed in the following subsections. Balanced detection will be briefly discussed in Chapter 3 as a method to compensate nonlinear beating interference introduced by square-law detection, while the performance of the developed direct-detection transceiver technology is compared with that of balanced detection and coherent detection in Chapter 9.

2.2.1 Principles of Operation

The single-polarisation direct-detection receiver considered throughout this thesis consists of an optical band-pass filter (OBPF) or wavelength demultiplexer, to select the WDM channel of interest, a single photodiode (PD) and an analogue-to-digital converter (ADC), as shown in Fig. 2.3. The PD detects the transmitted optical signal at THz optical carrier frequency and down-converts it to an electrical baseband signal. The output photocurrent of the PD is based on the received optical power and the normalized detected signal, $V_{DD}(n)$ can be written as:

$$
\begin{aligned}
V_{DD}(n) &= R \cdot \left(E_S(n) \cdot E_S^*(n)\right) \\
&= R \cdot \left[A_S(n) e^{j\omega_S n} e^{j\phi_S}\right] \cdot \left[A_S(n) e^{-j\omega_S n} e^{-j\phi_S}\right] \\
&= R \cdot A_S^2(n)
\end{aligned} \tag{2.18}
$$

where R is the PD responsivity, $E_S(n)$ is the optical field of the photodiode input signal, * signifies complex conjugate, n is the discrete time index, $A_S(n)$ is the time dependent signal amplitude, and ω_S and ϕ_S are the angular frequency and phase, respectively. It can be seen that the optical phase information is lost following the square-law detection.

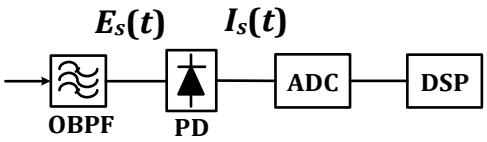

Fig. 2.3: A schematic of a direct-detection receiver.

The most straightforward DD transceiver is the intensity modulation direct detection (IM-DD) TRx, in which a double-sideband (DSB) real-valued signal is generated by a directly-modulated laser (DML) and detected by a single photodiode. However, since the performance of IM-DD system is significantly affected by dispersion–induced channel fading effect, such transceivers are not capable of supporting high capacity transmission over metro distances unless optical dispersion compensation is used [11, 12]. In contrast, the single-sideband subcarrier modulation direct-detection transceiver uses a CW laser and an external modulator (either an IQ-modulator or a dual-drive Mach-Zehnder modulator (DD MZM)). A digital SSB signal is generated together with an optical carrier, offering a number of advantages: it enables limitations due to fibre dispersion to be avoided using EDC, and allows higher spectral efficiency due to the use of a single sideband carrying a high-order modulation format. SSB SCM DD transceivers can therefore support higher transmission capacity [13]. Regarding the modulation formats that are used for direct detection, the simplest modulation formats are binary: on-off keying (OOK) [14-20] and duobinary [21-23]. However, the achievable ISD is limited to 1 b/s/Hz. To achieve ISD of more than 2 b/s/Hz, multiple amplitude levels need to be employed, such as pulse amplitude modulation (PAM) [24-27]. However, the performance of PAM systems is significantly degraded because of only one degree of freedom being used. In contrast, the SSB SCM signalling (SSB OFDM and SSB Nyquist-SCM) enables the use of quadrature amplitude modulation (QAM) in DD links, and consequently, higher ISDs can be achieved [28-29]. Different modulation formats used for DD system will be discussed in Chapter 3 in detail. Therefore, due to its advantages of more robust transmission performance and higher achievable spectral efficiency, the SSB SCM DD system is a promising solution for high capacity and spectrally-efficient metro applications.

2.2.2 Noise Theory of SSB SCM DD System

The square-law detection photodiode can be modelled as producing a photocurrent proportional to the square of the sum of all optical fields in an arbitrarily-chosen polarization, plus the square of the sum of all optical fields in the orthogonal polarization. This subsection explains the detection process in SSB SCM DD systems (both SSB OFDM and SSB Nyquist-SCM) considering a noisy channel.

In a SSB SCM DD system, the signal field, $E_0(n)$, is added to a real-valued optical carrier, $E_{carrier}(n)$ during the electrical-to-optical conversion. Assuming the accumulated chromatic dispersion is fully compensated by using either an optical or digital method and the effect of fibre nonlinearity is insignificant due to a relatively short transmission distance and low launch power, the system performance is mainly limited by ASE-noise. The ASE-noise spectrum is assumed to be white but band-limited by an OBPF before the detection, to filter out the out-of-band noise and at the same time demultiplex the WDM channels. The ASE-noise is unpolarised, with equal power in the polarization aligned to the signal ($E_{ASEX}(n)$) and its orthogonal component ($E_{ASEY}(n)$). Therefore, the optical field of the photodiode input signals in both polarizations, $E_{SX}(n)$ and $E_{SY}(n)$ are described as:

$$\begin{aligned} E_{SX}(n) &= E_{carrier}(n) + E_0(n) + E_{ASEX}(n) \\ E_{SY}(n) &= E_{ASEY}(n) \end{aligned} \tag{2.19}$$

The optical spectra of $E_{SX}(n)$ and $E_{SY}(n)$ are shown in Fig. 2.4 (left), with a subcarrier(s) bandwidth of B_{sc}, and a spectral guard band, B_{gap}, between the optical carrier and the subcarrier(s). After square-law detection, the normalized detected real-valued DSB signal, $V_{DD}(n)$ in Eq. 2.18 is given by:

$$\begin{aligned} V_{DD}(n) &= E_{SX}(n) \cdot E_{SX}^*(n) + E_{SY}(n) \cdot E_{SY}^*(n) \\ &= E_{carrier}^2(n) + \underbrace{2Re[E_{carrier}(n) \cdot E_0(n)]}_{CSBP} + \underbrace{|E_0(n)|^2}_{SSBI} \\ &\quad + \underbrace{2Re[E_{carrier}(n) \cdot E_{ASEX}(n)]}_{CABI} + \underbrace{2Re[E_0(n)^* \cdot E_{ASEX}(n)]}_{SABI} \\ &\quad + \underbrace{|E_{ASEX}(n)|^2 + |E_{ASEY}(n)|^2}_{AABI} \end{aligned} \tag{2.20}$$

where $Re[x]$ signifies the real part of x. The components of the optical spectrum beat with each other to produce the electrical beating products which can also be observed in Fig. 2.4 (middle) and (right). It should be mentioned that, for simplification of the noise analysis, the OBPF is assumed to be an ideal brickwall filter with the bandwidth of $B_{OBPF} = B_{gap} + B_{sc}$. Thus, the extra beating products caused by the ASE-noise in the negative frequency range can be neglected.

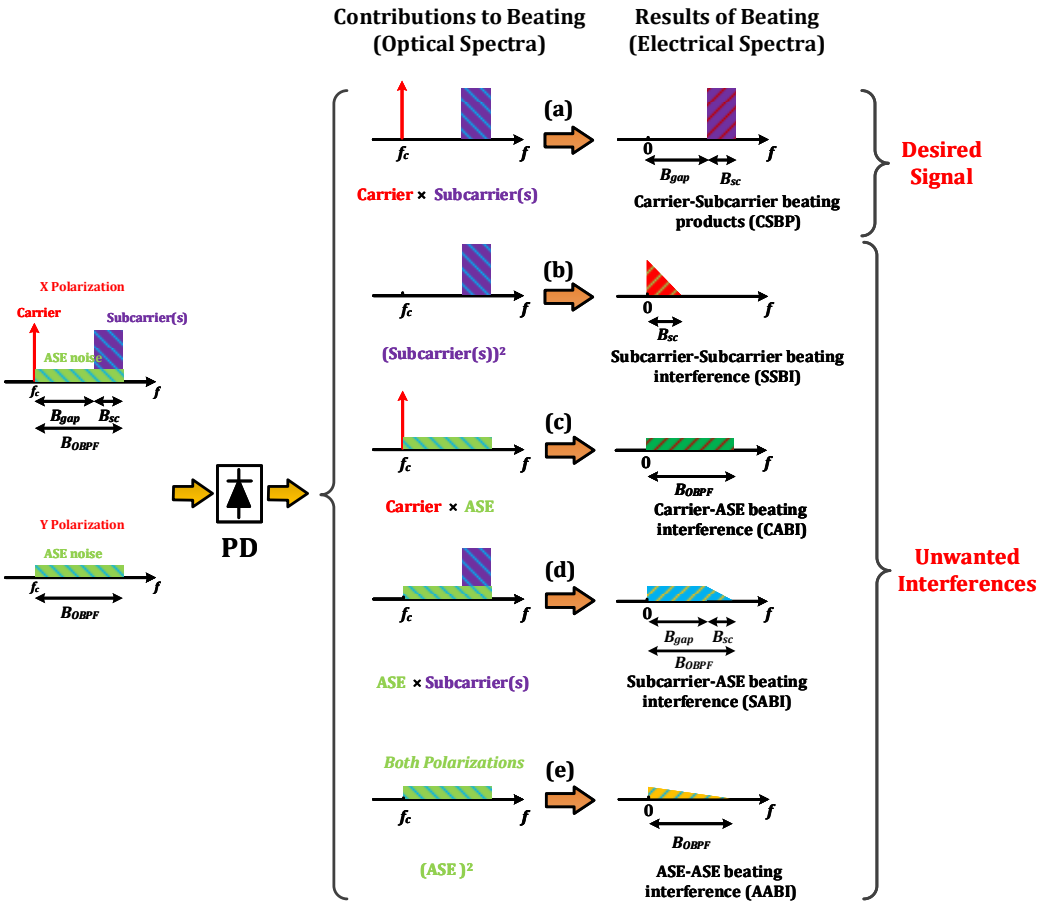

Fig. 2.4: Schematics of direct-detection process: receiver input optical spectrum (left), optical spectrum components which contribute to beating (middle) and the resulted beating products (right) [30].

The resulting electrical beating products (a)-(e) are [30, 31]:

(a) Carrier-Subcarrier beating product (CSBP), $2Re[E_{carrier}(n)\cdot E_0(n)]$: This is the desired electrical subcarrier signal, with the bandwidth of B_{sc}.

(b) Subcarrier-Subcarrier beating interference (SSBI), $|E_0(n)|^2$: This produces an unwanted nonlinear distortion, which is maximum close to zero frequency and falls to zero at the frequency equal to the bandwidth B_{sc} in the frequency domain (a triangular-shaped spectrum). In currently demonstrated SSB SCM DD system, the SSBI can either be avoided by leaving a spectral guard band with $B_{gap} \geq B_{sc}$ between the optical carrier and the subcarrier band [32] or can be compensated by using optical [33, 34] or digital methods [35-40].

(c) Carrier-ASE beating interference (CABI) (one polarization), $2Re[E_{carrier}(n)\cdot E_{ASEX}(n)]$: The optical carrier, and the component of the ASE noise in the same polarization as the carrier, beat with each other, with the resulting products falling across the full bandwidth of the signal ($B_{OBPF} = B_{gap} + B_{sc}$).

(d) Subcarrier-ASE beating interference (SABI) (in the same polarization), $2Re[E_0(n)^*\cdot E_{ASEX}(n)]$: This is more complex than the CABI penalty due to ASE-noise and subcarrier(s) both occupying a finite bandwidth. Based on the convolution in the frequency domain, the SABI is maximum between 0 and B_{gap} frequency (rectangular-shaped) and it

falls to zero at a point equal to the bandwidth of the ASE-noise (triangular-shaped between B_{gap} and B_{OBPF}).

(e) ASE-ASE beating interference (AABI) (either polarization), $|E_{ASEX}(n)|^2$ or $|E_{ASEY}(n)|^2$: The band-limited ASE-noise beats with itself, producing products with maximum power close to zero frequency and falling to zero at the bandwidth of the signal (triangle shaped with a bandwidth of B_{OBPF}). This beating interference becomes significant at low OSNRs and can be neglected at higher OSNRs.

In an ideal SSB SCM DD system, if the SSBI effect is eliminated, the CABI effect becomes the dominant noise source affecting the SNR of the received electrical signal. However, even when SSBI is present, the penalty due to CABI remains an additional significant nonlinear penalty which degrades the receiver sensitivity, in comparison to the effects of SABI and AABI. Discussions about the relationship between these penalties will be presented in the following subsection.

2.2.3 Noise Management of SSB SCM DD System

In spectrally-efficient WDM SSB SCM DD system, a narrow or zero frequency guard band ($B_{gap} < B_{sc}$) should be used between the optical carrier and the SSB SCM to minimize the signal bandwidth. In this case, all the beating interference effects discussed in the above subsection may occur in the signal spectral region. The system performance can be evaluated by measuring the detected electrical signal-to-noise power ratio (SNR), which is given by:

$$SNR = \frac{P_{desired}}{P_{distortion}} = \frac{P_{CSBP}}{P_{SSBI} + P_{CABI} + P_{SABI} + P_{AABI}} \tag{2.21}$$

where $P_{desired}$ and $P_{distortion}$ are the powers of desired signal (CSBP) and interfering products, (SSBI, CABI, SABI and AABI) respectively. According to the theory of beating in square-law detection, the CSBP and CABI are optical carrier related beating terms; their impacts are proportional to the applied optical carrier. Thus, a parameter termed the carrier-to-signal power ratio (CSPR) is utilized to determine the detected electrical SNR expressed in Eq. 2.21. The CSPR is defined as:

$$CSPR = \frac{P_{carrier}}{P_{subcarrier(s)}} \tag{2.22}$$

Fig. 2.5 shows the relationship between the system performance (measured by bit-error-ratio (BER)) and the employed CSPR value with two different OSNRs ($OSNR_1 < OSNR_2$). It can be seen that there is a trade-off between the system distortions, thus leading to an optimum CSPR value which offers the best system performance. Signals with lower CSPR suffer more from higher nonlinear distortions, contributed by the SSBI, SABI and AABI, while high CSPR leads to a high required OSNR value due to excessive optical carrier power, which is included in the OSNR calculation. In addition, for different OSNR values, the contributions of the ASE noise-related beating terms (CABI, SABI and AABI) change, leading to a noise-dependent trade-off between these interferences. The optimum CSPR of system operating at higher OSNR ($OSNR_2$ in Fig. 2.5) is higher than that for system employing lower OSNR ($OSNR_1$). Consequently, it is important that the CSPR is re-optimized for each OSNR value. Furthermore, if beating interference compensation techniques are applied to the system, due to the reduction in the impact of the nonlinear beating terms, the optimum CSPR value reduces to a lower value. In the situation where the optical guard

band is sufficiently narrow and the OSNR is sufficiently high, the impact of SABI and AABI are insignificant, and the trade-off is mainly between the SSBI and CABI penalties. The selection of the optimum CSPR value and its reduction in compensated systems will be described in detail in Chapters 4-7 and 9.

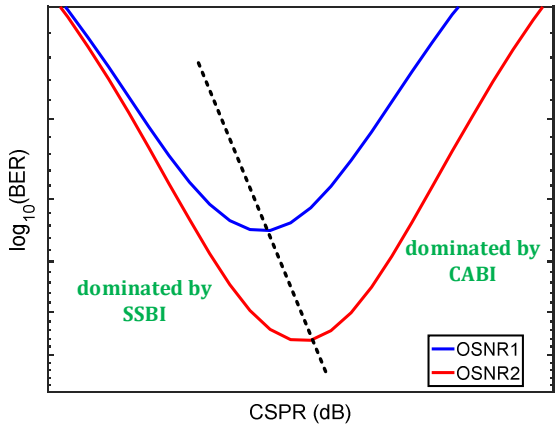

Fig. 2.5: Schematic of BER versus CSPR at two different OSNR values ($OSNR_1 < OSNR_2$). The dashed black line indicates the shift in the optimum CSPR value.

2.3 Subsystems for cost-effective and spectrally-efficient direct-detection systems

In this section, the digital subsystems used for SSB SCM DD transceivers are discussed. It covers the single-sideband (SSB) signal generation using the Hilbert transform, the EDC technology to mitigate the accumulated dispersion along the fibre transmission and digital equalization techniques to recover the clock and minimise BER. Overall system designs showing the SSB SCM modulation and demodulation can be found in Chapter 3, Section 3.1.4.

2.3.1 Discrete Hilbert Transform (HT) for Single-Sideband Filtering

Double sideband (DSB) SCM is possible. However, this halves the achievable optical ISD [41]. Since both signal sidebands carry the same information, it is preferable to perform SSB modulation in order to double the ISD without any loss of information. A digital discrete Hilbert transform (HT) filter can be applied to generate the SSB signal electrically. In the HT, all negative frequency components of the signal are phase-advanced by 90° whereas all positive ones are phase-delayed by 90°. The amplitude of the signal spectrum remains unchanged [42, 43]. In other words, the HT introduces an 180° phase difference between the negative and positive frequency components of an input signal. The HT frequency response ($H_{HT}(\omega)$) is described as:

$$H_{HT}(\omega) = \begin{cases} e^{-\frac{j\pi}{2}}, & \omega > 0 \\ 0, & \omega = 0 \\ e^{\frac{j\pi}{2}}, & \omega < 0 \end{cases} \tag{2.23}$$

where ω is the angular frequency. The output of the HT is phase shifted by θ (multiplied by $e^{j\theta}$) and added to the original DSB signal to cancel the negative frequency components, thus creating a SSB signal, as shown in Fig. 2.6.

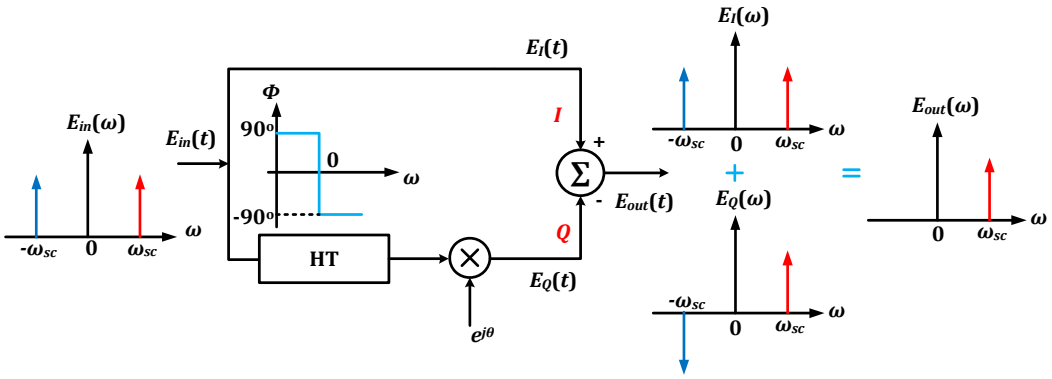

Fig. 2.6: Schematic of digital Hilbert transform sideband filter.

Analytically, the I and Q components ($E_I(t)$ and $E_Q(t)$) of the filter output signal, $E_{out}(t)$, can be written as:

$$\begin{aligned} E_I(t) &= A[1+\gamma\cos(\omega_{sc}t)] \\ E_Q(t) &= A[1+\gamma\cos(\omega_{sc}t-\pi/2)]e^{j\theta} \end{aligned} \tag{2.24}$$

where A is the amplitude, γ denotes the modulation index and ω_{sc} is the angular frequency of the SCM signal. According to Euler's formula: $\cos(x)=\frac{1}{2}(e^{jx}+e^{-jx})$, the filter output, which is the sum of the I and Q components, can be written as:

$$\begin{aligned} E_{out}(t) &= E_I(t)+E_Q(t) \\ &= A\left\{\begin{array}{c} 1+e^{j\theta}+\frac{\gamma}{2}e^{j\omega_{sc}t}\left[1+e^{j(\theta-\pi/2)}\right] \\ +\frac{\gamma}{2}e^{-j\omega_{sc}t}\left[1+e^{j(\theta+\pi/2)}\right] \end{array}\right\} \end{aligned} \tag{2.25}$$

In this equation, the lower or upper sideband of the input signal shown can be suppressed when the value of θ is chosen as $\pi/2$ or $-\pi/2$.

Alternatively, the DSB-to-SSB conversion can be performed optically by employing an optical filter [44-46] or an optical HT based on a fibre Bragg grating (FBG) [47-49]. A drawback of using optical sideband filtering is the requirement of an optical filter with a very steep profile (transition bandwidth). In addition, the ISD is significantly reduced due to requirement of placing a spectral gap between the optical carrier and subcarrier signal. Sideband filtering using an optical HT based on a FBG suffers from the degradation of the receiver sensitivity due to the reflectivity [50] and relatively poor stability due to the wavelength drift of the FBG [47]. Hence, in our work, we employ digital HT-based sideband filtering and a complex (IQ- or dual drive Mach Zehnder) modulator.

2.3.2 Electronic Dispersion Compensation (EDC)

A key attribute of the transceiver in optical fibre communication systems is its tolerance to fibre chromatic dispersion (CD). For complexity and cost reasons, it is preferable to compensate the accumulated CD with digital method, referred to as electronic dispersion compensation (EDC), rather than the optical methods such as dispersion compensating fibre (DCF). The EDC technique was proposed in [51-53] and is carried out by linear convolution with the inverse of the linear

lossless channel response due to CD, either at the transmitter (Tx-EDC) or at the receiver (Rx-EDC).

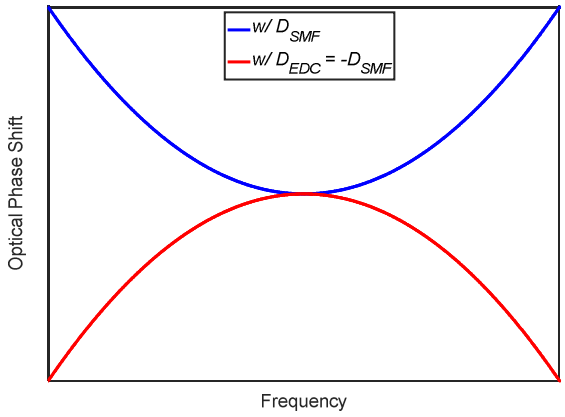

Fig. 2.7: Schemetic of optical phase shift versus frequency.

Fig. 2.7 shows a schematic of the optical phase shift with respect to frequency in a SSMF link and its inversion as a function of frequency. The inverse of the linear lossless channel response due to CD in the frequency domain, $H^{-1}(\omega)$, is calculated by simply inverting the sign of the dispersion parameter of a SSMF, D_{SMF} as expressed in Eq. 2.9 (D_{EDC} = -D_{SMF}), thus, $H^{-1}(\omega)$ can be written as:

$$H^{-1}(\omega) = \exp\left(j\frac{D_{EDC}}{4\pi c}\lambda_0{}^2\omega^2 L\right) \tag{2.26}$$

The signal spectrum following the EDC, $E(\omega)$ is given by:

$$\begin{aligned} E(\omega) &= E(\omega, L)H^{-1}(\omega) \\ &= E(\omega, L)\exp\left(j\frac{D_{EDC}}{4\pi c}\lambda_0{}^2\omega^2 L\right) \end{aligned} \tag{2.27}$$

where $E(\omega, L)$ is the signal spectrum before the EDC. The EDC can be implemented efficiently in the frequency domain using Fast Fourier Transforms (FFTs) and the overlap-and-save method (discarding the output samples corrupted by time aliasing each frame, and overlapping the input frames by the same amount) [64]. Alternatively, time-domain finite impulse response (FIR) filters have been proposed. A closed form solution for tap weights of the FIR filter with the bounds on the number of taps required for a given amount of dispersion is presented in [54].

In SSB SCM DD systems, transmitter-based electronic dispersion compensation (Tx-EDC) can be carried out using the complex (IQ- and dual-drive Mach-Zehnder) modulator and has shown very good performance [55-57], while the performance of the receiver-based EDC (Rx-EDC) is significantly impaired by the nonlinear effect known as SSBI caused by square-law detection [58]. However, the utilization of Tx-EDC also brings the drawback of increased system operation complexity due to the need for feedback from the receiver including the dispersion information. Our latest research results have shown that, the Tx and Rx-EDCs can achieve similar performance if the SSBI penalty is effectively suppressed with the utilization of receiver linearization techniques, which therefore simplifies the system operation [59]. Details of such comparisons between Tx and Rx-EDCs in the presence of different receiver linearization schemes on a SSB SCM DD system will be presented in Chapter 8.

2.3.3 Digital Equalization

Due to the difference in the sampling rates between the transmitter and receiver, it is essential to apply digital synchronization for symbol re-timing to recover the transmitted symbols. The algorithms discussed in this section implement blind equalization (non data-aided) where the tap weights, expressed as $h(n)$, are adaptively updated based on the received signal, expressed as $x(n)$. The tap weights of the equalizer are updated based on the error signal (e) at each iteration. In general, the least mean squares (LMS) algorithm is used to update the filter taps, due to its stability, fast convergence rate and lower computational complexity compared with implementing the recursive least squares algorithm or a Kalman filter [60]. In the LMS algorithm, the tap weights are adapted by utilizing the steepest-descent algorithm based on the derivative of the cost (error) function with respect to the filter coefficients. For a single-input, single-output complex channel, the filter taps are adjusted as:

$$h(n+1) = h(n) - \mu\widehat{\nabla}J(n) \tag{2.28}$$

where $h(n)$ is the tap vector at instant n, μ is the step-size and $\widehat{\nabla}J(n)$ is the estimated gradient of the cost surface with respect to $h(n)$. The error signal, $e(n)$ is often used to formulate the adaptation of a filter, which is given by:

$$\begin{aligned} e(n) &= -\frac{x(n)y(n)^*}{\widehat{\nabla}J(n)} \\ y(n) &= h(n)^H x(n) \end{aligned} \tag{2.29}$$

where $x(n)$ is the input vector at instant n, $y(n)$ represents the instantaneous output of the equalizer at instant n, * signifies the complex conjugate and H is the Hermitian conjugate. According to Eq. 2.29, the estimated gradient, $\widehat{\nabla}J(n)$ is written as:

$$\widehat{\nabla}J(n) = e(n)y^*(n)x(n) \tag{2.30}$$

Hence, Eq. 2.28 is re-written by:

$$h(n+1) = h(n) + \mu e(n)y^*(n)x(n) \tag{2.31}$$

As given in Eq. 2.29, the cost (error) function indicates the instantaneous symbol's deviation with respect to the desired symbol. To compute the error signal and subsequently, update tap weights of the filter, two main cost functions being implemented are the constant modulus algorithm (CMA), proposed by Godard [61], and decision-directed LMS. In the CMA algorithm, it is assumed that all the input symbols have a constant modulus or power, such as M-PSK symbols, thus the error function, $e(n)$ can be written as:

$$e(n) = R - |x(n)|^2 \tag{2.32}$$

where R is the desired constant modulus that the equalizer attempts to approach. For M-QAM symbols (M > 2), which have more than one constant modulus, the CMA algorithm needs to be modified by adding decision boundaries between the modulus rings, and it should be done before the computation of the error function and the adaptation of tap weights, a method referred to as a

radius directed equalizer (RDE) [62]. Although operating on modulation formats with a constant modulus or power is a limitation of the CMA algorithm, it enables very fast convergence and high robustness. Therefore, the CMA algorithm can be applied for pre-convergence before switching to decision-directed mode to minimize the error function, thus leading to an improved SNR performance.

In decision-directed mode, the error signal can be calculated by subtracting the instantaneous equalizer output, $y(n)$ from the output signal following the hard decision:

$$e(n) = D[y(n)] - y(n) \tag{2.33}$$

where $D[\cdot]$ signifies the operator of hard decision. For a QPSK signal, $D[y_{QPSK}(n)]$ is given by:

$$D[y_{QPSK}(\mathrm{n})] = \frac{1}{\sqrt{2}}[sgn\{Re[y(n)]\} + jsgn\{Im[y(n)]\}] \tag{2.34}$$

where $sgn\{\cdot\}$ denotes the signum operator. Implementing the FIR filter with decision-directed LMS algorithm is used as the second equalization stage, in which the received symbols are converged to their hard decision levels. Hence, the symbol decision process can be simplified. However, a drawback of this method is that its convergence depends on making a sequence of successive correct symbol decisions, and consequently the convergence is slowed down or even sometimes blocked by incorrect decisions. Therefore, a decision-directed mode equalizer is always initiated with CMA to initialize the filter coefficients [63]. Note that, all the equalizers used throughout this thesis operate at 2 Sa/symbol.

References

[1] G.P. Agrawal, Fiber-optic Communication Systems. 3rd ed. (John Wiley & Sons, 2010).

[2] J.M. Senior, Optical Fiber Communications: Principles and Practice. 3rd ed. (Pearson Education, 2009).

[3] G.P. Agrawal, Nonlinear Fiber Optics. 4th ed. (Academic Press, 2001).

[4] G.P. Agrawal, Applications of Nonlinear Fiber Optics. 2nd ed. (Academic Press, 2008).

[5] L.G. Cohen, C. Lin, and W. G. French, "Tailoring zero chromatic dispersion into the 1.5-1.6 μm low-loss spectral region of single-mode fibres," in Electron. Lett. 15(12), 334-335 (1979).

[6] C.T. Chang, "Minimum dispersion at 1.55 μm for single-mode step-index fibres," in Electron. Lett. 15(23), 765-767 (1979).

[7] V.A. Bhagavatula, M.S. Spotz, W.F. Love, and D.B. Keck, "Segmented-core single-mode fibres with low cost and low dispersion," in Electron. Lett. 19(9), 765-767 (1983).

[8] B.J. Ainslie and C.R. Day, , "A review of single-mode fibers with modified dispersion characteristics," in J. Lightw. Technol. 4(8), 967-979 (1986).

[9] E. Desurvire, D. Bayart, B. Desthieux, and S. Bigo, Erbium-doped Fiber Amplifiers: Device and System Developments. (John Wiley & Sons, 2002).

[10] R.W. Boyd, Nonlinear Optics. 3rd ed. (Academic Press, 2008).

[11] Z. Liu, G. Hesketh, B. Kelly, J. O'Caroll, R. Phelan, D.J. Richardson, and R. Slavik, , "300-km transmission of dispersion pre-compensated PAM4 using direct modulation and direct detection," in Optical Fiber Communication Conference, OSA Technical Digest Series (CD) (Optical Society of America, 2017), paper Th3D.6.

[12] Z. Liu, M.S. Erilinç, B. Kelly, J.O'Carroll, R. Phelan, B.C. Thomsen, R.I. Killey, D.J. Richardson, P. Bayvel, and R. Slavik, , "49 Gbit/s direct-modulation and direct-detection transmission over 80 km SMF-28 without optical amplification or filtering," in European Conference and Exhibition on Optical Communication (ECOC 2016), 145-147.

[13] W.-R. Peng, X. Wu, V.R. Arbab, K.-M. Feng, B. Shamee, L.C. Christen, J.Y. Yang, A.E. Willner, and S. Chi, "Theoretical and experimental investigations of direct-detected RF-tone-assisted optical OFDM systems," J. Lightw. Technol., 27(10), 1332-1339 (2007).

[14] W. Idler, S. Bigo, Y. Frignac, B. Franz and G. Veith, "Vestigial side-band demultiplexing for ultra-high capacity (0.64 bit/s/Hz) of 128×40 Gbit/s channels," in Optical Fiber Communication Conference, OSA Technical Digest Series (CD) (Optical Society of America, 2001), paper MM3.

[15] W. Idler, G. Charlet, R. Dischler, Y. Frignac and S. Bigo, "0.8 bit/s/Hz of information spectral density by vestigial side-band filtering of 42.66 Gb/s NRZ," in European Conference and Exhibition on Optical Communication (ECOC 2002), paper 8.1.5.

[16] K. Schuh, E. Lach, B. Junginger, G. Veith, J. Renaudier and G. Charlet, "8 Tbit/s (80×107 Gbit/s) DWDM ASK-NRZ VSB transmission over 510 km NZDSF with 1 bit/s/Hz spectral efficiency," in European Conference and Exhibition on Optical Communication (ECOC 2007), paper 1.8.

[17] J.-X. Cai, M. Nissov, C.R. Davidson, Y. Cai, A.N. Pilipetskii, H. Li et al., "Transmission of thirty-eight 40 Gb/s channels (>1.5 Tb/s) over transoceanic distance," in Optical Fiber Communication Conference, OSA Technical Digest Series (CD) (Optical Society of America, 2002), paper PD FC4.

[18] Y. Frignac, G. Charlet, W. Idler, R. Dischler, P. Tran, S. Lanne et al., "Transmission of 256 wavelength-division and polarization-division multiplexed channels at 42.7 Gb/s (10.2 Tb/s capacity) over 3×100 km of TeraLight fiber," in Optical Fiber Communication Conference, OSA Technical Digest Series (CD) (Optical Society of America, 2002), paper PD FC5.

[19] D. F. Grosz, A. Agarwal, S. Banerjee, A.P. Kung, D.N. Maywar, A. Gurevich et al., "5.12 Tb/s (128×42.7 Gb/s) transmission with 0.8 bit/s/Hz spectral efficiency over 1280 km of standard single-mode fiber using all-Raman amplification and strong signal filtering," in European Conference and Exhibition on Optical Communication (ECOC 2002), paper PD4.3.1.

[20] I. Morita, T. Tsuritani, N.Yoshikane, A. Agata, K. Imai and N. Edagawa, "100% Spectral–efficient 25 x 42.7 Gbit/s transmission using asymmetric filtered CS-RZ signal and a novel crosstalk suppressor," in European Conference and Exhibition on Optical Communication (ECOC 2002), paper PD4.7.

[21] G. Charlet, S. Lanne, L. Pierre, C. Simonneau, P. Tran, H. Mardoyan et al., "Cost-optimized 6.3 Tbit/s-capacity terrestrial link over 17×100 km using Phase-Shaped Binary Transmission in a conventional all-EDFA SMF-based system," in Optical Fiber Communication Conference, OSA Technical Digest Series (CD) (Optical Society of America, 2003), paper , PD2.5.

[22] T. Ono, Y. Yano, K. Fukuchi, T. Ito, H. Yamazaki, M. Yamaguchi and K. Emura, "Characteristics of optical duobinary signals in terabit/s capacity, high-spectral efficiency WDM systems," J. Lightw. Technol., 16(5), 788-797 (1998).

[23] H. Bissessur, G. Charlet, W. Idler, C. Simonneau, S. Borne, L. Pierre et al., "3.2 Tbit/s (80× 40 Gbit/s) phase-shaped binary transmission over 3× 100 km with 0.8 bit/s/Hz efficiency," Electron. Lett., 38(8), 377–379 (2002).

[24] K. Szczerba, P. Westbergh, J. Karout, J. Gustavsson, Å. Haglund, M. Karlsson, P. Andrekson, E. Agrell, and A. Larsson "30 Gbps 4-PAM transmission over 200 m of MMF using an 850 nm VCSEL," Opt. Express, 19(26), B203-B208 (2011).

[25] K. Szczerba, M. Karlsson, P. Andrekson, A. Larsson, and E. Agrell, "35.2 Gbps 8-PAM transmission over 100 m of MMF using an 850 nm VCSEL," in European Conference and Exhibition on Optical Communication (ECOC 2013), paper Th.F.1.

[26] K. Zhong, X. Zhou, Y. Gao, W. Chen, J. Man, L. Zeng, A.P.T. Lau, and C. Lu, "140Gbit/s 20km Transmission of PAM-4 Signal at 1.3 μm for Short Reach Communications," IEEE Photon. Technol. Lett., 27(16), 1757-1760 (2015).

[27] K. Szczerba, P. Westbergh, M. Karlsson, P.A. Andrekson, and A. Larsson, "70 Gbps 4-PAM and 56 Gbps 8-PAM Using an 850 nm VCSEL," J. Lightw. Technol., 33(7), 1395-1401 (2015).

[28] A.O. Wiberg, B.-E. Olsson, and P.A. Andrekson, "Single cycle subcarrier modulation," in Optical Fiber Communication Conference, OSA Technical Digest Series (CD) (Optical Society of America, 2009), paper OTuE.1.

[29] A.S. Karar and J.C. Cartledge, "Generation and detection of a 56 Gb/s signal using a DML and half-cycle 16-QAM Nyquist-SCM," IEEE Photon. Technol. Lett., 25(8), 757-760 (2013).

[30] A.J. Lowery, "Amplified-spontaneous noise limit of optical OFDM lightwave systems," Opt. Express, 16(2), 860-865 (2008).

[31] J. Ma and W. Zhou, "Joint influence of the optical-to-sideband ratio and guard band on direct-detection SSB-OOFDM system," IEEE Photon. J., 7(5), 7801713 (2015).

[32] B.J.C. Schmidt, A.J. Lowery, and L.B. Du, "Low sample rate transmitter for direct-detection optical OFDM," in Optical Fiber Communication Conference, OSA Technical Digest Series (CD) (Optical Society of America, 2009), paper OWM4.

[33] S.A. Nezamalhosseini, L.R. Chen, Q. Zhuge, M. Malekiha, F. Marvasti, and D.V. Plant, "Theoretical and experimental investigation of direct detection optical OFDM transmission using beat interference cancellation receiver," Opt. Express, 21(13), 15237-15246 (2013).

[34] W. Peng, I. Morita, and H. Tanaka, "Enabling high capacity direct-detection optical OFDM transmissions using beat interference cancellation receiver," in European Conference and Exhibition on Optical Communication (ECOC 2010), paper Tu.4.A.2.

[35] W. Peng, X. Wu, K. Feng, V.R. Arbab, B. Shamee, J. Yang, L.C. Christen, A.E. Willner, and S. Chi, "Spectrally efficient direct-detected OFDM transmission employing an iterative estimation and cancellation technique," Opt. Express, 17(11), 9099-9111 (2009).

[36] Z. Li, M. S. Erkilinc, S. Pachnicke, H. Griesser, R. Bouziane, B. C. Thomsen, P. Bayvel, R. I. Killey, "Signal-signal beat interference cancellation in spectrally-efficient WDM direct-detection Nyquist-pulse-shaped 16-QAM subcarrier modulation," Opt. Express 23(18), 23694-23709 (2015).

[37] S. Randel, D. Pilori, S. Chandrasekhar, G. Raybon, and P. Winzer, "100-Gb/s discrete-multitone transmission over 80-km SSMF using single-sideband modulation with novel interference-cancellation scheme," in European Conference and Exhibition on Optical Communication (ECOC 2015), paper Mo.4.5.2.

[38] K. Zou, Y. Zhu, F. Zhang and Z. Chen, "Spectrally efficient terabit optical transmission with Nyquist 64-QAM half-cycle subcarrier modulation and direct-detection," Opt. Lett. 41(12), 2767-2770 (2016).

[39] Z. Li, M. S. Erkilinc, R. Maher, L. Galdino, K. Shi, B. C. Thomsen, P. Bayvel, and R. I. Killey, "Two-stage linearization filter for direct-detection subcarrier modulation", IEEE Photon. Technol. Lett. 28(24), 2838-2841 (2016).

[40] Z. Li, M. S. Erkilinc, R. Maher, L. Galdino, K. Shi, B. C. Thomsen, P. Bayvel, and R. I. Killey, "Reach enhancement for WDM direct-detection subcarrier modulation using low-complexity two-stage signal-signal beat interference cancellation", in European Conference and Exhibition on Optical Communication (ECOC 2016), paper M 2.B.1.

[41] M.S. Erkılınç, S. Kilmurray, R. Maher, M. Paskov, R. Bouziane, S. Pachnicke, H. Griesser, B.C. Thomsen, P. Bayvel, and R.I. Killey, "Nyquist-shaped dispersion-precompensated subcarrier modulation with direct detection for spectrally-efficient WDM transmission," Opt. Express, 22(8), 9420-9431 (2014).

[42] J.G. Proakis, Digital Communications. 5th ed. (McGraw-Hill Higher Education, 2007).

[43] S.S. Haykin, Digital Communication System. 4th ed. (John Wiley & Sons, 2001).

[44] J. Park, W. Sorin, and K. Lau, "Elimination of the fibre chromatic dispersion penalty on 1550 nm millimetre-wave optical transmission," Electron Lett., 33(6), 512-513 (1997).

[45] J. Yu, M.-F. Huang, Z. Jia, T. Wang, and G.-K. Chang, "A novel scheme to generate single-sideband millimter-wave signals by using low-frequency local oscillator signal," IEEE Photon. Technol. Lett., 20(7), 478-480 (2008).

[46] Z. Tang, S. Pan, and J. Yao, "A high resolution optical vector network analyzer based on a wideband and wavelength-tunable optical single-sideband modulator," Opt. Express, 20(6), 6555-6560 (2012).

[47] Z. Li, H. Chi, X. Zhang, and J. Yao, "Optical single-sideband modulation using a fiber-bragg-grating-based optical Hilbert transformer," IEEE Photon. Technol. Lett., 23(9), 558-560 (2011).

[48] Y. Ogiso, Y. Tsuchiya, S. Shinada, S. Nakajima, T. Kawanishi, and H. Nakajima, "High extinction-ratio integrated mach-zehnder modulator with active y-branch for optical SSB signal generation," IEEE Photon. Technol. Lett., 22(12), 941-943 (2010).

[49] K. Takano, N. Hanzawa, S. Tanji, and K. Nakagawa, "Experimental demonstration of optically phase-shifted SSB modulation with fiber-based optical Hilbert transformers," in Optical Fiber Communication Conference, OSA Technical Digest Series (CD) (Optical Society of America, 2007), paper JThA48.

[50] M. Attygalle, C. Lim, G. Pendock, A. Nirmalathas, and G. Edvell, "Transmission improvement in fiber wireless links using fiber bragg gratings," IEEE Photon. Technol. Lett., 17(1), 190-192 (2005).

[51] R.I. Killey, P.M. Watts, V. Mikhailov, M. Glick, and P. Bayvel, "Electronic dispersion compensation by signal predistortion using digital processing and a dual-drive Mach-Zehnder modulator," IEEE Photon. Technol. Lett., 17(3), 714-716 (2005).

[52] J. McNicol, M. O'Sullivan, K. Roberts, A. Comeau, D. McGhan, and L. Strawczynski, "Electrical domain compensation of optical dispersion," in Optical Fiber Communication Conference, OSA Technical Digest Series (CD) (Optical Society of America, 2005), paper OThJ3.

[53] M.M.E. Said, J. Sitch, and M.I. Elmasry, "An electrically pre-equalized 10-Gb/s duobinary transmission system," J. Lightw. Technol., 23(1), 388-400 (2005).

[54] S.J. Savory, "Digital filters for coherent optical receivers," Opt. Express, 16(2), 804-817 (2008).

[55] Z. Li, M. S. Erkılınç, S. Pachnicke, H. Griesser, R. Bouziane, B.C. Thomsen, P. Bayvel, and R.I. Killey, “Signal-signal beat interference cancellation in spectrally-efficient WDM direct-detection Nyquist-pulse-shaped 16-QAM subcarrier modulation,” Opt. Express 23(18), 23694-23709 (2015).

[56] Z. Li, M. S. Erkilinc, R. Maher, L. Galdino, K. Shi, B. C. Thomsen, P. Bayvel, and R. I. Killey, "Reach enhancement for WDM direct-detection subcarrier modulation using low-complexity two-stage signal-signal beat interference cancellation", in European Conference and Exhibition on Optical Communication (ECOC 2016), paper M 2.B.1.

[57] K. Zou, Y. Zhu, F. Zhang and Z. Chen, “Spectrally efficient terabit optical transmission with Nyquist 64-QAM half-cycle subcarrier modulation and direct-detection,” Opt. Lett. 41(12), 2767-2770 (2016).

[58] M. Sieben, J. Conradi, and D.E. Dodds, “Optical single sideband transmission at 10 Gb/s using only electrical dispersion compensation” J. Lightw. Technol., 17(10), 1742-1749 (1999).

[59] Z. Li, M.S. Erkılınç, K. Shi, E. Sillekens, L. Galdino, B.C. Thomsen, P. Bayvel, and R.I. Killey, "SSBI mitigation and Kramers-Kronig scheme in single-sideband direct-detection transmission with receiver-based electronic dispersion compensation", J. Lightw. Technol., 35(10), 1887-1893 (2017).

[60] S.S. Haykin, Adaptive Filter Theory. 4th ed. (Pearson Education, 2005).

[61] D. Godard, “Self-recovering equalization and carrier tracking in two-dimensional data communication systems,” IEEE Trans. Commun. 28(11), 1867-1875 (1980).

[62] I. Fatadin, D. Ives, and S.J. Savory, “Blind equalization and carrier phase recovery in a 16-QAM optical coherent system,” J. Lightw. Technol., 27(15), 3042-3049 (2009).

[63] G. Picchi and G. Prati, “Blind equalization and carrier recovery using a “stop-and-go” decision-directed algorithm,” IEEE Trans. Commun. 35(9), 877-887 (1987).

[64] A.V. Oppenheim and R.W.Schafer, Digital Signal Processing, Englewood Cliffs, NJ: Prentice-Hall, 1975.

CHAPTER 3

LITERATURE REVIEW & STATE OF THE ART

The purpose of this review is to give an overview of the techniques used for direct detection systems in short- and medium- haul applications. It consists of two sections: In the first section, digital modulation formats that can be used for DD links are described, and ISDs, capacities and transmission reaches achieved using them are presented. The second section focuses on a number of effective optical and digital linearization techniques to eliminate the nonlinearities introduced by square-law detection, aiming to improve the performance of the DD transceiver.

3.1 Modulation Formats for Direct-Detection Transceiver

In DD links, the electrical signal is first converted into an optical signal at the transmitter, the resulting optical signal is transmitted over the optical fibre and then detected by a DD receiver, carrying out square-law detection, which allows detection of only the intensity of the light. Therefore, the first step in the design of an optical fibre communication system is determining how to modulate the electrical signal onto an optical carrier. This section covers the modulation techniques that can be applied in short- and medium- haul links.

Because of their implementation with a cost-effective transceiver architecture, binary modulation formats, *e.g.,* on-off keying (OOK) and duobinary have, until recently, been used for most of the installed optical transmission links. In these formats, the simplest optical receiver, which only consists of a single photodiode without a delay-line interferometer (DLI), is employed to detect the transmitted signal. However, the achievable ISDs are limited up to 1 bit/s/Hz since only 1 bit is encoded per symbol. With the continuously increasing demand for high bandwidth transmission due to data intensive services such as IP video, scientific and cloud computing in access, inter-data centre, back-haul, metropolitan and regional optical links [1, 2], it is becoming challenging to meet this demand using binary modulation formats. Higher order modulation formats, which encode $\log_2(M)$ bits per symbol ($M \geq 4$), *e.g., M-ary* phase-shift keying (M-PSK) and *M-ary* quadrature amplitude modulation (M-QAM) inherited from digital wireless communications, enabling more efficient utilization of the available optical bandwidth, have attracted much research interest in the last decade. The M-PSK formats encode the data by modulating only the phase of an optical field, whereas M-QAM formats modulate the data in multiple dimensions (both amplitude and phase) [3]. It is preferable to use the M-QAM formats rather than M-PSK formats since they have a lower SNR requirement for the same value of M due to their larger Euclidean symbol spacing [4].

M-QAM modulation formats with polarization multiplexing, utilizing coherent receivers and DSP-based fibre impairment mitigation techniques enable the highest bit rates with the highest ISDs [5-9], but require complex optical hardware structure. In contrast, single-polarization optical links with direct detection receivers use a simpler receiver structure and hence may be favourable for short- and medium-haul links; service providers have recently started using 100 Gb/s metro solutions based on 4 × 28 Gb/s using direct detection technology, with cost-effectiveness being the

primary requirement in such links [10]. Therefore, DD transceivers offering ISDs greater than 2 b/s/Hz will be required in the near future.

M-ary pulse amplitude modulation (M-PAM) is a simple multi-level amplitude modulation format that potentially offers ISD greater than 1 b/s/Hz with low transceiver hardware complexity and can be used as an alternative to binary modulation. However, in contrast to the complex modulation formats, since only one degree of freedom is used, the power efficiency of M-PAM is relatively low. Even so, it is still attractive for short-haul links, for instance, interconnects and data centres [11-14]. In comparison to M-PAM, *M-ary* differential phase-shift keying (DPSK) formats have been proposed to enable ISDs of more than 1 bit/s/Hz with better transmission performance. Nevertheless, the utilization of one or more balanced photodetectors (BPDs) combined with DLIs leads to an increased receiver complexity.

Thanks to the ongoing development of silicon complementary metal oxide semiconductor (CMOS) technology, especially high-speed digital signal processing (DSP), digital-to-analogue converters (DACs) and analogue-to-digital converters (ADCs), much of the transceiver complexity can be moved from the optical domain to the electrical domain. This allows the use of multi-level and multi-dimensional coding in DD links with a single-ended photodiode and without the need for DLIs, consequently allowing higher ISDs with reasonable OSNR performance to be achieved using cost-effective optical transceiver designs. The subcarrier modulation (SCM) technique which enables the use of M-QAM signalling implemented using a DSP-based transceiver architecture with a simple single photodiode, is a potentially attractive and practical solution for low-cost, spectrally-efficient access, metro and regional links. Fig. 3.1 shows a brief overview of the signal modulation techniques for direct-detection optical transceivers.

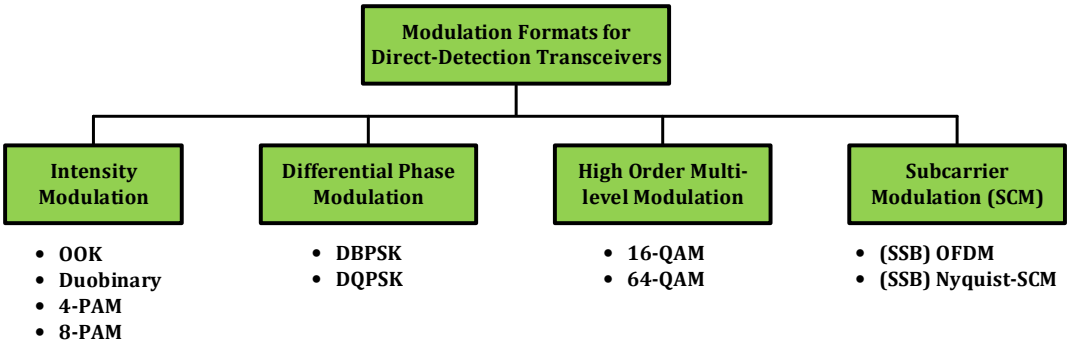

Fig. 3.1: Brief overview of the signal modulation techniques in direct-detection optical transceivers.

This section focuses on the modulation techniques used for short- and medium-haul links employing direct-detection. First, intensity modulation formats are described, following which, differential phase modulation and multi-level modulation formats are introduced. The last subsection covers two subcarrier modulation (SCM) approaches: optical orthogonal frequency division multiplexing (OFDM) and Nyquist pulse-shaped subcarrier modulation (Nyquist-SCM). Note that only single polarization transmission systems are investigated, due to their lower complexity than those using polarization multiplexing.

3.1.1 Intensity Modulation Formats

On-Off Keying (OOK)

On-off keying (OOK) is the most primitive modulation format and the cheapest solution for optical fibre communications. The transmitter simply changes the signal power between two levels, sending high power to encode a '1', and low power for a '0' when transmitting a continuous wave (CW) lightwave. The transceiver design for signal generation and detection is shown in Fig. 3.2. At the transmitter, a single-drive modulator or directly modulated laser is used to modulate a series of bit sequences onto the intensity of an optical carrier. At the receiver, a single photodiode is applied to perform the optical to electrical conversion.

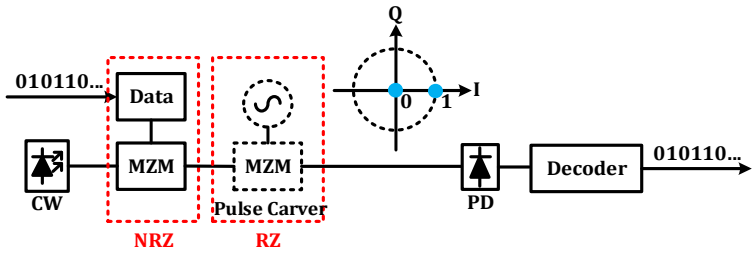

Fig. 3.2: Schematic of transceiver design for NRZ- and RZ-OOK signal generation and detection [15].

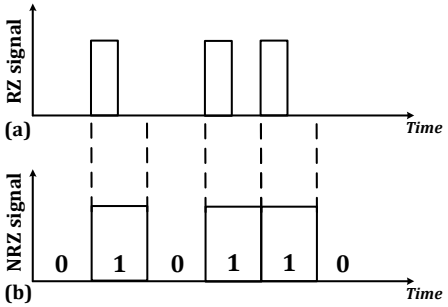

Fig. 3.3: Digital bit stream 010110… coded by using (a) RZ and (b) NRZ modulation formats.

There are two formats for OOK, termed return-to-zero (RZ) and non-return-to-zero (NRZ). As shown in Fig. 3.3, in the RZ-OOK format, each optical pulse representing a '1' is shorter than the bit slot, and its power level returns to the zero level before the bit duration is over. In the NRZ-OOK format, the optical pulse remains on throughout the bit slot and its power level does not drop to zero between consecutive '1' bits. A pulse carver, including an additional single-drive Mach-Zehnder modulator (MZM) driven sinusoidal signal following the optical modulator can be used to generate the RZ-OOK pulses with duty cycles of 33%, 50% and 67%, the latter being termed carrier-suppressed RZ (CS-RZ) [15]. The different duty cycles of the RZ-OOK signal are determined by different amplitude and biasing point of the sinusoidal driving signals. Detailed discussions about RZ-OOK signal generation are presented in [15-17].

In contrast to NRZ, the duration of a RZ pulse is shorter than the bit slot which gives more transition points from bit one to bit zero. According to Fourier transform theory, if the duration of a pulse in time is shorter, the spectrum becomes wider in frequency [17]. Hence, the spectra of RZ formats are broader than those of NRZ formats, leading to its power spectral density (PSD) lower than NRZ. As a result of this reduced PSD, the system's tolerance to fibre nonlinearities is improved [18], which is vitally necessary for long-haul applications (> 1000 km). However, since this characteristic also results in a reduced robustness to chromatic dispersion as well as a lower ISD (typically $\leq$ 0.5 b/s/Hz), it is not favourable for short- and medium- haul transmissions [19,

20]. The CS-RZ format provides the highest resilience to fibre nonlinearity compared to the other binary modulation formats.

Experimental demonstrations of NRZ signalling without applying transmitter-based optical filtering have been presented for submarine links [21, 22], with achieved ISDs of less than 0.5 b/s/Hz. Since the real-valued signal's (DSB) spectrum is symmetric around the carrier frequency, one of the sidebands can be filtered out whilst preserving the full information content of the signal and square-law detectability. Vestigial sideband (VSB) signalling can be applied to partially suppress or completely remove one of the sidebands to further improve the achievable ISD as well as the resilience to chromatic dispersion. In VSB signalling, an optical filter with a defined roll-off and optical carrier frequency offset is used to partially suppress one of the sidebands. Hence, the real-valued DSB signal is transformed into a complex-valued VSB signal. However, a drawback of using VSB signalling is its requirement of optical filters with very steep profile [23, 24], which is not cost-effective. The VSB-OOK techniques have been experimentally demonstrated at 40 and 100 Gb/s per channel to achieve ISDs from 0.64 to 1 b/s/Hz [25-28]. In addition, utilizing VSB signalling to improve the dispersion robustness of CS-RZ has also been reported for 40 Gb/s per channel links to achieve ISDs of 0.8 and 1 b/s/Hz for transoceanic and metro applications respectively [29, 30].

Duobinary

OOK signalling (NRZ and RZ) has been utilized for decades in optical fibre links at up to 10 Gb/s per channel. However, due to the accumulated chromatic dispersion and polarization mode dispersion (PMD), significant penalties can be observed if the bit rate per channel is further increased to 40 or 100 Gb/s. Therefore, correlative coding, referred to as partial-response signalling, is employed to compress the optical signal spectrum [31] and the duobinary, which is a three-level modulation format, is the most widely used technique. Different approaches can be utilized to generate the duobinary signals, either utilizing an optical delay-and-add method, referred to as optical duobinary [32] or electrical or optical low-pass filtering method, called electrical or optical phase-shaped binary transmission (PSBT) [33, 34].

The duobinary transceiver design is shown in Fig. 3.4. At the transmitter, the binary data-stream (a_n) is combined with its predecessor (p_{n-1}) using an XOR-gate and generates differential pre-coded data (b_n). Following this, a delay-and-add circuit or a Bessel low-pass filter (BLPF) with a 3-dB bandwidth of 25% of the symbol rate ($f_s/4$) is applied to b_n to obtain the duobinary signal. Finally, the generated 3-level duobinary signal is modulated by a push-pull MZM around its minimum transmission point (different transmitter configurations can be found in [35]). Since the phase information is lost upon square-law detection, the total system throughput is not increased by using this format. Nevertheless, this characteristic effectively improves the system's dispersion tolerance compared to NRZ-OOK. This is mainly because the '0' levels are preserved better due to the destructive interference of '+1' and '-1' levels [36]. The signal spectral compression of duobinary results from the smoother transitions between '-1', '0' and '+1' levels in contrast to the sharper transitions between '-1', '0' and '+1' levels in OOK.

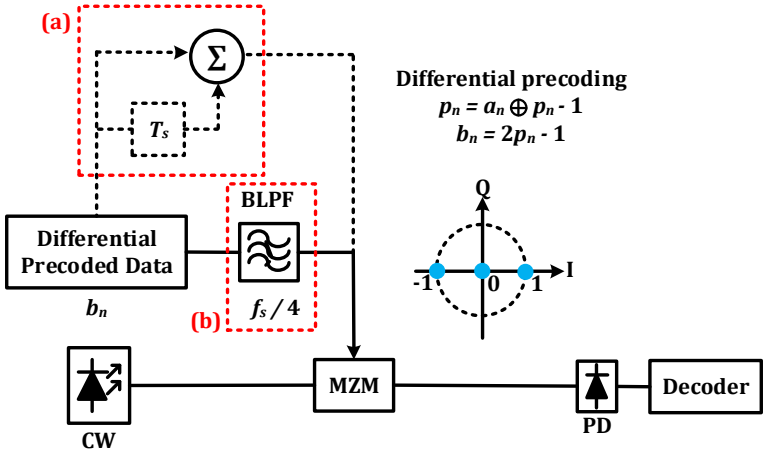

Fig. 3.4: Schematic of transceiver design for duobinary signal generation and detection using (a) delay-and-add circuit or (b) Bessel low-pass filter (BLPF) with a bandwidth of $f_s / 4$ [15].

Compared with OOK, duobinary signalling offers advantages such as improved resilience to chromatic dispersion, higher achievable ISDs (though typically less than 1 b/s/Hz) due to narrower optical spectrum, and better receiver sensitivity due to the absence of an optical carrier, thus making it a favourable and widely-used cost-effective solution for dense wavelength-division-multiplexing (DWDM) metro and core links at 40 Gb/s per channel [37]. As reported in [38, 39], duobinary signalling has been presented at 40 Gb/s per channel to achieve ISDs of 0.6 and 0.8 b/s/Hz.

Four-level Pulse Amplitude Modulation (4-PAM)

To achieve ISDs of more than 1 bit/s/Hz, multiple amplitude levels should be employed. The Nyquist-pulse-shaped four-level pulse amplitude modulation (Nyquist 4-PAM) is a simple multi-level modulation format that potentially offers increased ISDs with low transceiver hardware complexity and can be used as an alternative to binary modulations (OOK and duobinary). The transceiver design of Nyquist 4-PAM can be found in Fig. 3.5. At the transmitter, the bit sequence is input to a PAM encoder, and Nyquist pulse shaping is carried out using a Nyquist filter. Following this, the generated Nyquist 4-PAM signal is modulated by a MZM. At the receiver, the signal is detected by a single photodiode and is then passed through a second Nyquist filter for matched filtering. Finally, a 4-PAM decoder is used for signal recovery.

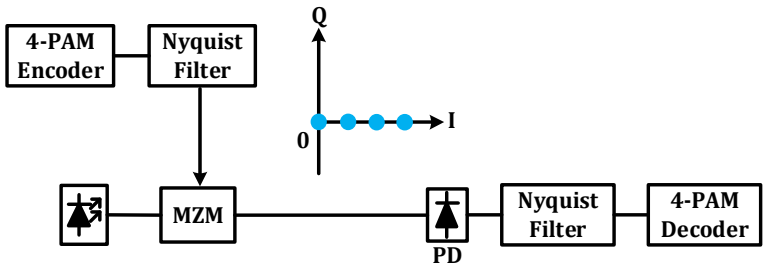

Fig. 3.5: Schematic of transceiver design for Nyquist 4-PAM signal generation and detection.

Although the achievable ISDs of Nyquist 4-PAM can be increased by performing both multi-level amplitude modulation and Nyquist pulse shaping, the OSNR performance of the Nyquist 4-PAM signalling degrades significantly because of only one degree of freedom being used, *i.e.*,

encoding data onto the amplitude of an optical field [11-14]. However, since complexity is critical in interconnects and data centres, and Nyquist 4-PAM offers the lowest implementation complexity of all the multilevel modulation format with spectral efficiency of 2 bits/s/Hz, it is still an appealing spectrally efficient and cost-effective short- haul optical links. The 4-PAM signalling has been demonstrated at up to 160 Gb/s for short reach (< 20 km) transmissions [40-46]. Moreover, 8-PAM signalling has been recently reported to achieve a further increased ISD with DD receiver [47].

3.1.2 Differential Phase Modulation Formats

As discussed above, the intensity modulation formats modulate the data onto the intensity of the optical field alone, and the signal can be recovered by using a single photodiode. Although the achievable ISDs can be increased by applying M-PAM signalling, the problem of poor receiver sensitivity resulting from only one degree of freedom being utilized, makes this system only suitable for short-range optical links. In order to obtain ISDs of greater than 1 b/s/Hz as well as better receiver sensitivity leading to an enhanced transmission reach to medium-range, the phase information of the optical field should be utilized. Therefore, differential encoding schemes, which enables each symbol to behave as a phase reference for the subsequent symbols, with balanced detection receivers [48] can be applied to increase ISDs while at the same time retaining phase information upon square-law detection.

Differential binary ($M = 2$) phase-shift keying (DBPSK)

In this format, like duobinary, differential precoding is utilized to encode the binary data-stream (a_n) on the binary phase changes between adjacent bits. A '1' bit is represented by a π phase shift and '0' bit encoded with zero phase shift. It should be mentioned that, if the tested bit-stream is a pseudo-random binary sequence (PRBS), differential precoding has no effect on the PRBS, which has auto- and cross-correlation properties, and thus it can be bypassed in experimental demonstrations [49].

As shown in Fig. 3.6, a DBPSK signal can be generated by using the same transmitter design as the RZ- or NRZ-OOK format. The main difference is that the symbol spacing on the IQ-plane is increased from 1 for OOK to $\sqrt{2}$ for DBPSK at a fixed average optical power. At the receiver, for the purpose of recovering the phase information of the optical signal without applying a local oscillator (LO), it is desirable to convert phase modulation into intensity modulation before detection. This can be achieved by detecting the DBPSK signal with a single balanced photodetector (BPD) combined with a delay line interferometer (DLI). The transmitted DBPSK signal is first split into two paths by applying a 3-dB coupler. One path is delayed by a bit duration, *e.g.*, 100 ps for a 10 Gb/s signal, and combined with the original signal with a 3-dB coupler. In this way, the preceding symbol in the DBPSK data stream is utilized as a phase reference based on the constructive or destructive relation between two adjacent symbols. Although a single-ended photodiode is sufficient for DBPSK signal detection, a BPD is usually applied because the increased symbol spacing allows DBPSK to accept $\sqrt{2}$ more Guassian noise which translates into a 3 dB gain over OOK in required OSNR at a given BER value [50].

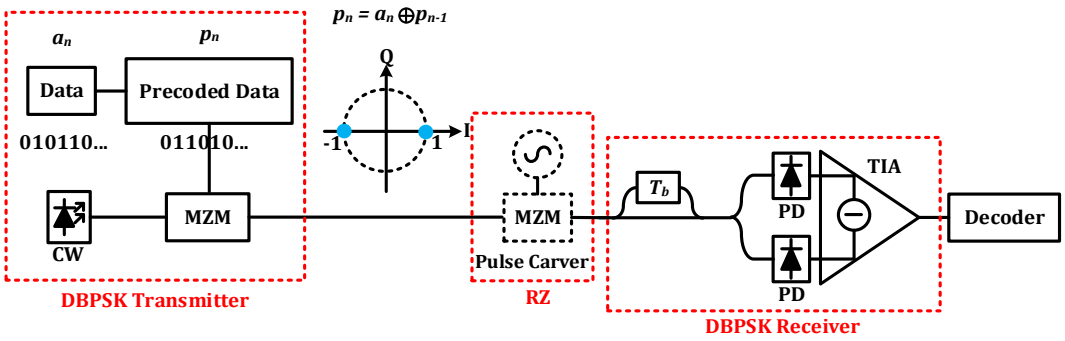

Fig. 3.6: Schematic of transceiver design for DBPSK signal generation and detection [15].

Similar to other binary modulation format (OOK and duobinary), the maximum achievable ISD of DBPSK signalling is 1 b/s/Hz. Hence, DBPSK is not suitable for links operating beyond 40 Gb/s per channel due to the bandwidth limitations of optical and electrical components. In addition, it may not be the most cost-effective solution for metro and regional applications due to its increased optical receiver hardware complexity. However, some experiments have been reported for (ultra) long- haul applications to evaluate its fibre nonlinearity robustness. The nonlinear transmission performance of RZ-DBPSK over 13100 km submarine fibre was shown to be similar with OOK in terms of the optimum launch power levels at 10 Gb/s per channel with an ISD of 0.3 b/s/Hz [51]. Some other experiments operating at 40 Gb/s with an ISD of 0.8 b/s/Hz have demonstrated that RZ-DBPSK has greater tolerance to chromatic dispersion as well as intra-channel nonlinearities compared with OOK formats [52-54].

Differential quadrature (M =4) phase-shift keying (DQPSK)

To achieve ISDs of greater than 1 b/s/Hz, higher order M-level modulation formats, which encode $\log_2(M)$ bits per symbol ($M \geq 4$) should be used. DQPSK, which is one of the simplest multi-level formats, was first proposed by Griffin and Carter [55]. It makes use of four optical phase shifts {0, $+\pi/2$, $+\pi$, $-\pi/2$} to modulate symbols {'00', '01', '11', '01'}, thus its symbol rate is half the total bitrate.

As shown in Fig. 3.7, the transmitter design of DQPSK requires two 3 dB couplers (one for splitting the CW laser source into two paths of equal intensity and one for combing them into one path), two nested MZMs operated as amplitude modulator for in-phase (I) and quadrature (Q) components, referred to as an IQ- modulator, and one optical $\pi/2$ phase shifter applied in one path. Moreover, a pulse carver can be added to obtain a RZ-DQPSK signal [56-58] to improve system resilience to fibre nonlinearity in (ultra) long- haul applications. At the receiver, the incoming optical signal is first split into two paths and two DBPSK receivers are applied to separately detect the I and Q components of the signal. Since a DQPSK signal has the same optical bandwidth as a DBPSK signal, its achievable ISD is doubled compared with binary modulation formats, thus make it suitable for spectrally-efficient WDM systems. Nevertheless, as discussed above, this improved ISD is achieved at the expense of using complex optical transceiver designs (multiple BPDs combined with DLIs), which is not cost-effective.

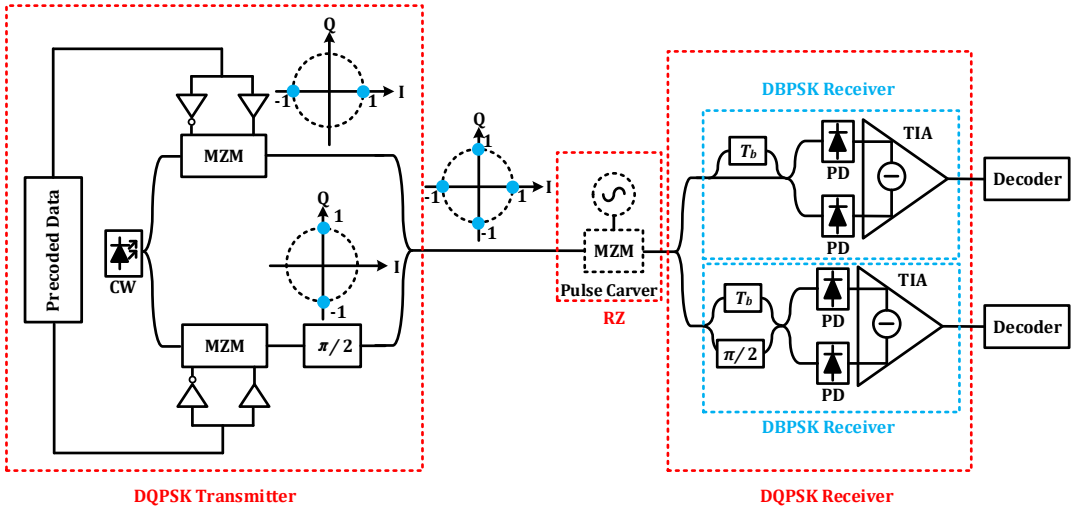

Fig. 3.7: Schematic of transceiver design for DQPSK signal generation and detection [15].

The DQPSK techniques have been experimentally demonstrated at bit rates of 12.5 Gb/s, 20 Gb/s, 40 Gb/s, 80 Gb/s and 100 Gb/s [59-63] to achieve ISDs of up to 1.6 b/s/Hz. However, since the symbol spacing dramatically decreases for higher order ($M > 4$) phase modulation formats, leading to an increased OSNR requirement at a given BER and reduced resilience to fibre nonlinearity, the transmission reach is consequently significantly reduced.

3.1.3 High order Multi-level (> 2 bits per symbol) Modulation Formats

To further increase the achievable ISDs, it is desirable to develop higher modulation formats. Thanks to the ongoing development of high-speed DAC/ADC technologies, DSP-based transceivers enables the generation of high order quadrature amplitude modulation, for example 16-QAM or 64-QAM [64] signalling with minimum Euclidean symbol spacing, as shown in Fig. 3.8 (a and b). An experimental demonstration of 16-QAM signalling has been presented for transmission over 160 km of uncompensated SSMF at a symbol rate of 10 GBaud using DACs [65].

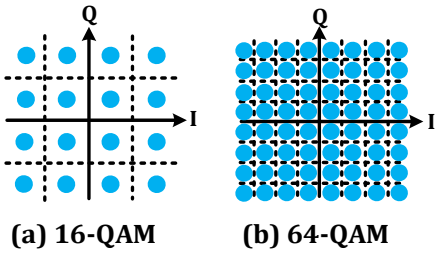

Fig. 3.8: Constellation diagrams for high order (a) 16-QAM and (b) 64-QAM modulaton formats.

3.1.4 Subcarrier Modulation (SCM) Formats

As discussed above, the use of cascaded modulators combined with one or more BPDs and DLIs to generate and detect high order modulation formats leads to increases in transceiver optical hardware complexity. Moreover, the implementation of dispersion compensating fibre (DCF) for chromatic dispersion mitigation further increases the cost. In order to overcome the above problems, DSP-based transceivers can be utilized for the implementation of high order modulation

formats instead of using cascaded modulators with BPDs and DLIs in short- and medium-haul links. Due to the ongoing development of CMOS technology and reduction of its size, cost and power consumption, it is expected that the utilization of high speed DACs and ADCs will be acceptable in future low-cost systems. Through the use of DSP, much of the transceiver complexity can be shifted from the optical domain to the electrical domain, making it possible to encode the M-QAM symbols with the minimum Euclidean spacing and to carry out electronic dispersion compensation. Therefore, the system OSNR requirement and robustness to chromatic dispersion are significantly improved without employing any DCFs or optical dispersion compensation (ODC) units.

In the last few years, the subcarrier modulation, which enables the use of M-QAM signalling with the minimum Euclidean spacing based on DSP-based transceiver architecture with a single-ended photodiode, has been proposed as a potentially attractive solution for low-cost, spectrally-efficient access, metro and regional links. Although only a single photodiode is utilized, and the phase information is lost upon square law detection, the amplitude and phase of the subcarrier(s) can be recovered at the receiver through beating with the optical carrier, making it possible to utilize high order QAM signalling to achieve high ISDs. In addition, since the EDC technique can be implemented in such transceivers, the system's resilience to chromatic dispersion can be improved as well.

There are two SCM approaches being studied for DD systems: optical orthogonal frequency division multiplexing (OFDM) [66] and Nyquist-SCM [67, 68]. OFDM utilizes multiple subcarriers that are orthogonal to each other with minimum frequency spacing (also called Nyquist spacing), while Nyquist-SCM uses only a single subcarrier with digital Nyquist pulse shaping. In order to further increase the achievable ISDs, sideband filtering can be utilized to generate SSB OFDM or SSB Nyquist-SCM, which are favourable for low-cost direct-detection WDM transceivers offering dispersion tolerance and high ISDs. The following subsection mainly describes the signal characteristics, transceiver structure and notable experimental demonstrations of these two SCM schemes.

Orthogonal Frequency Division Multiplexing (OFDM)

In optical OFDM signalling, the main difference in contrast to the previous formats is the implementation of inverse fast Fourier transforms (IFFT) at the transmitter and fast Fourier transforms (FFT) at the receiver. OFDM is a spectrally efficient multiple carrier modulation technique in which a high-speed serial data stream is divided into a number of parallel low-speed streams and modulated onto multiple subcarrier at different frequencies for simultaneous transmission. Based on the fast IFFT/FFT algorithm, multicarrier modulation and demodulation are efficiently implemented with OFDM. If the IFFT input signal satisfies the Hermitian symmetry, the generated OFDM signal is real-valued and is referred to as discrete multi-tone (DMT).

As shown in Fig. 3.9, the total signal frequency band is divided into a number of non-overlapping or overlapping frequency subcarriers, referred to as FDM and OFDM respectively. It can be seen that the FDM signalling allows to eliminate inter-channel interference (ICI) but makes inefficient use of the bandwidth. In contrast, the OFDM signalling overlaps the spectra of individual subcarriers to achieve increased spectral efficiency and the ICI is minimized due to orthogonality between adjacent subcarriers [69].

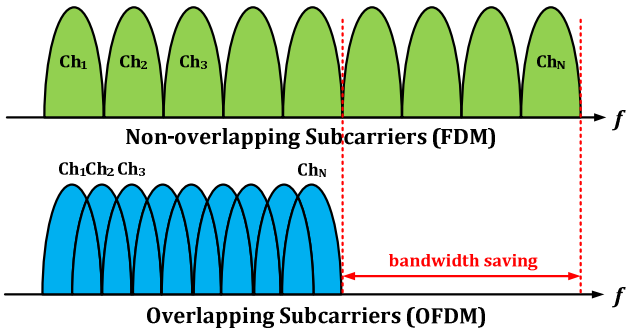

Fig. 3.9: Spectral efficient OFDM spectrum illustration.

In OFDM signaling [70-77], no ICI occurs between the adjacent subcarriers because each subcarrier has a *sinc*-function $(sin(x)/x)^2$ shaped spectrum that intercepts with the other *sinc* spectra at their null points. This orthogonality condition comes at the expense of strict time alignment/synchronization requirements between the generated OFDM symbols at the demultiplexing stage. Since OFDM signalling is highly susceptible to time and sampling frequency offset between the transmitter and receiver, proper management is also required, otherwise, the system suffers from significant performance degradation due to the crosstalk. Because of the much narrower bandwidth of each subcarrier compared to the total bandwidth, the OFDM signal's resilience to multi-path propagation is increased. Since the data is transmitted on a number of different frequencies, unlike with single-carrier NRZ or M-QAM signalling, the symbol period of each OFDM symbol is much longer than that of a serial system. Inter-symbol interference (ISI) due to time skew (for example, caused by chromatic dispersion) can be eliminated using a cyclic prefix (CP) and frequency domain single-tap equalizers as demonstrated in [70, 71]. After applying an IFFT to the encoded signal, the CP, which is a copy of the last fraction of each OFDM symbol, is added to the start of the symbol. Thus, the extended symbol can combat the time skew due to dispersion along the channel up to the duration of the CP, because the signal remains periodic within the Fourier-Transform window at the receiver. Since it does not carry any information, the CP costs additional bandwidth, and hence impacts the achievable ISD. A detailed discussion about the use of the CP can be found in [72, 73]. There are two major groups of OFDM DD systems [74-77], called intensity modulated (IM-) OFDM DD and SSB-OFDM DD. A drawback of IM-OFDM DD systems is that, since the modulated signal is DSB, the chromatic dispersion accumulated along the fibre transmission causes a relative phase rotation between the two sidebands, producing nulls in the carrier-signal beating terms at certain frequencies after square-law detection, termed dispersion induced power fading [78]. IM-OFDM DD and its comparison with OOK are described in detail in [79]. In order to avoid the power fading impairment and at the same time to increase the spectral efficiency, one of the signal sidebands can be removed either by optical filtering [80-82] or driving the IQ- modulator with a OFDM signal and its HT [83], as described in Chapter 2.

The transceiver design to implement SSB-OFDM DD signalling is shown in Fig. 3.10 [84]. In the transmitter digital signal processing (DSP), asymmetric zero padding is performed on the parallel QAM symbols to carry out frequency upconversion, the CP is then inserted after the IFFT to combat the dispersion. After the parallel-to-serial conversion, the SSB OFDM signal is generated. Since the relative phases of the OFDM subcarriers can add constructively, leading to high peak-to-average power ratio (PAPR), clipping needs to be performed to reduce the PAPR. Following this, a linear field modulation is carried out by biasing the IQ-modulator within its linear

regime (at or close to the quadrature point) and an optical carrier is added to the SSB OFDM signal. At the receiver, a single photodiode is utilized to detect the signal [85]. In the receiver DSP, after the serial to parallel conversion, the CP is first removed from the detected signal. Then, the FFT is applied and consequently frequency domain single-tap equalization with complex multiplication is performed for dispersion compensation. Finally, the QAM demapped parallel data carried by the subcarriers are converted to serial data.

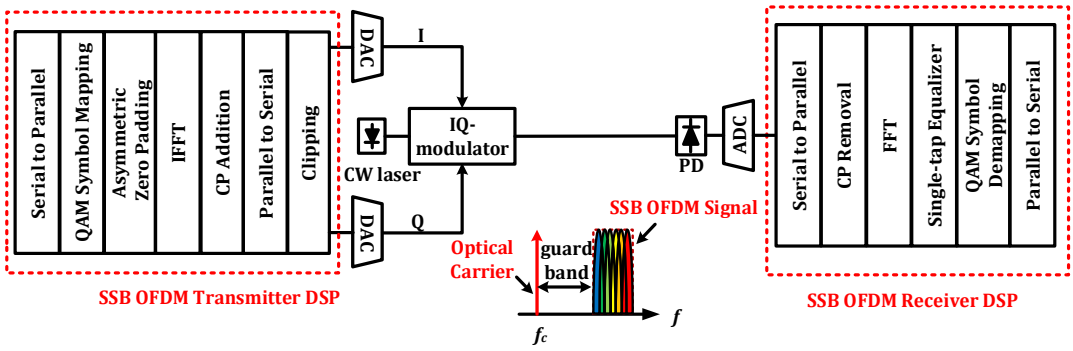

Fig. 3.10: Schematic of transceiver design for SSB OFDM DD signal generation and detection.

As discussed in Chapter 2, to avoid the distortion caused by SSBI on the desired CSBP, two methods can be applied: either the use of a sufficient spectral guard band between the sideband signal and the optical carrier, or the employment of linearization techniques. The first method halves the achievable ISD and wastes approximately 50% of the bandwidth of the electrical and optical components, such as DACs/ADCs, optical modulator(s), and photodiode(s). Thus it is not a spectrally-efficient solution and the bandwidth requirements for such components are nearly doubled. In contrast, the use of effective linearization techniques, removing the signal-signal beat products, enables the use of a narrower or zero guard band with improved system performance, making it attractive for spectrally-efficient applications. A number of recently proposed SSBI compensation techniques will be discussed in detail in Section 3.2.

SSB-OFDM DD technology has attracted much research attention for short- and medium-haul applications due to its robustness to chromatic dispersion, higher receiver sensitivity and achievable ISDs of greater than 1 b/s/Hz. Experimental demonstrations of WDM SSB-OFDM DD systems have been reported, with transmission over SSMF at ISDs of up to 2 b/s/Hz at 10, 20, 40 and 100 Gb/s per channel [86-89].

Nyquist-pulse-shaped subcarrier modulation (Nyquist-SCM)

As mentioned above, the main disadvantage of OFDM signalling is the high PAPR, thus causing a degradation in system performance. Clipping and other techniques for reducing the PAPR have been discussed, but they all have drawbacks such as increased complexity or overheads, resulting in nonlinear distortion and penalties [76, 77]. Alternatively, single subcarrier modulation, introduced in wireless infrared communications [90, 91], can be used for high order modulation with direct direction [92]. In this technique, the baseband signal is electrically modulated onto a single RF-subcarrier, in contrast to the multiple subcarriers used in OFDM. The lower PAPR due to the use of only a single RF-subcarrier reduces the quantization noise from the DACs/ADCs and, at the same time, offers a lower optimum carrier-to-signal power ratio (CSPR), thus potentially providing a better OSNR performance compared to OFDM signalling [93].

In order to maximize the spectral efficiency, high-order QAM encoding, Nyquist pulse shaping, and a subcarrier frequency lower than the symbol rate can be implemented, a technique called intensity-modulated Nyquist-SCM DD signalling [94-98]. To further improve the robustness to dispersion induced power fading, digital sideband filtering is implemented for generating the SSB Nyquist-SCM DD signalling. Fig. 3.11 shows the transceiver design of SSB Nyquist-SCM DD system. In the transmitter DSP, digital root-raised-cosine (RRC) filters are applied to the I- and Q-components of the baseband QAM signal to perform Nyquist pulse shaping. Then the filtered I- and Q-components are up-converted to an RF-subcarrier frequency (f_{sc}) and added to each other to generate a DSB Nyquist-SCM signal. A digital HT sideband filter (as discussed in Chapter 2) is applied to remove the lower frequency sideband (sideband suppression ratio > 30 dB) and, by biasing the IQ-modulator, an optical carrier is transmitted along with the sideband. The electrical and optical spectra in the generation process of SSB Nyquist-SCM signalling are shown in Fig. 3.12 (a) and (b) respectively. At the receiver, the transmitted signal is detected by a single photodiode. In the receiver DSP, down-conversion to baseband and matched filtering with a RRC filter are performed. Finally, the QAM symbol demapping is carried out following the equalization stage. Similar to SSB OFDM DD signalling, in order to improve system's robustness to the SSBI effect, either a sufficient frequency guard-band or an effective linearization scheme needs to be applied.

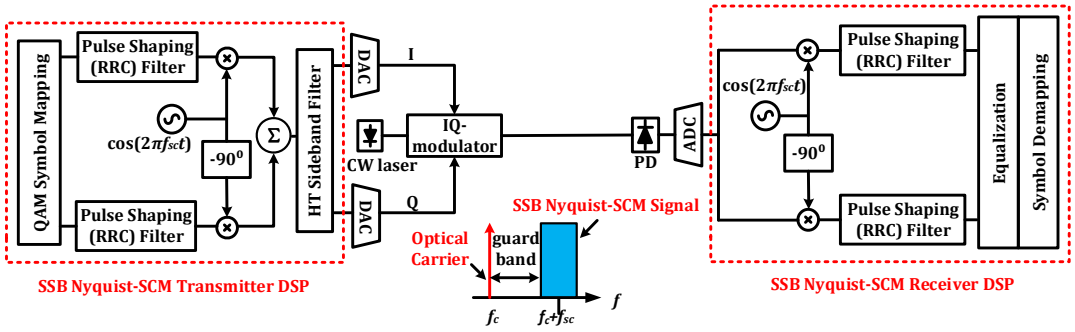

Fig. 3.11: Schematic of transceiver design for SSB Nyquist-SCM DD signal generation and detection.

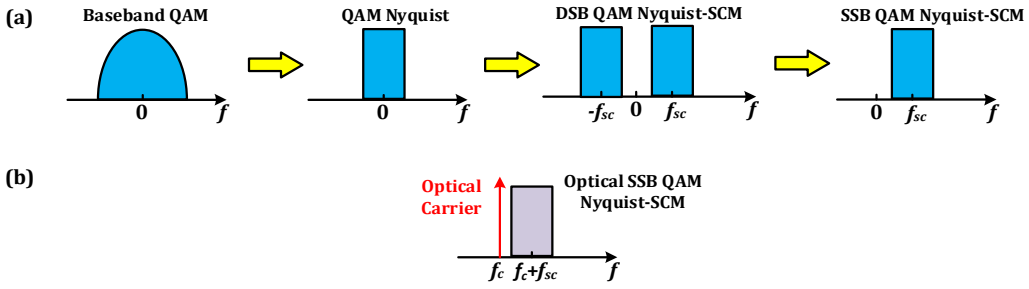

Fig. 3.12: Schematics of SSB Nyquist-SCM signal generation: (a) Digital signal spectra: Nyquist pulse shaping, up-conversion to the subcarrier frequency and sideband filtering. (b) Optical signal spectrum.

A number of experimental demonstrations have shown that Nyquist-SCM with direct detection is a promising and practical spectrally-efficient modulation technique for access, metro and regional networks. DD single-cycle QPSK, RZ-DQPSK and 16-QAM SCM in which f_{sc} is set equal to the symbol rate (f_b) have been demonstrated in [94-96], respectively. To further increase the spectral efficiency, half-cycle subcarrier modulation with and without Nyquist pulse shaping were demonstrated in back-to-back and transmission over VCSEL-based short optical links (up to 20

km) in [97, 98]. WDM DD SSB Nyquist-SCM combined with transmitter-based EDC to mitigate chromatic dispersion have been reported, transmitting over 800 km and 320 km at bit rates of 14 and 25 Gb/s per channel with ISDs of up to 2 b/s/Hz [99, 100].

3.2 Linearization Techniques for Single-Sideband Direct-Detection Transceiver

As described in Chapter 2, nonlinear distortion arises in SSB SCM DD schemes (both SSB OFDM and SSB Nyquist-SCM) from signal-signal beating during the square-law detection, generating unwanted mixing products which interfere with the desired signal-carrier beat terms. Among all these unwanted mixing products, the effect known as SSBI, which falls within the bandwidth of the subcarrier signal, causes the most significant degradation in the system's OSNR performance [101]. In order to avoid the SSBI penalty, two methods can be utilized: either the use of a sufficient spectral guard band ($B_{gap} \geq B_{sc}$) or employment of linearization techniques. Since the first method has the significant drawback of halving the spectral efficiency, it is necessary to develop effective techniques to cancel the SSBI and thus allows to use a narrow or zero guard band with improved system performance.

Recently, a number of linearization techniques have been investigated for both SSB OFDM and SSB Nyquist-SCM systems, including the use of beating interference cancellation balanced receiver, digital iterative SSBI cancellation, digital single-stage linearization filter, digital iterative linearization filter, digital two-stage linearization filter and the Kramers-Kronig DSP scheme. The principle of operation and characteristics of all these techniques are described in this section. Additionally, the advantages and drawbacks of each technique are also discussed.

3.2.1 Beat Interference Cancellation Balanced Receiver (BICBR)

The beat interference cancellation balanced receiver (BICBR) was first demonstrated for a SSB-OFDM DD system in [102-104]. The experimental results showed that the BER is significantly improved compared to the conventional DD receiver in transmission over SSMF, and a reduction of the frequency guard band can consequently be achieved.

The receiver structure of a BICBR is shown in Fig. 3.13 and its operation can be described as follows: (a) An optical 3 dB coupler splits the transmitted optical SSB SCM signal into two parallel branches. (b) The upper branch is sent directly to a photodiode (PD1) yielding both the desired CSBP and SSBI; while the lower branch suppressing the optical carrier with a carrier suppression filter (CSF) results in only SSBI after the square-law detection by PD2. (c) By simply subtracting the output of the lower branch from that of the upper branch, the desired signal without SSBI can be obtained at the output of the balanced detector, thus potentially allowing to achieve SSB SCM signalling with a smaller frequency guardband.

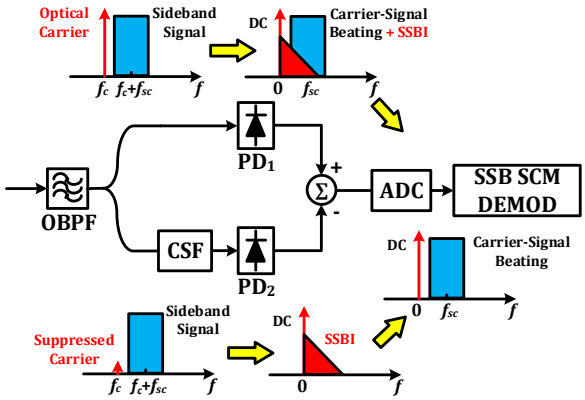

Fig. 3.13: Working principle of the BICBR technique. CSF: carrier suppression filter. SSB SCM DEMOD: single-sideband subcarrier modulation signal demodulation.

The key advantage of this technique is that, in the ideal case, in which the CSF can fully remove the optical carrier and at the same time does not affect the SSB signal, the signal-signal beating products can be fully constructed in the lower branch and the unwanted SSBI terms can be fully mitigated by subtraction. Moreover, this BICBR cancels out not only the SSBI, but also part of other unwanted beating interferences, *e.g.*, SABI and AABI and can therefore provide superior linearization performance. However, this scheme has the drawback of the significantly increased complexity of the receiver optical hardware, requiring a balanced receiver which includes two single-ended photodiodes and a very narrow optical filter (<1 GHz) to suppress the optical carrier from the transmitted signal.

3.2.2 Digital Iterative SSBI Estimation and Cancellation

As an alternative to the complex optical linearization technique described above, digital linearization techniques have also been proposed and demonstrated. This subsection describes the digital iterative SSBI estimation and cancellation (E&C) schemes implemented either at the transmitter or at the receiver.

Transmitter-based Digital Iterative SSBI Estimation and Cancellation

The transmitter-based digital iterative SSBI E&C or digital iterative SSBI pre-distortion technique was proposed for virtual SSB (VSSB) OFDM [105, 106] and then applied to VSSB Nyquist-SCM [107]. The experimental results have shown receiver sensitivity improvements after applying such technique.

As shown in Fig. 3.14, the principle of this iterative pre-distortion technique can be described as follows: The transmitted signal is pre-distorted so that the received signal is as close as possible to the desired ideal signal, through the following digital processing steps within the transmitter. (a) After QAM mapping, the signal waveform is first stored in memory, and a sampled representation of an optical SSB SCM signal is generated. (b) The linear modulator and single-ended photodetector are digitally represented by applying a DC term and a square-law calculation, and an approximation of the waveform of the detected signal including the unwanted SSBI is obtained. (c) The signal is demodulated to QAM symbols and an accurate calculation of the interference terms is carried out by comparing the detected signal with the ideal QAM symbols.

(d) The calculated interference is then subtracted from the stored waveform to obtain the newly updated signal. Then, the original signal in the memory is replaced with this updated signal; (e) This compensation process is repeated iteratively until the constellation of the received symbols converges. (f) Finally, the generated pre-distorted electrical signal is sent to the DACs.

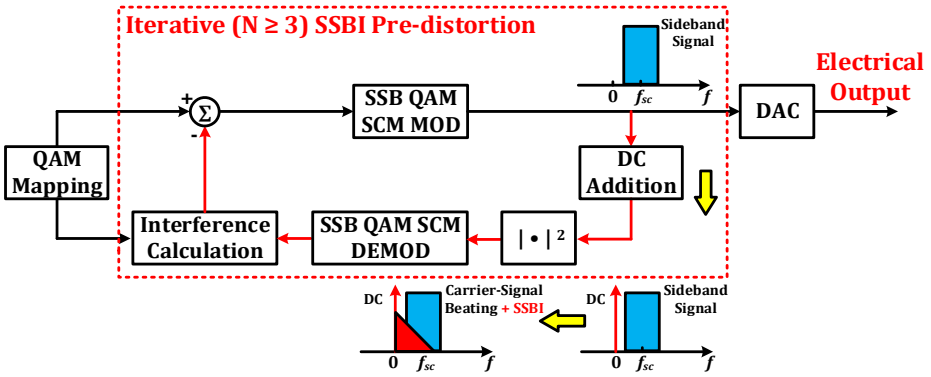

Fig. 3.14: DSP design of the literative SSBI predistortion technique. SSB SCM MOD&DEMOD: single-sideband subcarrier modulation signal demodulation and modulation.

This digital iterative SSBI pre-distortion technique can effectively compensate for SSBI and only requires a single-ended photodetector leading to a simpler receiver structure compared with the BICBR technique discussed in the above subsection. However, the use of iterative pre-distortion leads to increased PAPR and imperfect SSBI cancellation due to the introduction of extra unwanted beating products after square-law detection, which potentially impair the system performance. Furthermore, since this technique requires accurate CSPR estimation and the use of multiple (typically more than three) iterations to achieve saturated compensation performance, the digital hardware complexity at the transmitter is significantly increased.

Receiver-based Digital Iterative SSBI Estimation and Cancellation

A receiver-based digital iterative SSBI E&C technique has been proposed and investigated for VSSB OFDM DD systems [108, 109], and this technique has been refined and extended to the SSB Nyquist-SCM system in our work [110-112]. The principle of the technique is shown in Fig. 3.15.

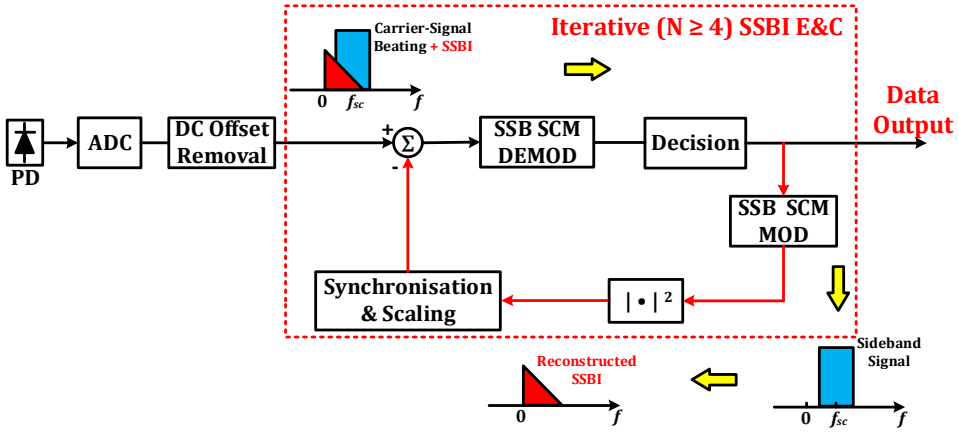

Fig. 3.15: DSP design of the receiver-based iterative SSBI estimation and cancellation technique. SSB SCM MOD&DEMOD: single-sideband subcarrier modulation signal demodulation and modulation.

The operation can be described as follows: (a) The detected signal waveform, which includes both the desired signal (CSBP) and the unwanted SSBI term, is stored in memory, and then SSB SCM demodulation and equalization stages are applied to the detected signal; (b) after making symbol decisions, a digital representation of the ideal SSB QAM SCM signal, with the received symbol sequence, is re-generated, and an approximation of the waveform of the signal-signal beat products is obtained by implementing the square-law detection process on this ideal re-generated SSB QAM SCM signal without the optical carrier; (c) after synchronization and amplitude scaling, the reconstructed signal-signal beating products' waveform is then subtracted from the stored received signal to partially eliminate the SSBI; (d) this compensation process is iteratively repeated until saturation of the compensation performance is reached. Note that, the scaling factor controls the compensation effectiveness of such technique, thus needs to be swept and set to an optimum value to minimize the BER. The compensation effectiveness is degraded if incorrect symbol decisions are made.

As for the digital SSBI pre-distortion scheme described above, the receiver-based digital iterative SSBI E&C technique only requires a single photodiode, and thus also has the advantage of lower optical hardware complexity compared with the above-mentioned BICBR technique. In addition, since the technique does not cause an increase in the PAPR or unwanted extra interfering beating products, it offers a potentially better compensation performance over the SSBI pre-distortion scheme. However, the drawback of this technique is that the digital hardware complexity of the receiver is high due to the requirement of multiple (typically more than four) iterations, *i.e.* multiple demodulation and modulation operations. Further technical details and performance assessments of this technique are presented in Chapter 4.

3.2.3 Receiver-based Digital Single-stage Linearization Filter

Since the iterative SSBI E&C scheme includes symbol decision-based SSBI reconstruction with multiple demodulation and modulation operations, its performance has a high dependency on the accuracy of symbol decision making and suffer from significantly increased DSP complexity. A receiver-based digital single-stage linearization filter was proposed for SSB-OFDM DD system [113] and has shown effective compensation performance with very simple digital hardware structure.

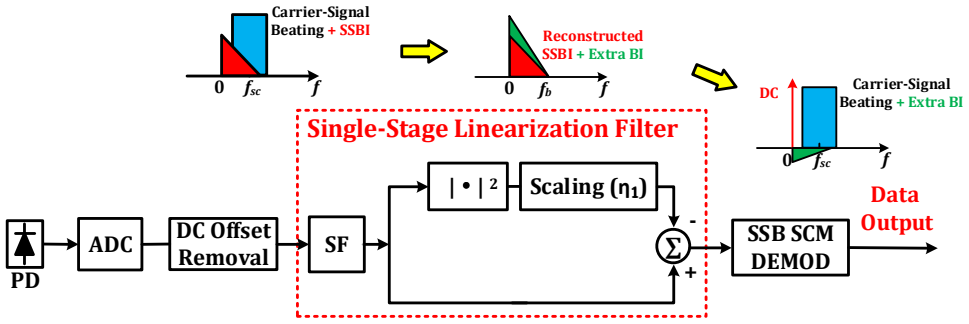

Fig. 3.16: DSP design of the receiver-based digital single-stage linearization filter. SSB SCM DEMOD: single-sideband subcarrier modulation signal demodulation. SF: sideband filter.

Fig. 3.16 shows the DSP design of the single-stage linearization filter. The detected DSB (real-valued) signal is passed through the single-stage linearization filter: a SSB signal is first generated

using a sideband filter (SF), which is performed by an ideal digital Hilbert transform filter (details can be found in Chapter 2), and an approximation of the signal-signal beating products is calculated based on the filtered SSB signal, which is then subtracted from the original SSB signal to partially compensate the SSBI. Note that, this technique aims to replicate the process of generating signal-signal beating products from the transmitted SSB signal. The use of the SF avoids unwanted beating products which would otherwise be generated by the negative frequency part of the detected DSB signal spectrum. DC offset removal is performed to ensure the re-generation of only the signal-signal beating products. The amplitude scaling factor (η_1) controls the effectiveness of the single-stage linearization filter and is inversely proportional to the utilized CSPR value, hence needs to be optimally adjusted to maximise its effectiveness.

The advantage of this scheme is its use of a very simple DSP structure. Moreover, unlike the above-mentioned iterative SSBI E&C schemes, such scheme avoids the symbol decision-based compensation process. However, as the calculation of the signal-signal beating products is based on the received distorted signal, this technique itself introduces extra unwanted beating interferences (shown as the dark green spectrum in Fig. 3.16), thus limiting the compensation gain. Additionally, in the real-time digital circuit implementation, the performance of this technique has a strong dependence on the SF filter design, hence the performance may be degraded due to limited symbol length utilized. Further technical details and performance evaluations of such scheme can be found in Chapter 5.

3.2.4 Receiver-based Digital Iterative Linearization Filter

As mentioned above, the compensation performance of the single-stage linearization filter is limited by its introduced extra beating interference. To achieve further improved compensation performance, the single-stage linearization filter can be iteratively repeated, a technique which has been demonstrated for SSB Nyquist-SCM signalling in [114, 115].

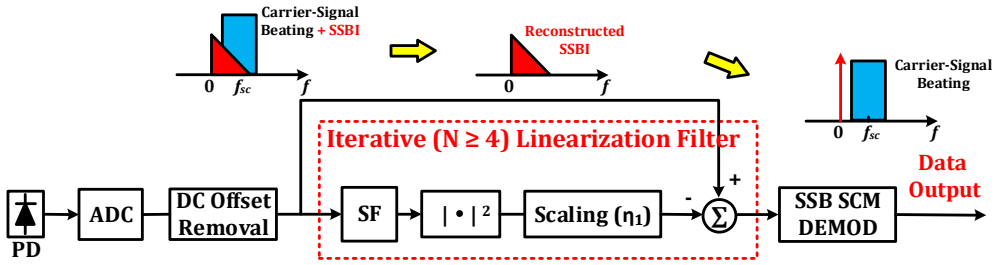

Fig. 3.17: DSP design of the receiver-based digital iterative linearization filter. SSB SCM DEMOD: single-sideband subcarrier modulation signal demodulation. SF: sideband filter.

Fig. 3.17 shows the DSP design with the iterative linearization filter, and its working principle is described as follows: the waveform of the detected signal is first stored in memory, and the signal-signal beating products are calculated based on the filtered SSB signal, which are then subtracted from the stored signal waveform in the memory, to mitigate the SSBI. It can be seen that if no iterative update is carried out, this technique is the same as the process in the single-stage linearization filter, as described in the above subsection. Since the signal-signal beating products are approximated by performing the square-law calculation on the filtered detected signal, inaccuracies occur due to the inclusion of the SSBI term in the detected signal. However, this

process can be repeated multiple times in order to reduce the inaccuracies and achieve the maximum compensation gain.

This iterative linearization filtering technique improves the performance of the single-stage linearization filter by using the stored received signal waveform and iteratively repeating the SSBI reconstruction process until the performance improvement saturates. Due to the multiple (four times or more) iterations performed, its DSP complexity is significantly increased, however. It should be mentioned that the sideband filter has to stay inside of the iterative process to keep the input signal of each iteration being single sideband, and the value of the optimum scaling factor is fixed once it is optimally adjusted in the first iteration.

3.2.5 Receiver-based Digital Two-stage Linearization Filter

An alternative method to further improve the compensation performance of the single-stage linearization filter is to utilize a two-stage linearization filter, which has been proposed and demonstrated for SSB Nyquist-SCM system in our latest works [116, 117].

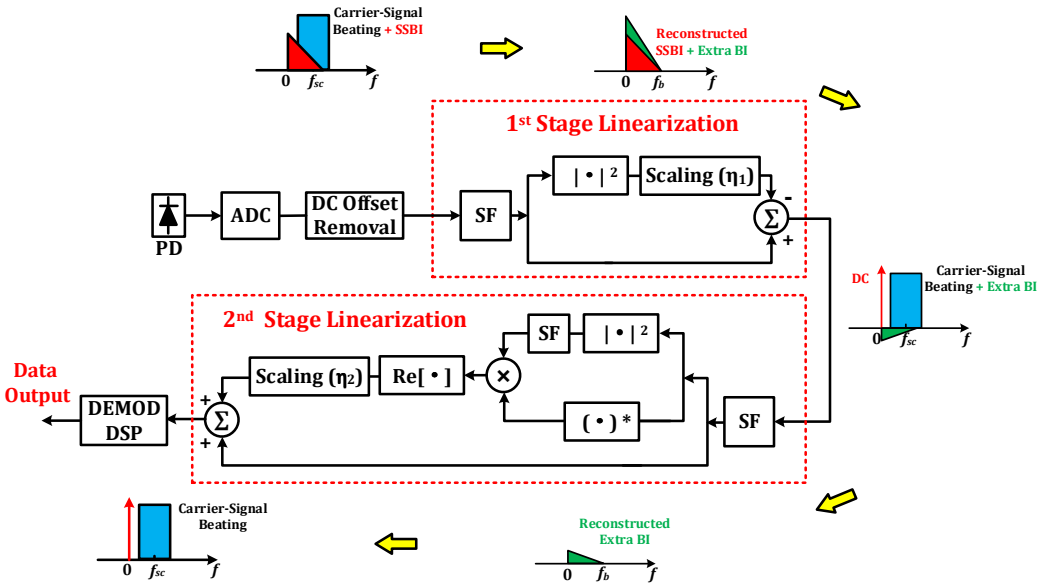

Fig. 3.18: DSP design of the receiver-based digital two-stage linearization filter. SSB SCM DEMOD: single-sideband subcarrier modulation signal demodulation. SF: sideband filter.

The DSP design with the two-stage linearization filter is shown in Fig. 3.18. There are two linearization stages in such scheme, the first linearization stage is the same as the single-stage linearization filter discussed in the subsection 3.2.3. With the optimum adjustments of the two scaling factors (η_1 and η_2), the SSBI penalty and majority of the unwanted beating interference (mainly the signal-SSBI beating terms) introduced by the first linearization stage can be removed in each of the two linearization stages respectively. Note that, the utilization of sideband filters in both of the linearization stages suppresses the unwanted beating products generated at negative frequencies and thus improves the accuracy of beating interference reconstruction.

Compared with the single-stage linearization filter, such scheme offers enhanced compensation performance. Since the two-stage linearization filter avoids the utilization of multiple iterations such as the iterative SSBI E&C and iterative linearization filter mentioned in subsections 3.2.2 and

3.2.4, although the digital hardware complexity is more than twice of the single-stage linearization filter, it is still relatively lower than the other approaches. Therefore, the two-stage linearization filter can be a good tradeoff between the compensation effectiveness and the digital hardware complexity. Further technical details and experimental assessments of this technique can be found in Chapter 6.

3.2.6 Kramers-Kronig (KK) Receiver

It can be seen that the above-mentioned digital linearization approaches (SSBI E&C, single-stage linearization filter, iterative linearization filter and two-stage linearization filter) treat the SSBI terms as a perturbation to the signal. The system compensation works by calculating these perturbations and subtracting them from the detected signal. In contrast, a recently proposed technique, termed the Kramer-Kronig (KK) scheme, reconstructs the optical phase of the transmitted signal from the detected amplitude waveform, making use of the assumption that it is an ideal single-sideband and minimum phase signal. The KK scheme digitally reconstructs the transmitted optical SSB signal before the detector, and is therefore immune to the SSBI penalty. It was first proposed and assessed by simulations in [118, 119] and was further demonstrated by experiments for SSB Nyquist-SCM and SSB OFDM systems in [120, 121].

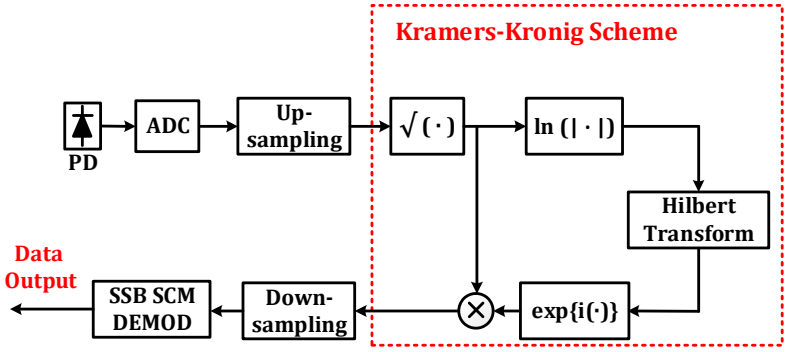

Fig. 3.19: DSP design of the receiver-based Kramers-Kronig scheme. SSB SCM DEMOD: single-sideband subcarrier modulation signal demodulation. SF: sideband filter.

The DSP design of the receiver-based KK scheme is shown in Fig. 3.19. The minimum phase condition ensures that the phase of the signal can be uniquely extracted from its intensity [131]. We consider a complex valued signal $s(n)$, whose spectrum is symmetric and has a frequency range between $-B/2$ and $B/2$. The transmitted optical single sideband signal, $h(n)$ can be written as:

$$h(n) = A + s(n)\exp(-i\pi Bn) \tag{3.1}$$

where n is the discrete time index, A is a positive bias (optical carrier) value that serves to ensure non-negative values of $h(n)$. In order to fulfil the condition of minimum phase, the optical carrier is required to have an amplitude larger than that of the sideband signal ($|A| > |s(n)|$). When $h(n)$ is a minimum phase signal, its phase $\varphi(n)$ and absolute value $|h(n)|$ are uniquely related by the Hilbert transform:

$$\varphi(n) = \frac{1}{\pi} p.v. \int_{-\infty}^{\infty} dn' \frac{log[|h(n')|]}{n - n'} \tag{3.2}$$

where *p.v.* is the principle value. Eq. 3.2 is termed the Kramers-Kronig relation [122]. By utilizing the Kramers-Kronig relation, the phase of the transmitted signal is linked to its intensity. Hence, following direct detection of the total field intensity, the complex-valued electric field of the SSB signal is extracted from the measured photocurrent. Note that, due to the high bandwidth resulting from the square-root and logarithm ($ln(|h(n)|)$) operations, a relatively higher oversampling rate (typically 4 samples per symbol or more) needs to be utilized in this part of the DSP. With sufficiently high oversampling rate, the KK scheme provides superior linearization effectiveness over the other currently demonstrated beating interference mitigation schemes. Technical details and performance evaluations of the KK scheme can be found in Chapter 7.

3.2.7 Other Linearization Techniques

A number of other optical or digital SSBI mitigation techniques have been proposed to improve the system performance and achieve increased ISD [123-130]. One approach is to modulate the envelope of the optical signal instead of the field, a technique known as compatible SSB (cSSB) OFDM [123]. However, significant degradation in the OSNR performance can be observed when implementing this technique due to the high required optical carrier power to avoid clipping at the receiver thus preventing the system from operating at the optimum CSPR value. Another SSBI cancellation technique is to utilize an interleaver combined with turbo coding, which requires approximately 30% overhead, thus introducing extra bandwidth redundancy [124-126]. Furthermore, nonlinear equalization by using a Volterra nonlinear filter have also been proposed [127, 128] but the computational complexity of using this technique is significantly increased.

References

[1] Alcatel-Lucent, "Bell labs metro network traffic growth: architecture impact study," Strategic White Paper (2013).

[2] Cisco, "Cisco visual networking index: forecast and methodology, 2014-2019," White Paper (2015).

[3] J.G. Proakis, Digital Communications. 5th ed. (McGraw-Hill Higher Education, 2007).

[4] S.S. Haykin, Digital Communication System. 4th ed. (John Wiley & Sons, 2001).

[5] S. Chandrasekhar, X. Liu, B. Zhu, and D.W. Peckham, "Transmission of a 1.2-Tb/s 24-carrier no-guard-interval coherent OFDM superchannel over 7200-km of ultra-large-area fiber," in European Conference and Exhibition on Optical Communication (ECOC 2009), paper 1, 2.

[6] J.-X. Cai, Y. Sun, H.G. Batshon, M. Mazurczyk, H. Zhang, D.G. Foursa, and A.N. Pilipetskii , "54 Tb/s transmission over 9,150 km with optimized hybrid Raman-EDFA amplification and coded modulation," in European Conference and Exhibition on Optical Communication (ECOC 2014), paper PD.3.3.

[7] J. Zhang, J. Yu, Y. Fang, and N. Chi, "High speed all optical Nyquist signal generation and full-band coherent detection," Scientific Report 4, 6156 (2014).

[8] S. Beppu, M. Yoshida, K. Kasai, and M. Nakazawa, "2048 QAM (66 Gbit/s) single-carrier coherent optical transmission over 150 km with a potential SE of 15.3 bit/s/Hz," in Optical Fiber Communication Conference, OSA Technical Digest Series (CD) (Optical Society of America, 2014), paper W1A.6.

[9] T.J. Xia, S. Gringeri, and M. Tomizawa, "High- capacity optical transport networks," IEEE Commun. Mag. 50(11), 170-178 (2012).

[10] ADVA, Efficient 100G Transport (2014).

[11] K. Szczerba, P. Westbergh, J. Karout, J. Gustavsson, Å. Haglund, M. Karlsson, P. Andrekson, E. Agrell, and A. Larsson "30 Gbps 4-PAM transmission over 200 m of MMF using an 850 nm VCSEL," Opt. Express, 19(26), B203-B208 (2011).

[12] K. Szczerba, M. Karlsson, P. Andrekson, A. Larsson, and E. Agrell, "35.2 Gbps 8-PAM transmission over 100 m of MMF using an 850 nm VCSEL," in European Conference and Exhibition on Optical Communication (ECOC 2013), paper Th.F.1.

[13] K. Zhong, X. Zhou, Y. Gao, W. Chen, J. Man, L. Zeng, A.P.T. Lau, and C. Lu, "140Gbit/s 20km Transmission of PAM-4 Signal at 1.3 μm for Short Reach Communications," IEEE Photon. Technol. Lett., 27(16), 1757-1760 (2015).

[14] K. Szczerba, P. Westbergh, M. Karlsson, P.A. Andrekson, and A. Larsson, "70 Gbps 4-PAM and 56 Gbps 8-PAM Using an 850 nm VCSEL," J. Lightw. Technol., 33(7), 1395-1401 (2015).

[15] P.J. Winzer and R.J. Essiambre, "Advanced modulation formats for high-capacity optical transport networks," in J. Lightw. Technol. 24(12), 4711-4728 (2006).

[16] G. Charlet, "Progress in optical modulation formats for high-bit rate WDM transmissions," IEEE J. Sel. Topics Quantum Electron., 12(4), 469-483 (2006).

[17] E. Ip and J.M. Kahn, "Power spectra of return-to-zero optical signals," J. Lightw. Technol., 24(3), 1610-1618 (2006).

[18] D. Breuer and K. Petermann, "Comparison of NRZ- and RZ-modulation format for 40 Gb/s TDM standard-fiber systems," IEEE Photon. Technol. Lett., 9(3), 398-400 (1997).

[19] M. Hayee and A. Willner, "NRZ versus RZ in 10-40 Gb.s dispersion-managed WDM transmission systems," IEEE Photon. Technol. Lett., 11(8), 991-993 (1999).

[20] Y. Frignac, S. Bigo, and J.-P. Hamaide, "NRZ versus RZ format in N × 40 Gbit/s WDM terrestrial transmission systems with high spectral efficiency of 0.4 bit/(s·Hz)," in European Conference and Exhibition on Optical Communication (ECOC 2001), paper 524-525.

[21] G. Raybon, P.J. Winzer, and C.R. Doerr, "1-Tb/s (10 × 107 Gb/s) electrically multiplexed optical signal generation and WDM transmission," J. Lightw. Technol., 25(1), 233-238 (2007).

[22] G. Vareille, B. Julien, F. Pitel, and J.-F. Marcerou, "3.65 Tbit/s (365 ×,11.6 Gb/s) transmission experiment over 6850 km using 22.2 GHz channel spacing in NRZ format" in European Conference and Exhibition on Optical Communication (ECOC 2001), paper 14-15.

[23] S. Shimotsu, S. Oikawa, T. Saitou, N. Mitsugi, K. Kubodera, T. Kawanishi, and M. Izutsu, "Single side-band modulation performance of a $Linbo_3$ integrated modulator consisting of four-phase modulator waveguides," IEEE Photon. Technol. Lett., 13(4), 364-366 (2001).

[24] P. Watts, V. Mikhailov, M. Glick, P. Bayvel, and R. Killey, "Single sideband optical signal generation and chromatic dispersion compensation using digital filters," Electron. Lett. 40(15), 958-960 (2004).

[25] W. Idler, G. Charlet, R. Dischler, Y. Frignac, and S. Bigo, "0.8 bit/s/Hz of information spectral density by vestigial sideband filtering of 42.66 Gb/s NRZ," in European Conference and Exhibition on Optical Communication (ECOC 2002), paper 1-2.

[26] B. Bigo, Y. Frignac, G. Charlet, W. Idler, S. Borne, H. Gross, R. Dischler, W. Poehlmann, P. Tran, C. Simonneau et al., "10.2 Tbit/s (256 × 42.7 Gb/s PDM/WDM) transmission over 100 km Teralight fiber with 1.28 bit/Hz spectral efficiency," in Optical Fiber Communication Conference, OSA Technical Digest Series (CD) (Optical Society of America, 2001), paper PD25.

[27] S. L. Jansen, R. H. Derksen, C. Schubert, X. Zhou, M. Birk, C.-J. Weiske, M. Bohn, D. van de Borne, P.M. Krummrich, M. Moller et al., "107-Gb/s full-RTDM transmission over field installed fiber using vestigial sideband modulation," in Optical Fiber Communication Conference, OSA Technical Digest Series (CD) (Optical Society of America, 2007), paper OWE3.

[28] K. Schuh, E. Lach, B. Junginger, A. Klekamp, and G. Veith, "8 ×107 Gbit/s serial binary NRZ/VSB transmission over 480 km SSMF with 1 bit/s/Hz spectral efficiency and without optical equalizer" in European Conference and Exhibition on Optical Communication (ECOC 2007), paper Mo2.3.1.

[29] T. Tsuritani, A. Agata, I. Morita, K. Tanaka, and N. Edagawa, "Performance comparison between DSB and VSB signals in 20 Gbit/s-based ultra-long-haul WDM systems," in Optical Fiber Communication Conference, OSA Technical Digest Series (CD) (Optical Society of America, 2001), paper MM5.

[30] I. Morita, T. Tsuritani, N. Yoshikane, A. Agata, K. Imai, and N. Edagawa, "100% spectral-efficient 25 × 42.7 Gbit/s transmission using asymmetrically filtered CS-RZ signal and a novel crosstalk suppressor" in European Conference and Exhibition on Optical Communication (ECOC 2002), paper 1-2.

[31] A. Lender, "The duobinary technique for high-speed data transmission," Trans. Commun. Electron. 82(2), 214-218 (1963).

[32] K. Yonenaga, S. Kuwano, S. Norimatsu, and N. Shibata, "Optical duobinary transmission system with no receiver sensitivity degradation," in Electron. Lett. 31(4), 302-304 (1995).

[33] D. Penninckx, M. Chbat, L. Pierre, and J.-P. Thiery, "The phase-shaped binary transmission: A new technique to transmit far beyond the chromatic dispersion limit," IEEE Photon. Technol. Lett., 9(2), 259-261 (1997).

[34] J.B. Stark, J. Mazo, and R. Laroia, "Phased amplitude-shift signaling (pass) code: Increasing the spectral efficiency of DWDM transmission," in European Conference and Exhibition on Optical Communication (ECOC 1998), paper 373-374.

[35] C. Gosset, L. Dupont, A. Tan, A. Bezard, and E. Pincemin, "Experimental performance comparison of duobinary formats for 40 Gb/s long-haul transmission," in Optical Fiber Communication Conference, OSA Technical Digest Series (CD) (Optical Society of America, 2008), paper JThA55.

[36] D. Penninckx, L. Pierre, J.-P. Thiery, B. Clesca, M. Chbat, and J. Beylat, "Relation between spectrum bandwidth and the effects of chromatic dispersion in optical transmission," in Electron. Lett. 32(11), 1023-1024 (1996).

[37] E. Pincemin, C. Gosset, N. Boudrioua, A. Tan, D. Grot, and T. Guillossou "Experimental performance comparison of duobinary and PSBT modulation formats for long-hual 40 Gb/s transmission on G 0.652 fibre," Opt. Express, 20(27), 28171-28190 (2012).

[38] G. Charlet, J.-C. Antona, S. Lanne, and S. Bigo, "From 2,100 km to 2,700 km distance using phase-shaped binary transmission at 6.3 Tbit/s capacity," in Optical Fiber Communication Conference, OSA Technical Digest Series (CD) (Optical Society of America, 2003), paper 329-330.

[39] G. Charlet, S. Lanne, L. Pierre, C. Simonneau, P. Tran, H. Mardoyan, P. Brindel, M. Gorlier, J.-C. Antona, M. Molina et al., "Cost-optimized 6.3 Tbit/s-capacity terrestrial link over 17 × 100 km using phase-shaped binary transmission in a conventional all-EDFA SMF-based system," in Optical Fiber Communication Conference, OSA Technical Digest Series (CD) (Optical Society of America, 2003), paper PD25.P1.

[40] M. Chagnon, M. Osman, M. Poulin, C. Latrasse, J. Gagne, Y. Painchaud, C. Paguet, S. Lessard, and D. Plant, "Experimental study of 112 Gb/s short reach transmission employing PAM formats and SiP intensity modulator at 1.3 μm," Opt. Express, 22(17), 21018–21036 (2014).

[41] L.F. Suhr, J.J.V. Olmos, B. Mao, X. Xu, G.N. Liu, and I. T. Monroy, "112-Gbit/s × 4-lane duobinary-4-PAM for 400 G base," in European Conference and Exhibition on Optical Communication (ECOC 2014), paper Tu.4.3.2.

[42] K.P. Zhong, W. Chen, Q. Sui, J. Man, A.P.T. Lau, C. Lu, and L. Zeng, "Low cost 400 GE transceiver for 2 km optical interconnect using PAM4 and direct detection," in Asia Communications and Photonics Conference (ACP 2014), paper ATh4D.2.

[43] K.P. Zhong, W. Chen, Q. Sui, J. Man, A.P. Lau, C. Lu, and L. Zeng, "Experimental demonstration of 500 Gbit/s short reach transmission employing PAM4 signal and direct detection with 25 Gbps device," in Optical Fiber Communication Conference, OSA Technical Digest Series (CD) (Optical Society of America, 2015), paper TH3A.3.

[44] K.P. Zhong, X. Zhou, T. Gui, L. Tao, Y. Gao, W. Chen, J. Man, L. Zeng, A.P.T. Lau, and C. Lu, "Experimental study of PAM-4, CAP-16, and DMT for 100 Gb/s short reach optical transmission systems," Opt. Express, 23(2), 1176–1189 (2015).

[45] C. Caillaud, M.A.M. Adrover, F. Blache, F. Pommereau, J. Decobert, F. Jorge, P. Charbonnier, A. Konczykowska, J.-Y. Dupuy, H. Mardoyan, K. Mekkhazni, J.-F. Pare, M. Faugeron, F. Mallecot, and M. Achouche, "Low cost 112 Gb/s InP DFB-EAM for PAM-4 2 km transmission," in European Conference and Exhibition on Optical Communication (ECOC 2015), paper PDP.1.5.

[46] H.Yamazaki, M. Nagatani, S. Kanazawa, H. Nosaka, T. Hashimoto, A. Sano, and Y. Miyamoto, "160-Gbps Nyquist PAM4 transmitter using a digital-preprocessed analog-multiplexed DAC," in European Conference and Exhibition on Optical Communication (ECOC 2015), paper PDP.2.2.

[47] M.A. Mestre, H. Mardoyan, A. Konczykowska, R. Rios-Müller, J. Renaudier, F. Jorge, B. Duval, J-Y. Dupuy, A. Ghazisaeidi, P. Jennevé, and S. Bigo, "Direct Detection transceiver at 150-Gbit/s net data rate using PAM 8 for optical interconnects," in European Conference and Exhibition on Optical Communication (ECOC 2015), paper PDP.2.4.

[48] A. H. Gnauck and P. J. Winzer, "Optical phase-shift-keyed tranmission," J. Lightw. Technol., 23(1), 115-130 (2005).

[49] M. Rice, S. Tretter, and P. Mathys, "On differentially encoded M-sequence," IEEE Trans. Commun. 49(3), 421-424 (2001).

[50] P. A. Humblet and M. Azizoglu, "On the bit error rate of lightwave systems with optical amplifiers," in J. Lightw. Technol. 9(11), 1576-1582 (1991).

[51] J.-X. Cai, D. Foursa, L. Lu, C. Davidson, Y. Cai, W. Patterson, A. Lucero, B. Bakhshi, G. Mohs, P. Corbett et al., "RZ-DPSK field trial over 13 100 km of installed non-slope-matched submarine fibers," J. Lightw. Technol., 23(1), 95-103 (2005).

[52] J.-X. Cai, A. Turukhin, B. Anderson, W. Patterson, G. Berkowitz, J. Figueiredo, W. Kellner, M. Mazurczyk, T. Marino, F. Valvo et al., "40G field trial with 0.8 bit/s/Hz spectral efficiency over 6,550 km of installed undersea cable," in Optical Fiber Communication Conference, OSA Technical Digest Series (CD) (Optical Society of America, 2011), paper NThB6.

[53] W. Idler, A. Klekamp and A. Konczykowska, "System performance and tolerances of 43Gb/s ASK and DPSK modulation formats," in European Conference and Exhibition on Optical Communication (ECOC 2003), paper PDP.2.2.

[54] R. Dischler, A. Klekamp, J.A. Lazaro Villa, and W. Idler, "Experimental comparison of nonlinear threshold and optimum pre-dispersion of 43 Gb/s ASK and DPSK formats," in Optical Fiber Communication Conference, OSA Technical Digest Series (CD) (Optical Society of America, 2004), paper NThB6.

[55] R. Griffin and A. Carter, "Optical differential quadrature phase-shift key (ODQPSK) for high capacity optical transmission," in Optical Fiber Communication Conference, OSA Technical Digest Series (CD) (Optical Society of America, 2002), paper 367-368.

[56] A. Gnauck, P. Winzer, S. Chanrasekhar, and C. Dorrer, "Spectrally efficient (0.8 b/s/Hz) 1-Tb/s (25 × 42.7 Gb/s) RZ-DQPSK transmission over 28 100-km SSMF spans with 7 optical add/drops," in European Conference and Exhibition on Optical Communication (ECOC 2004), paper 40-41.

[57] G. Charlet, P. Tran, H. Mardoyan, M. Lefrancois, T. Fauconnier, F. Jorge, and S. Bigo, "151 × 43 Gb/s transmission over 4080 km based on return-to-zero-differential quadrature phase-shift keying," in European Conference and Exhibition on Optical Communication (ECOC 2005), paper 5-6.

[58] D. van den Borne, S.L. Jansen, G.-D. Khoe, H. de Waardt, and E. Gottwald, "Line optimization in long-haul transmission systems with 42.8-Gbit/s RZ-DQPSK modulation," in Optical Fiber Communication Conference, OSA Technical Digest Series (CD) (Optical Society of America, 2006), paper OFD2.

[59] T. Tokle, C. Davidson, M. Nissov, J.-X. Cai, D. Foursa, and A. Pilipetskii, "6500 km transmission of RZ-DQPSK WDM signals," Electron. Lett. 40(7), 444-445 (2004).

[60] K. Ishida, D.-S. Ly-Gagnon, K. Shimizu, T. Mizuochi, K. Motoshima, and K. Kikuchi, "Transmission of 20 × 20 Gb/s RZ-DQPSK signals over 5090 km with 0.53 b/s/Hz spectral efficiency," in Optical Fiber Communication Conference, OSA Technical Digest Series (CD) (Optical Society of America, 2004), paper FM2.

[61] S. Susskind and E.A. de Souza, "40 Gb/s RZ DQPSK transmission with SPM and ASE suppression by dispersion management," in International Microwave and Optoelectronics Conference (IMOC 2009), paper 106-109.

[62] N. Yoshikane and I. Morita, "1.14 b/s/Hz spectrally efficient 50 × 85.4-Gb/s transmission over 300 km using copolarized RZ-DQPSK signals," J. Lightw. Technol., 23(1), 108-114 (2005).

[63] X. Zhou, J. Yu, M. Du, and G. Zhang, "2 Tb/s (20 × 107 Gb/s) RZ-DQPSK straight-line transmission over 1005 km of standard single mode fiber (SSMF) without Raman amplification," in Optical Fiber Communication Conference, OSA Technical Digest Series (CD) (Optical Society of America, 2008), paper OMQ3.

[64] N. Kikuchi and S. Sasaki, "Incoherent 40-Gbit/s 16QAM and 30-Gbit/s staggered 8APSK (amplitude- and phase-shift keying) signaling with digital phase pre-integration technique," in 2008 IEEE/LEOS Summer Topical Meetings, paper 251-252.

[65] N. Kikuchi and S. Sasaki, "Highly sensitive optical multilevel transmission of arbitrary quadrature-amplitude modulation (QAM) signals with direct detection," J. Lightw. Technol., 28(1), 123-130 (2010).

[66] A.J. Lowery, L.B. Du, and J. Armstrong, "Performance of optical OFDM in ultralong-haul WDM lightwave systems," J. Lightw. Technol., 25(1), 131-138 (2007).

[67] A.O. Wiberg, B.-E. Olsson, and P.A. Andrekson, "Single cycle subcarrier modulation," in Optical Fiber Communication Conference, OSA Technical Digest Series (CD) (Optical Society of America, 2009), paper OTuE.1.

[68] J.C. Cartledge and A.S. Karar, "100 Gb/s intensity modulation and direct detection," J. Lightw. Technol., 32(16), 2809-2814 (2014).

[69] B. Saltzberg, "Performance of an efficient parallel data transmission system," IEEE Trans. Commun., 15(6), 805-811 (1967).

[70] J. Armstrong and B.J. Schmidt, "Comparison of asymmetrically clipped optical OFDM and DC-biased optical OFDM in AWGN," IEEE Commun. Lett., 12(5), 343-345 (2008).

[71] A.J. Lowery, "Improving sensitivity and spectral efficiency in direct-detection optical OFDM systems," in Optical Fiber Communication Conference, OSA Technical Digest Series (CD) (Optical Society of America, 2008), paper OMM4.

[72] A.J. Lowery and L.B. Du, "Optical orthogonal division multiplexing for long haul optical communications: A review of the first five years," Opt. Fiber Technol., 17(5), 421-438 (2011).

[73] J. Armstrong, "OFDM for optical communications," J. Lightw. Technol., 27(3), 189-204 (2009).

[74] X. Zheng, J.L, Wei, and J.M. Tang, "Transmission performance of adaptively modulated optical OFDM modems using subcarrier modulation over SMF IMDD links for access and metropolitan area networks," Opt. Express, 15(25), 20427-20440 (2008).

[75] J.M. Tang, P.M. Lane, and K.A. Shore, "30 Gb/s transmission over 40 km directly modulated DFB laser-based SMF links without optical amplification and dispersion compensation for VSR and metro applications" in Optical Fiber Communication Conference, OSA Technical Digest Series (CD) (Optical Society of America, 2006), paper JThB8.

[76] E. Giacoumidis, I. Tomkos, and J.M. Tang, "Adaptive modulation-induced reduction in filter concatenation impairment for optical OFDM metro/regional systems" in IEEE J. Opt. Commun. Netw, 3(7), 587-593 (2011).

[77] E. Giacoumidis, A. Tsokanos, C. Mouchos, G. Zardas, C. Alves, J.L. Wei, J.M. Tang, C. Gosset, Y. Jaouen,and I. Tomkos, "Extensive comparisons of optical fast-OFDM and conventional optical OFDM for local and access networks" in IEEE J. Opt. Commun. Netw, 4(10), 724-733 (2012).

[78] G. Meslener, "Chromatic dispersion induced distortion of modulated monochromatic light employing direct detection," IEEE J. Quantum Electron., 20(10), 1208-1216 (1984).

[79] D.J. Barros and J.M. Kahn, "Comparison of orthogonal frequency-division multiplexing and on-off keying in amplified direct-detection single-mode fiber systems," J. Lightw. Technol., 28(12), 1811-1820 (2010).

[80] J. Park, W. Sorin, and K. Lau, "Elimination of the fibre chromatic dispersion penalty on 1550 nm millimetre-wave optical transmission," Electron Lett., 33(6), 512-513 (1997).

[81] J. Yu, M.-F. Huang, Z. Jia, T. Wang, and G.-K. Chang, "A novel scheme to generate single-sideband millimter-wave signals by using low-frequency local oscillator signal," IEEE Photon. Technol. Lett., 20(7), 478-480 (2008).

[82] Z. Tang, S. Pan, and J. Yao, "A high resolution optical vector network analyzer based on a wideband and wavelength-tunable optical single-sideband modulator," Opt. Express, 20(6), 6555-6560 (2012).

[83] G. Smith, D. Novak, and Z. Ahmed, "Novel technique for generation of optical SSB with carrier using a single MZM to overcome fiber chromatic dispersion," in 1996 International Topical Meetings on Microwave Photonics, paper 5-8.

[84] B.J. Schmidt, A.J. Lowery, and J. Armstrong, "Experimental demonstrations of electronic dispersion compensation for long-haul transmission using direct-detection optical OFDM," J. Lightw. Technol., 26(1), 196-203 (2008).

[85] A.J. Lowery, and J. Armstrong, "Orthogonal-frequency-division multiplexing for dispersion compensation of long-haul optical systems," Opt. Express, 14(6), 2079–2084 (2006).

[86] D. Qian, J. Yu, and G.-K. Chang, "8 × 11.5-Gb/s OFDM transmission over 1000 km SSMF using conventional DFB lasers and direct-detection," in Optical Fiber Communication Conference, OSA Technical Digest Series (CD) (Optical Society of America, 2008), paper OMM3.

[87] S.-H. Fan, J. Yu, and G.-K. Chang, "Optical OFDM scheme using uniform power transmission to mitigate peak-to-average power effect over 1040 km single-mode fiber," IEEE J. Opt. Commun. Netw., 2(9), 711–715 (2010).

[88] B.J. Schmidt, A.J. Lowery, and J. Armstrong, "Experimental demonstration of 20 Gb/s direct-detection optical OFDM and 12 Gbit/s with a colorless transmitter," in Optical Fiber Communication Conference, OSA Technical Digest Series (CD) (Optical Society of America, 2007), paper OMI3.

[89] L. Mehedy, M. Bakaul, and A. Nirmalathas, "Single-channel directly detected optical-OFDM towards higher spectral efficiency and simplicity in 100 Gb/s Ethernet and beyond," IEEE J. Opt. Commun. Netw., 3(5), 426–434 (2011).

[90] J.R. Barry, Wireless Infrared Communications. 2nd ed. (Kluwer Academic Publishers, 1994).

[91] J. Kahn and J. Barry, "Wirless infrared communications," IEEE Proc., Invited Paper, 85(2), 265-298 (1997).

[92] S. Hranilovic, Wireless Optical Communications Systems. 4th ed. (Springer, 2005).

[93] M.S. Erkılınç, S. Pachnicke, H. Griesser, B.C. Thomsen, P. Bayvel, and R.I. Killey, "Performance comparison of single sideband direct-detection Nyquist-subcarrier modulation and OFDM," J. Lightw. Technol. 33(10), 2038-2046 (2015).

[94] A.O. Wiberg, B.-E. Olsson, and P.A. Andrekson, "Single cycle subcarrier modulation," in Optical Fiber Communication Conference, OSA Technical Digest Series (CD) (Optical Society of America, 2009), paper OTuE1.

[95] B.-E. Olsson, and M. Sköld, "QPSK transmitter based on optical amplitude modulation of electrically generated QPSK signal," in Asia Communications and Photonics Conference (ACP 2008), paper SaA3.

[96] B.-E. Olsson, and A. Apling, "Electron-optical subcarrier modulation transmitter for 100 GbE DWDM transport," in Asia Communications and Photonics Conference (ACP 2008), paper SaF3.

[97] T.-T. Pham, R. Rodes, J.B. Jensen, C.J. Chang-Hasnain, and I.T. Monroy, "Sub-cycle QAM modulation for VCSEL-based optical fiber links," Opt. Express, 21(2), 1830–1839 (2013).

[98] A.S. Karar and J.C. Cartledge, "Generation and detection of a 56 Gb/s signal using a DML and half-cycle 16-QAM Nyquist-SCM," IEEE Photon. Technol. Lett., 25(8), 757-760 (2013).

[99] M.S. Erkılınç, S. Kilmurray, R. Maher, M. Paskov, R. Bouziane, S. Pachnicke, H. Griesser, B.C. Thomsen, P. Bayvel, and R.I. Killey, "Nyquist-shaped dispersion-precompensated subcarrier modulation with direct detection for spectrally-efficient WDM transmission," Opt. Express, 22(8), 9420-9431 (2014).

[100] M. S. Erkilinc, Z. Li, S. Pachnicke, H. Griesser, B. C. Thomsen, P. Bayvel, and R. I. Killey, "Spectrally-Efficient WDM Nyquist Pulse-Shaped 16-QAM Subcarrier Modulation Transmission with Direct Detection", J. Lightw. Technol., 33(15), 3147-3155 (2015).

[101] A.J. Lowery, "Amplified-spontaneous noise limit of optical OFDM lightwave systems," Opt. Express 16(2), 860-865 (2008).

[102] W.R. Peng, I. Morita, and H. Tanaka, "Enabling high capacity direct-detection optical OFDM transmissions using beat interference cancellation receiver," in European Conference and Exhibition on Optical Communication (ECOC 2010), paper Tu.4.A.2.

[103] S.A. Nezamalhosseini, L.R. Chen, Q. Zhuge, M. Malekiha, F. Marvasti, and D.V. Plant, "Theoretical and experimental investigation of direct detection optical OFDM transmission using beat interference cancellation receiver," Opt. Express, 21(13), 15237-15246 (2013).

[104] J. Ma, “Simple signal-to-signal beat interference cancellation receiver based on balanced detection for a single-sideband optical OFDM signal with a reduced guard band,” Opt. Letters, 38(21), 4335-4338 (2013).

[105] C. Sánchez, B. Ortega, and J. Capmany, “System performance enhancement with pre-distorted OOFDM signal waveforms in DM/DD systems,” Opt. Express 22(6), 7269-7283 (2014).

[106] C. Ju, X. Chen, N. Liu, and L. Wang, “SSII cancellation in 40 Gbps VSB-IMDD OFDM system based on symbol pre-distortion,” in European Conference and Exhibition on Optical Communication (ECOC 2014), paper P.7.9.

[107] N. Liu, C. Ju, and X. Chen, “Nonlinear ISI cancellation in VSSB Nyquist-SCM system with symbol pre-distortion,” Opt. Commun. 338, 492–495 (2015).

[108] W. Peng, X. Wu, K. Feng, V.R. Arbab, B. Shamee, J. Yang, L.C. Christen, A.E. Willner, and S. Chi, “Spectrally efficient direct-detected OFDM transmission employing an iterative estimation and cancellation technique,” Opt. Express 17(11), 9099-9111 (2009).

[109] H. Shi, P. Yang, C. Ju, X. Chen, J. Bei, and R. Hui, “SSBI cancellation based on time diversity reception in SSB-DD-OOFDM transmission systems,” in Conference on Lasers and Electro-optics (CLEO 2014), paper JTh2A.14.

[110] Z. Li, M. S. Erkılınç, S. Pachnicke, H. Griesser, B.C. Thomsen, P. Bayvel, and R.I. Killey, “Direct-detection 16-QAM Nyquist-shaped subcarrier modulation with SSBI mitigation,” in IEEE International Conference on Communications (ICC 2015), paper 5204-5209.

[111] Z. Li, M. S. Erkılınç, S. Pachnicke, H. Griesser, R. Bouziane, B.C. Thomsen, P. Bayvel, and R.I. Killey, “Signal-signal beat interference cancellation in spectrally-efficient WDM direct-detection Nyquist-pulse-shaped 16-QAM subcarrier modulation,” Opt. Express, 23(18), 23694-23709 (2015).

[112] Z. Li, M.S. Erkilinc, S. Pachnicke, H. Griesser, R. Bouziane, B.C. Thomsen, P. Bayvel, and R.I. Killey, "Performance limits of spectrally-efficient WDM direct-detection SSB Nyquist subcarrier modulation with signal-signal beat interference cancellation", in European Conference on Network and Optical Communications (NOC), 1-6, (2015).

[113] S. Randel, D. Pilori, S. Chandrasekhar, G. Raybon, and P. Winzer, “100-Gb/s discrete-multitone transmission over 80-km SSMF using single-sideband modulation with novel interference-cancellation scheme,” in European Conference and Exhibition on Optical Communication (OFC 2015), paper Mo.4.5.2.

[114] K. Zou, Y. Zhu, F. Zhang and Z. Chen, “Spectrally efficient terabit optical transmission with Nyquist 64-QAM half-cycle subcarrier modulation and direct-detection,” Opt. Lett. 41(12), 2767-2770 (2016).

[115] K. Zou, Y. Zhu, and F. Zhang, “800Gb/s (8×100Gb/s) Nyquist half-cycle single sideband modulation direct detection transmission over 320km SSMF at C-band,” J. Lightw. Technol., 35(10), 1900-1905 (2017).

[116] Z. Li, M. S. Erkilinc, R. Maher, L. Galdino, K. Shi, B. C. Thomsen, P. Bayvel, and R. I. Killey, "Two-stage linearization filter for direct-detection subcarrier modulation", IEEE Photon. Technol. Lett. 28(24), 2838-2841 (2016).

[117] Z. Li, M.S. Erkılınç, K. Shi, E. Sillekens, L. Galdino, B.C. Thomsen, P. Bayvel, and R.I. Killey, "112 Gb/s/λ WDM direct-detection Nyquist-SCM transmission at 3.15 (b/s)/Hz over 240 km SSMF enabled by novel beating interference compensation", in Optical Fiber Communication Conference, OSA Technical Digest Series (CD) (Optical Society of America, 2017), paper Tu3I.4.

[118] A. Mecozzi, C. Antonelli, and M. Shtaif, “Kramers-Kronig coherent receiver,” Optica, 3(11), 1220-1227 (2016).

[119] C. Antonelli, A. Mecozzi, and M. Shtaif, “Kramers-Kronig PAM transceiver,” in Optical Fiber Communication Conference, OSA Technical Digest Series (CD) (Optical Society of America, 2017), paper Tu3I.5 (2017).

[120] Z. Li, M.S. Erkılınç, K. Shi, E. Sillekens, L. Galdino, B.C. Thomsen, P. Bayvel, and R.I. Killey, “SSBI mitigation and Kramer-Kronig scheme in single-sideband direct-detection transmission with receiver-based electronic dispersion compensation,” J. Lightw. Technol., 35(10), 1887-1893 (2017).

[121] X. Chen, C. Antonelli, S. Chandrasekhar, G. Raybon, J. Sinsky, A. Mecozzi, M. Shtaif, and P. Winzer, "218-Gb/s single-wavelength, single-polarization, single-photodiode transmission over 125-km of standard single-mode fiber using Kramers-Kronig detection", in Optical Fiber Communication Conference, OSA Technical Digest Series (CD) (Optical Society of America, 2017), paper Th5B.6 (2017).

[122] H. Voelcker, “Demodulation of single-sideband signals via envelope detection,” IEEE Trans. Commun. Technol. 14, 22-30, (1966).

[123] M. Schuster, S. Randel, C.A. Bunge, S.C.J. Lee, F. Breyer, B. Spinnler, and K. Petermann, “Spectrally efficient compatible single-sideband modulation for OFDM transmission,” IEEE Photon. Technol. Lett., 20(9), 670-672 (2008).

[124] Z. Cao, J. Yu, W. Wang, L. Chen, and Z. Dong, “Direct-detection optical OFDM transmission system without frequency guard band,” IEEE Photon. Technol. Lett., 22(11), 736-738 (2010).

[125] F. Li, Z. Cao, J. Yu, X. Li, and L. Chen, “SSMI cancellation in direct-detection optical OFDM with novel half-cycled OFDM,” Opt. Express, 21(23), 28543-28549 (2013).

[126] Z. Cao, J. Yu, M. Xia, Q. Tang, Y. Gao, W. Wang and L. Chen, "Reduction of intersubcarrier interference and frequency-selective fading in OFDM-ROF systems", J. Lightw. Technol., 28(16), 2423-2429 (2015).

[127] C.Y. Wong, S. Zhang, L. Liu, T. Wang, Q. Zhang, Y. Fang, S. Deng, G. N. Liu, and X. Xu, "56 Gb/s direct detected single-sideband DMT transmission over 320-km SMF using silicon IQ modulator," in Optical Fiber Communication Conference, OSA Technical Digest Series (CD) (Optical Society of America, 2015), paper Th4A.3.

[128] L. Zhang, T. Zuo, Y. Mao, Q. Zhang, E. Zhou, G.N. Liu, and X. Xu. "Beyond 100-Gb/s transmission over 80-km SMF using direct-detection SSB-DMT at C-band." J. Lightw. Technol., 34(2), 723-729 (2016).

[129] Z. Li, M. S. Erkilinc, R. Bouziane, B. C. Thomsen, P. Bayvel, and R. I. Killey, "Simplifed DSP-based signal-signal beat interference mitigation technique for direct detection OFDM", J. Lightw. Technol., 34(3), 866-872 (2016).

[130] Z. Li, M. S. Erkilinc, R. Bouziane, R. Maher, L. Galdino, K. Shi, B. C. Thomsen, P. Bayvel, and R. I. Killey, "Simplifed DSP-based signal-signal beat interference mitigation for direct detection subcarrier modulation", in Optical Fiber Communication Conference, OSA Technical Digest Series (CD) (Optical Society of America, 2016), paper W1A.3, (2016).

[131] A. Mecozzi, “A necessary and sufficient condition for minimum phase and implications for phase retrieval,” (2016) available at http://arxiv.org/abs/1606.04861.

CHAPTER 4

ITERATIVE SIGNAL-SIGNAL BEAT INTERFERENCE ESIMATION AND CANCELLATION

This chapter focuses on the technical details and performance evaluation of the receiver-based digital iterative SSBI estimation and cancellation (E&C) technique. Section 4.1 presents a mathematical description of its principle of operation. The experimental test-bed for system evaluation, a dispersion pre-compensated 112 Gb/s per channel spectrally-efficient WDM SSB 16-QAM Nyquist-SCM direct detection system with transmission over straight-line multi-span uncompensated SSMF links of up to 240 km, is described in Section 4.2. Section 4.3 presents the obtained experimental results on its back-to-back and transmission performance. Section 4.4 summarises this work.

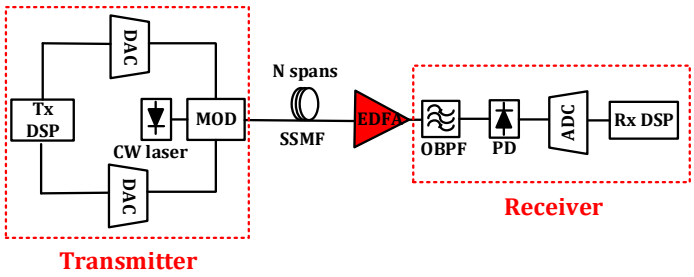

Fig. 4.1: Schematic diagram of the direct-detection system architecture. Tx & Rx DSP: Transmitter and receiver DSP, DAC: Digital-to-analogue converter, MOD: Optical modulator, SSMF: Standard single-mode fibre, EDFA: Erbium-doped fibre amplifier, OBPF: Optical band-pass filter, PD: Photodiode, ADC: Analog-to-digital converter.

The schematic diagram of the direct-detection system architecture is shown in Fig. 4.1. In the transmitter DSP, the SSB subcarrier modulated signal, $E_0(n)$, is generated by modulation DSP (MOD DSP), where n is the discrete time index. Afterwards, digital transmitter-based electronic dispersion compensation (EDC) [1] and pre-emphasis are implemented to mitigate the accumulated dispersion of the fibre and the low-pass filtering effects of the transceiver electronics. Following digital to analogue conversion, electrical to optical conversion is carried out, during which the real-valued optical carrier, $E_{carrier}(n)$, is added to the SSB SCM signal by optimally biasing the IQ-modulator. Following transmission over the fibre, direct detection and analogue to digital conversion, the detected DSB signal after direct current (DC) offset removal, $V_{DD}(n)$, can be written as [2]:

$$\begin{aligned} V_{DD}(n) &= K[|E_{carrier}(n) + E_0(n)|^2] \\ &= 2Re[E_{carrier}(n) \cdot E_0(n)] + |E_0(n)|^2 \end{aligned} \tag{4.1}$$

where $K[\cdot]$ signifies the DC offset removal operator, and $Re[x]$ represents the real part of x. In the RHS of this equation, the first term is the desired carrier signal beating product (CSBP), and the second term is the unwanted SSBI term. Following this, the linearization scheme is applied to the waveform of $V_{DD}(n)$.

4.1 Principle of Operation

The receiver-based iterative SSBI E&C technique can be utilized for SSB SCM (both OFDM and Nyquist-SCM) DD systems [3-5] and its working principle has been functionally described in Chapter 3, Section 3.2.2. This section presents a more detailed mathematical description of its operation.

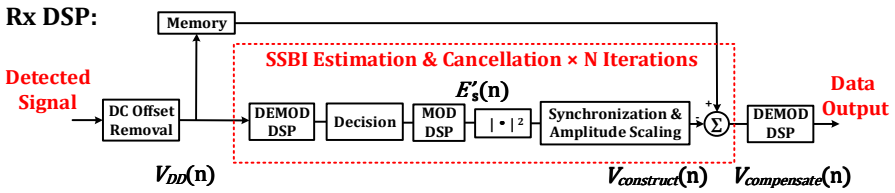

Fig. 4.2: Receiver DSP design with the receiver-based iterative SSBI E&C technique. MOD & DEMOD DSP: SSB SCM signal generation and demodulation.

The receiver DSP design with the receiver-based iterative SSBI E&C approach is shown in Fig. 4.2. Within the iterative E&C process at the receiver, after demodulation and symbol decision making, modulation DSP is used to generate a digital representation of the ideal SSB SCM signal (without the optical carrier), $E_0'(n)$, and an approximation of the waveform of the signal-signal beating products is obtained by implementing the square-law detection process:

$$V_{construct}(n) = |E_0'(n)|^2 \tag{4.2}$$

where $V_{construct}(n)$ is the reconstructed signal-signal beating products. This is then subtracted from the stored received signal waveform, $V_{DD}(n)$, partially cancelling the distortion due to signal-signal beating. Since the symbol decisions, and, consequently, $V_{construct}$ are not accurate for all the symbols, multiple iterations of the demodulation/modulation and SSBI cancellation are required until no further significant gains are observed. The amplitude scaling factor value utilized within such technique needs to be optimized to minimize the BER value and is fixed for all the iterations. When the performance improvement saturates (no further reduction of the BER is observed), $E_0'(n) \approx E_0(n)$, and the compensated signal, $V_{compensate}(n)$ is written as:

$$\begin{aligned} V_{compensate}(n) &= V_{DD}(n) - V_{construct}(n) \\ &\approx 2Re[E_{carrier}(n) \cdot E_0(n)] \end{aligned} \tag{4.3}$$

Therefore, the effect of SSBI is almost fully eliminated and the compensated signal only contains the desired CSBP. In contrast to the optical methods such as the beating interference cancellation balanced receiver [6-8], this approach only requires a single photodiode and avoids the need for a narrow optical bandpass filter, and consequently significantly reduces optical hardware complexity. At the same time, since all the digital compensation is carried out at the receiver, there is no introduction of unwanted extra beating interferences caused by SSBI pre-distortion [9-11], and this technique offers potentially improved compensation performance. However, the iterative SSBI E&C scheme typically requires more than four iterations to reach the maximum compensation gain, and it is impossible to reuse the same digital hardware iteratively for continuous transmitted data. The DSP complexity is directly related to the number of applied iterations and is therefore significantly increased. In addition, another limitation of this technique

is its dependency on the accuracy of the symbol decision making, thus noticeably degrading its compensation performance at lower OSNR levels.

4.2 Experimental Setup

As shown in Fig. 4.3, in order to assess the performance of DD transceivers with the above-mentioned receiver-based digital iterative SSBI E&C scheme and later the other digital linearization schemes in the following chapters, transmission experiments were carried out. The optical transmission test-bed consists of a 4 × 112 Gb/s SSB 16-QAM Nyquist-SCM transmitter, a straight-line standard single-mode fibre (SSMF) link and an optical bandpass filter (OBPF) followed by a single-ended photodiode-based direct-detection receiver to select and recover the channel of interest.

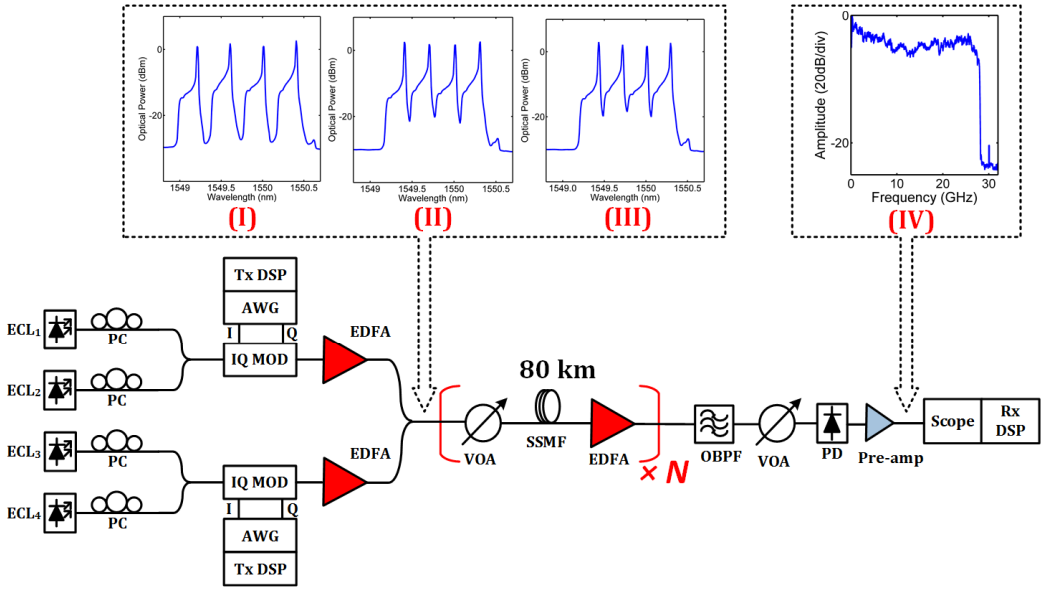

ECL: External cavity laser, AWG: Arbitrary-waveform generator, PC: Polarization controller, EDFA: Erbium-doped fiber amplifier, VOA: Variable optical attenuator, SSMF: Standard single mode fiber, OBPF: Optical Band-pass filter, PD: Photodiode.

Fig. 4.3: Experimental test-bed for 4 × 112 Gb/s WDM DD SSB 16-QAM Nyquist-SCM transmission with multiple-span transmission link structures. Insets: WDM signal spectra with (I) 50 GHz, (II) 37.5 GHz and (III) 35 GHz channel spacing; (IV) detected digital signal spectrum.

At the transmitter, two high-speed arbitrary-waveform generators (Keysight M8196A AWG) operating at a 92 GSa/s sampling rate and with 33 GHz 3-dB bandwidth were used to drive each IQ-modulator. The I- and Q- components of the SSB 16-QAM Nyquist-SCM signals were generated offline using MATLAB, and subsequently, uploaded to the AWGs to serve as the IQ-modulators' driving signals. The modulation DSP generating the SSB Nyquist-SCM signal is described in detail in Chapter 3. Four 2^{15} de Bruijn bit sequences were encoded onto a 16-QAM signal at 112 Gb/s (a symbol rate (f_s) of 28 GBd). A pair of root-raised cosine (RRC) filters with a roll-off factor (β) of 0.01 were utilized to carry out Nyquist pulse shaping on the I- and Q-components of the signal. Note that, to limit the size of the pulse shaping filter and matched filter, the roll-off factor was chosen to be 0.01 rather than 0. The filtered components were up-converted to a subcarrier frequency of 14.28 GHz ($f_{sc} = 0.51 \cdot f_s$) and added to each other to obtain a DSB Nyquist-SCM signal. The subcarrier frequency and β were selected such that the spectral guard-

band between the signal and the optical carrier was negligible. Following this, the lower frequency sideband was removed using a digital Hilbert transform sideband filter to generate a SSB Nyquist-SCM signal. Finally, to mitigate the accumulated chromatic dispersion, EDC was applied.

Four external cavity lasers (ECLs) with a linewidth of 100 kHz grouped around a wavelength of 1550 nm were utilized to generate odd and even channels. After passing through the IQ-modulators with the addition of optical carriers, the modulated odd and even channels were multiplexed to generate a 4×112 Gb/s WDM signal. The WDM channel spacing was set to three different values: 50 GHz, 37.5 GHz and 35 GHz, corresponding to gross optical ISDs of 2.2 (b/s)/Hz, 3.0 (b/s)/Hz and 3.2 (b/s)/Hz, respectively. The insets (I – III) of Fig. 4.3 show the optical WDM spectra, measured with an optical spectrum analyser (OSA) at a 0.01 nm resolution. The peak and asymmetric shapes of the optical spectra show the optical carriers and SSB signals, respectively. Note that, the optimization of the carrier-to-signal power ratio (CSPR) is crucial to achieve the optimum performance of SSB SCM DD systems. In the experiment, the optical carrier was generated by biasing the IQ-modulators above the null point and the biases were adjusted to achieve the desired CSPR values.

The transmission scenario investigated in the transmission experiments was a straight-line multiple span fibre link, consisting of spans of 80 km SSMF followed by erbium-doped fibre amplifiers (EDFAs) with a 5 dB noise figure.

At the receiver, an OBPF (Yenista Optics XTM50-Ultrafine) with an adjustable bandwidth was used to demultiplex the channel of interest and remove the out of band ASE noise. Note that the 3-dB bandwidth of the filter was set to 31 GHz for optimum system performance. The filtered signal was then detected using a single-ended PIN photodiode. The detected electrical signal was pre-amplified and digitized by a single ADC (Agilent DSA-X 96204Q) operating at 80 GSa/s. The received digital spectrum is plotted in the inset (IV) of Fig. 4.3. In the receiver DSP, following the DC offset removal, the digital linearization scheme was applied to eliminate the SSBI penalty. In the demodulation DSP (DEMOD DSP), frequency down-conversion and matched filtering with a RRC filter (β = 0.01) were carried out. For symbol synchronisation, a 5-tap constant modulus algorithm with least mean square (CMA-LMS) finite impulse response (FIR) filter was initially carried out for fast convergence before switching to decision-directed LMS mode. The adopted step size was set to 1.0×10^{-3} and a pilot tone was not used for synchronisation. Finally, the signal was demodulated and the BER and error-vector-magnitude (EVM) [13] were calculated, the former by error counting over 2^{18} bits.

4.3 Experimental Results

Both the optical back-to-back and WDM transmission evaluations were carried out with the experimental test-bed described in Section 4.2. System performance with different WDM channel spacing, transmitting over the multiple span SSMF link structures is presented in this section. Due to the similar performance of all WDM channels, one of the central channels (channel #2) was used as the channel under test in the case of WDM measurements here, and throughout the measurements described in this thesis. Four iterations were utilized in the iterative SSBI E&C approach to achieve the maximum compensation gain (no further BER reduction was observed after four iterations).

4.3.1 WDM Back-to-Back Performance Evaluation

Initially, the optical back-to-back performance was evaluated by performing ASE-noise loading at the receiver, with the experimental results plotted in Figs. 4.4 to 4.7.

To determine the minimum WDM channel spacing for the highest achievable optical ISD, initially, the channel spacing was varied from 33 to 50 GHz and the required OSNR at the hard-decision forward-error-correction (HD-FEC) BER threshold of 3.8×10^{-3} was monitored without carrying out any linearization (Fig. 4.4). In order to maintain the linear crosstalk penalty caused by neighbouring channel at less than 1 dB, the minimum WDM channel spacing was set to 35 GHz, yielding a gross ISD of 3.2 (b/s)/Hz.

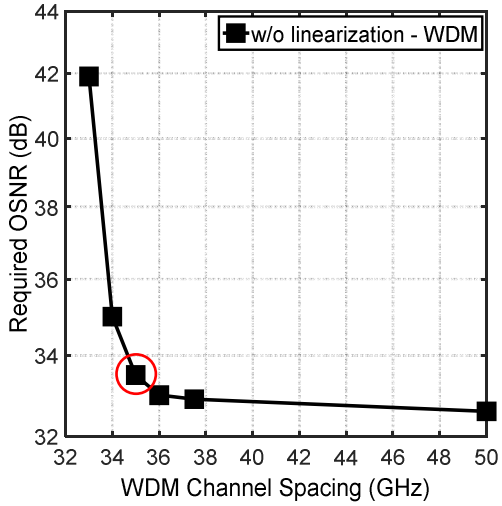

Fig. 4.4: Required OSNR at BER = 3.8×10^{-3} versus WDM channel spacing without digital receiver linearization scheme.

At a channel spacing of 35 GHz, to show the sensitivity of the systems to the applied CSPR value, BER versus CSPR without and with the iterative SSBI E&C approach at 31 dB OSNR was plotted in Fig. 4.5. A tradeoff between the system penalties can be observed, signals with lower CSPR values suffered more from high nonlinear distortion, contributed by the SSBI, while high CSPR led to a high required OSNR value duer to excessive optical carrier power, which is included in the numerator of the OSNR calculation. Due to the change in this tradeoff by using the iterative SSBI E&C scheme, the optimum CSPR value was reduced by approximately 3 dB with respect to the case without performing any linearization.

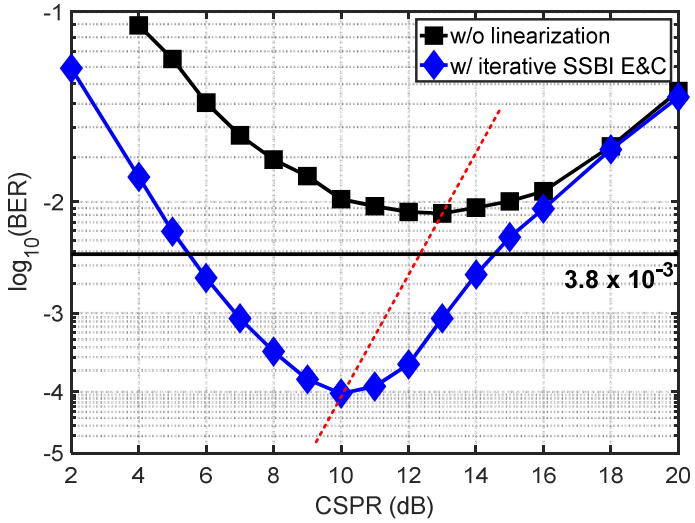

Fig. 4.5: BER versus CSPR without and with iterative SSBI E&C scheme at OSNR = 31 dB.

An assessment of the dependence of the optimum CSPR value on the OSNR level using the iterative SSBI E&C scheme was carried out by plotting the optimum CSPR as a function of OSNR, as shown in Fig. 4.6. The optimum performance was achieved by sweeping the CSPR value from 2 dB to 20 dB and setting it to the optimum value for each OSNR level, as described in Chapter 2, Section 2.2. The optimum CSPR value increased with the OSNR, as described in Chapter 2, Section 2.2. In comparison to the uncompensated case, the optimum CSPR values was reduced when the iterative SSBI E&C scheme was applied. Since the compensation effectiveness relies on the accuracy of symbol decision making, the reduction was 3 dB for high OSNRs ($\geq$ 27 dB), gradually reducing to 1.5 dB for low OSNRs ($\leq$ 21 dB).

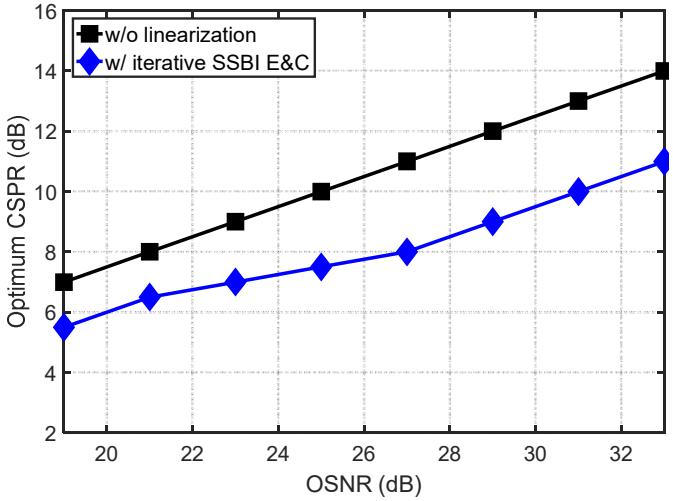

Fig. 4.6: Optimum CSPR versus OSNR without and with iterative SSBI E&C scheme in back-to-back operation.

The BER versus OSNR for the cases without and with the receiver-based iterative SSBI E&C scheme was plotted in Fig. 4.7, the optimum CSPR values at each OSNR were obtained from the results shown in Fig. 4.6. It can be seen that the required OSNR at the HD-FEC threshold (BER = 3.8×10^{-3}) was 33.5 dB without using linearization, reduced to 26.4 dB (7.1 dB gain) by applying the iterative SSBI E&C technique.

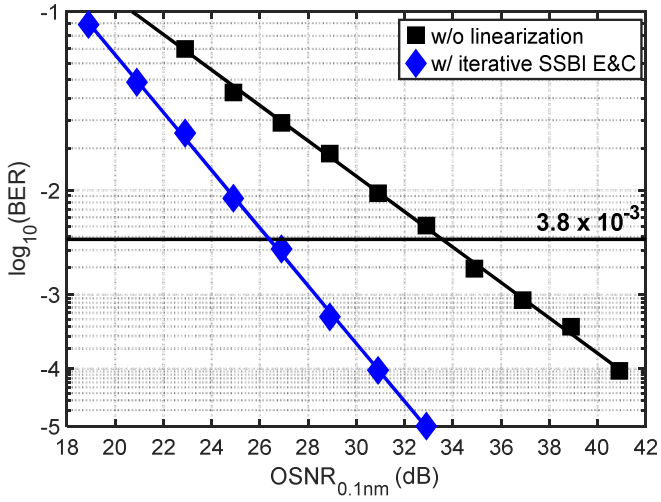

Fig. 4.7: BER versus OSNR at 35 GHz WDM channel spacing without and with receiver-based digital iterative SSBI E&C scheme.

4.3.2 WDM Transmission Performance Evaluation

In the transmission experiments using multiple span fibre link (Fig. 4.3), BER versus optical launch power per channel at 35 GHz channel spacing was plotted in Fig. 4.8, illustrating the transmission performance at different optical launch powers at 240 km WDM transmission. It can be seen that the optimum optical launch power was reduced by up to 1 dB after applying the iterative SSBI E&C scheme. The optimum CSPR remained the same for all the optical launch powers, at 12 dB without using linearization and 9 dB using the iterative scheme.

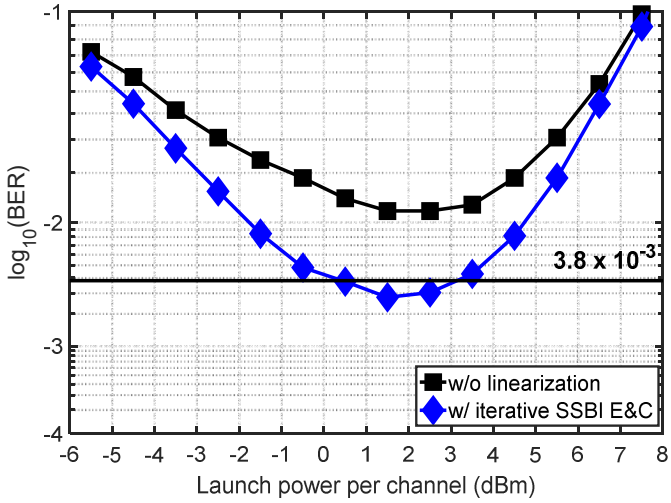

Fig. 4.8: BER versus optical launch power per channel at 35 GHz channel spacing without and with the iterative SSBI E&C scheme over 240 km WDM transmission.

As mentioned before, the accuracy of the symbol decisions needs to be improved by carrying out multiple iterations in the compensation DSP. The plot of BER versus the applied number of iterations in the receiver DSP at 240 km transmission was shown in Fig. 4.9. It can be seen that, more than four iterations were required in order to achieve the maximum compensation gain. Additionally, the number of iterations required varies with the transmission distance due to the

variation in accuracy of the symbol decision making; fewer iterations are required for shorter transmission distances.

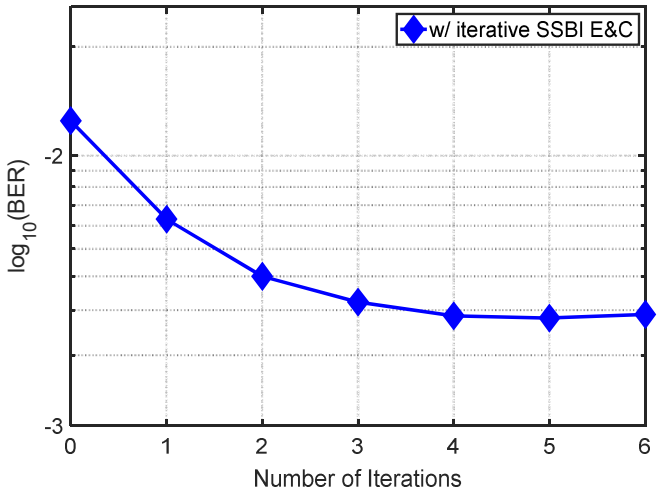

Fig. 4.9: BER versus receiver iteration numbers with the iterative SSBI E&C scheme over 240 km WDM transmission.

The BER (at the optimum optical launch power and CSPR) versus transmission distances from 80 km to 240 km multiple span (N = 1, 2 and 3) without and with the iterative SSBI E&C scheme was plotted in Fig. 4.10. It can be observed that the WDM transmission performance was significantly improved at all distances, and the BER at 240 km was decreased from 1.2×10^{-2} to 2.8×10^{-3} using the iterative SSBI E&C scheme. Since the tradeoff between the ASE-noise and fibre nonlinearity remained unchanged in multiple span fibre links, the optimum launch power was found to be 1.5 dBm for all three transmission distances. To observe the compensation effectiveness, the received constellation diagrams, without and with the iterative SSBI E&C scheme after transmission over 240 km, were plotted in the insets (a) and (b). It can be seen that after the iterative SSBI E&C scheme, the compensated constellation was significantly less distorted than the uncompensated one, especially in the four points in the corners, which were mostly affected by the SSBI due to their high symbol energies. The EVM was decreased from 21.2 % to 17.1% with this compensation method.

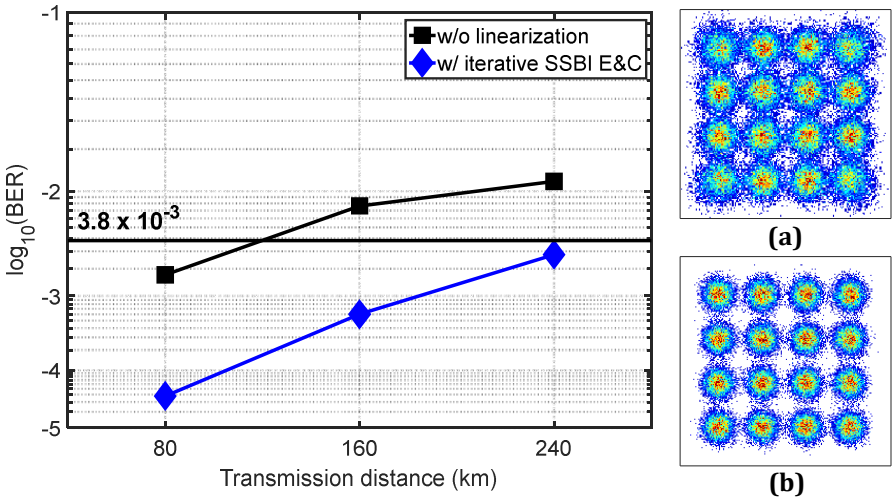

Fig. 4.10: BER versus transmission distance at 35 GHz WDM channel spacing without and with the iterative SSBI E&C scheme. Insets: Received constellation diagrams over 240 km WDM transmission, (a) without (21.2%), and (b) with iterative SSBI E&C scheme (17.1%).

Finally, the performance of all four WDM channels was shown in Fig. 4.11 at a distance of 240 km. The average BER for all the channels was decreased from 1.1×10^{-2} without SSBI cancellation, to 2.5×10^{-3} (nearly one-order magnitude) using the iterative SSBI E&C approach. To calculate the theoretical upper bound on the achievable net optical ISD, based on the theoretical hard-decision decoding bound for the binary symmetric channel [14] at 2.5×10^{-3} BER (p), the maximum code rate (r) is given by:

$$r = 1 + p \cdot log_2 p + (1-p) \cdot log_2 (1-p) \tag{4.4}$$

The value of r was found to be 0.97, hence the net bit rate per channel was 109 Gb/s, and the achieved maximum net optical ISD was 3.11 (b/s)/Hz.

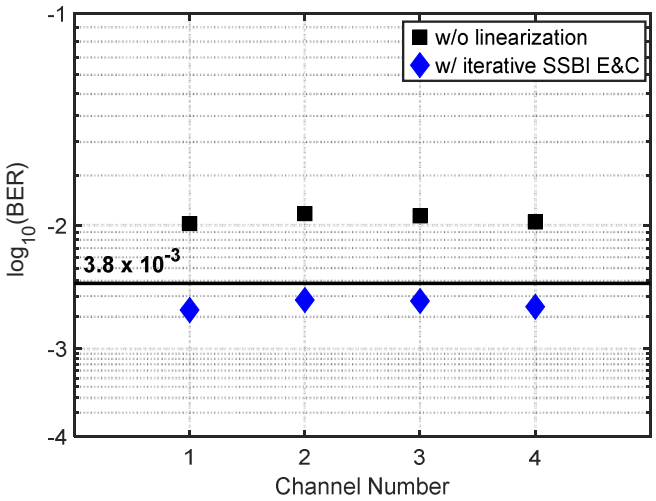

Fig. 4.11: BERs for each WDM channel without and with the iterative SSBI E&C scheme over 240 km transmission.

4.4 Summary

Technical details and experimental performance evaluations of the receiver-based digital iterative SSBI E&C technique were presented in this chapter. Both theoretical analysis and practical experimental assessments indicated that the digital iterative SSBI E&C approach can effectively eliminate the SSBI penalty by iteratively reconstructing the signal-signal beating products according to the symbol decision making, and then subtracting them from the detected signal. Since such scheme avoids the utilization of complex balanced receiver-based SSBI mitigation, the optical hardware complexity is significantly reduced. However, due to requirement of multiple iterations in the compensation DSP, the dramatically increased digital hardware complexity becomes the main drawback of this scheme. Moreover, the SSBI estimation is affected by the accuracy of the symbol decision making, and noticeable degradation of the compensation effectiveness can be observed at lower OSNR levels as a consequence.

References

[1] R.I. Killey, P.M. Watts, V. Mikhailov, M. Glick, and P. Bayvel, "Electronic dispersion compensation by signal predistortion using digital processing and a dual-drive Mach-Zehnder modulator," IEEE Photon. Technol. Lett. 17(3), 714-716 (2005).

[2] Z. Li, M. S. Erkilinc, L. Galdino, K. Shi, B. C. Thomsen, P. Bayvel, and R. I. Killey, " Comparison of digital signal-signal beat interference compensation techniques in direct-detection subcarrier modulation systems", Opt. Express, 24(25), 29176-29189, (2016).

[3] W. Peng, X. Wu, K. Feng, V.R. Arbab, B. Shamee, J. Yang, L.C. Christen, A.E. Willner, and S. Chi, "Spectrally efficient direct-detected OFDM transmission employing an iterative estimation and cancellation technique," Opt. Express 17(11) 9099-9111 (2009).

[4] J.-H. Yan, Y.-W. Chen, B.-C. Tsai, and K.-M. Feng, "A multiband DDO-OFDM System with spectral efficient iterative SSBI reduction DSP," IEEE Photon. Technol. Lett. 28(2), 119-122 (2016).

[5] Z. Li, M. S. Erkılınç, S. Pachnicke, H. Griesser, R. Bouziane, B.C. Thomsen, P. Bayvel, and R.I. Killey, "Signal-signal beat interference cancellation in spectrally-efficient WDM direct-detection Nyquist-pulse-shaped 16-QAM subcarrier modulation," Opt. Express 23(18), 23694-23709 (2015).

[6] W.R. Peng, I. Morita, and H. Tanaka, "Enabling high capacity direct-detection optical OFDM transmissions using beat interference cancellation receiver," in European Conference and Exhibition on Optical Communication (ECOC 2010), paper Tu.4.A.2.

[7] S.A. Nezamalhosseini, L.R. Chen, Q. Zhuge, M. Malekiha, F. Marvasti, and D.V. Plant, "Theoretical and experimental investigation of direct detection optical OFDM transmission using beat interference cancellation receiver," Opt. Express, 21(13), 15237-15246 (2013).

[8] J. Ma, "Simple signal-to-signal beat interference cancellation receiver based on balanced detection for a single-sideband optical OFDM signal with a reduced guard band," Opt. Letters, 38(21), 4335-4338 (2013).

[9] C. Sánchez, B. Ortega, and J. Capmany, "System performance enhancement with pre-distorted OOFDM signal waveforms in DM/DD systems," Opt. Express 22(6), 7269-7283 (2014).

[10] C. Ju, X. Chen, N. Liu, and L. Wang, "SSII cancellation in 40 Gbps VSB-IMDD OFDM system based on symbol pre-distortion," in European Conference and Exhibition on Optical Communication (ECOC 2014), paper P.7.9.

[11] N. Liu, C. Ju, and X. Chen, "Nonlinear ISI cancellation in VSSB Nyquist-SCM system with symbol pre-distortion," Opt. Commun. 338, 492–495 (2015).

[12] M.S. Erkılınç, Z. Li, S. Pachnicke, H. Griesser, B.C. Thomsen, P. Bayvel, and R.I. Killey, "Spectrally-efficient WDM Nyquist-pulse-shaped 16-QAM subcarrier modulation transmission with direct detection," J. Lightw. Technol. 33(15), 3147-3155 (2015).

[13] R.A. Shafik, M.S. Rahman, and A.R. Islam, “On the extended relationships among EVM, BER and SNR as performance metrics,” in International Conference on Electrical and Computer Engineering (ICECE 2006), paper 408-411.

[14] C.E. Shannon, “A mathematical theory of communication,” Bell System Technical Journal, 27(3), 379-423, (1948).

CHAPTER 5

RECEIVER-BASED DIGITAL SINGLE-STAGE LINEARIZAITON FILTER

As discussed in Chapter 4, the digital iterative SSBI E&C technique includes symbol decision-based SSBI reconstruction with multiple demodulation and modulation operations, its compensation performance has a high dependency on the accuracy of symbol decision making and it comes with significantly increased DSP complexity. In this chapter, a simple structured receiver-based digital linearization filter is demonstrated. In Section 5.1, its operating principle and its further application as a non-iterative SSBI E&C scheme are first described mathematically. In Section 5.2, the experimental performance including optical back-to-back and WDM transmission is assessed in a dispersion pre-compensated 35 GHz-spaced 112 Gb/s per channel spectrally-efficient WDM SSB 16-QAM Nyquist-SCM DD system operating over SSMF links of up to 240 km. Section 4.3 summaries this chapter.

5.1 Principle of Operation

The digital single-stage linearization filter studied in this section was recently proposed and demonstrated for SSB OFDM DD system in [1] and has shown effective compensation performance with very simple digital hardware structure. The functional description of such scheme has been presented in Chapter 3, Section 3.2.3. In this section, its working principle is further described with mathematical expressions.

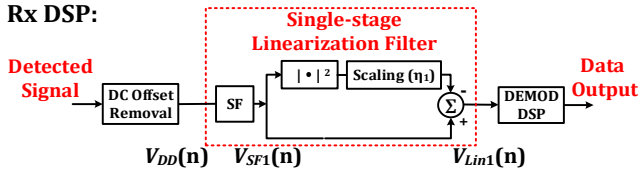

Fig. 5.1: Receiver DSP design with the receiver-based single-stage linearization filter. SF: sideband filter. DEMOD DSP: SSB SCM signal demodulation.

The receiver DSP design with the single-stage linearization filter is shown in Fig. 5.1. Following the square-law detection, the detected DSB signal after the DC offset removal, $V_{DD}(n)$ (expressed in Eq. 4.1) is passed through the single-stage linearization filter. The signal after the sideband filter, $V_{SF1}(n)$, and the output of the single-stage linearization filter, $V_{Lin1}(n)$, are written as follows:

$$V_{SF1}(n) = \alpha \cdot E_0(n) + \Lambda[|E_0(n)|^2] \tag{5.1}$$

$$\begin{aligned} V_{Lin1}(n) &= V_{SF1}(n) - \eta_1 \cdot |V_{SF1}(n)|^2 \\ &= \alpha \cdot E_0(n) + \Lambda[|E_0(n)|^2] - \alpha^2\eta_1 \cdot |E_0(n)|^2 - 2\alpha\eta_1 \\ &\quad \cdot Re\left[E_0^*(n) \cdot \Lambda[|E_0(n)|^2]\right] - \eta_1 \cdot |\Lambda[|E_0(n)|^2]|^2 \end{aligned} \tag{5.2}$$

where α is an amplitude scaling factor inversely proportional to the optical carrier value, $\Lambda[\cdot]$ is the SF operator, and η_1 is a second amplitude scaling factor which controls the effectiveness of the single-stage linearization filter. In the RHS of Eq. 5.2, the first term is the desired SSB CSBP; since we only demodulate the signal spectrum in the positive frequency domain, the second term (SSBI) can be partially eliminated by the third term with the optimum adjustment of η_1. On the other hand, since the introduced fourth (signal-SSBI beating) and fifth (SSBI-SSBI beating) terms are comparatively lower than the SSBI term, the nonlinear penalty is reduced with respect to the case without implementing this single-stage linearization filter [2]. It should be mentioned that, the use of the SF avoids unwanted beating products which would otherwise be generated by the negative frequency part of the detected DSB signal spectrum. DC offset removal is performed to ensure the re-generation of only the signal-signal beating products.

An advantage of this single-stage linearization filter is its use of a very simple DSP structure. In addition, in comparison with the iterative SSBI E&C approach [3-5] discussed in Chapter 4, the single-stage linearization filter does not carry out symbol decision-based compensation, and hence its performance does not reply on the accuracy of the decision making. However, as shown in Eq. 5.2, as the calculation of the signal-signal beating products is based on the received distorted signal, this scheme itself introduces extra unwanted beating interference, thus preventing the filter from achieving the maximum compensation performance.

Another application of the single-stage linearization filter is to combine it with the SSBI E&C scheme described in the previous chapter, to realise a non-iterative SSBI E&C scheme. Results of our simulation and experimental studies have indicated that this non-iterative SSBI E&C scheme offers compensation performance matching the iterative scheme [6]. Fig. 5.2 shows the receiver DSP with the non-iterative SSBI E&C technique.

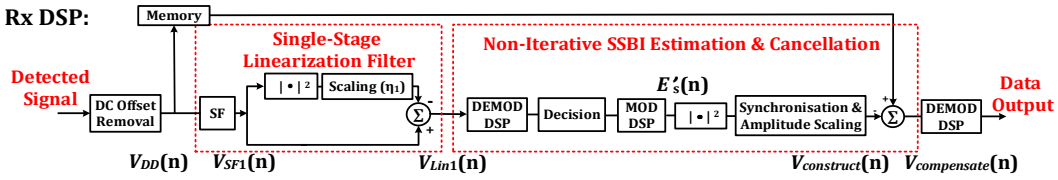

Fig. 5.2: Receiver DSP design with the receiver-based non-iterative SSBI E&C technique. SF: sideband filter. MOD & DEMOD DSP: SSB SCM signal generation and demodulation.

Two copies of the detected DSB signal waveform, $V_{DD}(n)$ are made with one being stored in memory and the other being passed through the single-stage linearization filter to partially eliminate the SSBI terms. Following this, non-iterative SSBI E&C is performed. Since symbol decisions are significantly more accurate due to the preceding single-stage linearization filtering stage, multiple iterations of the signal demodulation and modulation are not required to achieve the maximum compensation gain, thus leading to a speed-up of the convergence process and reduction of the DSP complexity. Moreover, unlike the single-stage linearization filter, no additional beating interferences (fourth and fifth terms in Eq. 5.2) are introduced, and hence it offers potentially better compensation performance, especially at high OSNR levels. However, similarly to the iterative SSBI E&C approach, the performance of this technique is also noticeably degraded at lower OSNR levels, resulting from its dependency on the accuracy of the symbol decision making.

5.2 Experimental Results

Experimental assessments of the system performance in both WDM back-to-back and transmission operations with the single-stage linearization filter and the non-iterative SSBI E&C scheme were carried out on the transmission test-bed discussed in Chapter 4, Section 4.2. Their compensation performance was also compared with that of the iterative SSBI E&C technique, with four iterations being utilized for the latter to achieve the maximum possible effectiveness.

5.2.1 WDM Back-to-Back Performance Evaluation

In the WDM optical back-to-back assessment, the BER with respect to CSPR at an OSNR of 31 dB was plotted in Fig. 5.3 for the system without and with the different digital linearization schemes. In comparison to the system without linearization, optimum CSPR value of the system utilizing single-stage linearization filter was reduced by approximately 2 dB, which was 1 dB lower than the cases with SSBI E&C schemes. The difference in the reduction of the optimum CSPR values is mainly because the SSBI E&C schemes offer stronger capability in suppressing the SSBI penalty over the single-stage linearization filter at such OSNR level.

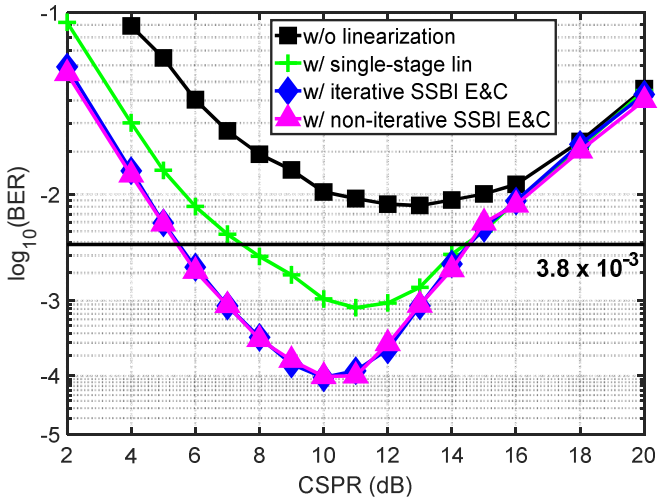

Fig. 5.3: BER versus CSPR without and with digital single-stage linearization filter, iterative and non-iterative SSBI E&C schemes at OSNR = 31 dB.

Following this, the dependence of the optimum CSPR values on the OSNR level was assessed by plotting the optimum CSPR versus OSNR, as shown in Fig. 5.4. In comparison to the uncompensated case, the optimum CSPR values were reduced by 2 dB for all the OSNRs for the single-stage linearization filter, while the SSBI E&C schemes exhibited greater reduction (3 dB) at high OSNRs (≥ 27 dB) and less reduction (1.5 dB) for low OSNRs (≤ 21 dB) because the compensation effectiveness of such schemes is determined by the accuracy of the decision makings.

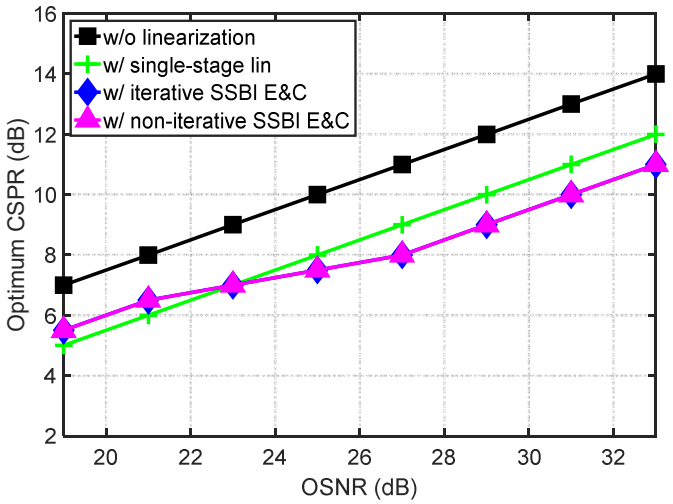

Fig. 5.4: Optimum CSPR versus OSNR without and with digital single-stage linearization filter, iterative and non-iterative SSBI E&C schemes in back-to-back operation.

To show the sensitivity of the systems to the applied amplitude scaling factors (η_1, $\eta_{dB} = 10 \times \log_{10}(\eta_{linear})$) in the single-stage linearization filter, BER versus applied amplitude scaling factor at 31 dB OSNR and 11 dB CSPR was plotted in Fig. 5.5. It can be seen that the value of η_1 controlled the compensation effectiveness of the single-stage linearization filter and needed to be adjusted to the optimum value (-10 dB in this figure). Reduced compensation effectiveness can be observed with low values of η_1, while the high valued η_1 leads to overcompensation. It should be mentioned that, the optimum η_1 is inversely proportional to the utilized CSPR value [2]. Therefore, the optimum η_1 varies with OSNR, transmission distances and launch powers due to the utilization of different CSPRs.

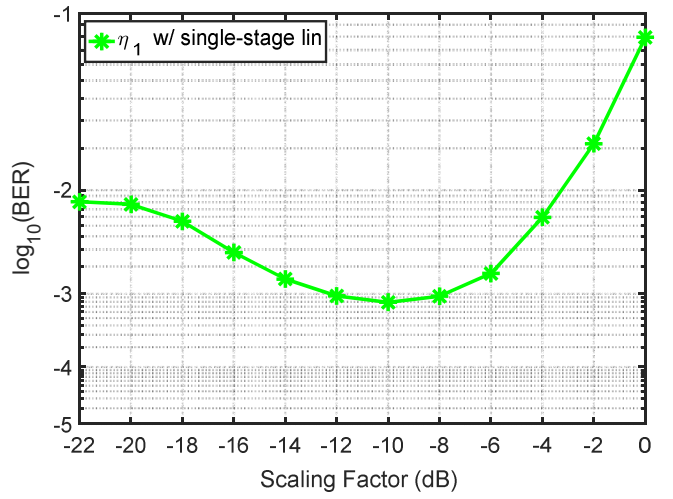

Fig. 5.5: BER versus scaling factor (η_1) with digital single-stage linearization filter at OSNR = 31 dB, CSPR = 11 dB.

Furthermore, the BER versus OSNR was plotted in Fig. 5.6 for the cases without and with the single-stage linearization filter, iterative and non-iterative SSBI E&C schemes. The CSPR was adjusted to the optimum value at each OSNR level, as shown in Fig. 5.4. It can be seen that, the required OSNR at the 3.8×10^{-3} BER threshold was 28.2 dB for the case with single-stage linearization filter (5.3 dB total compensation gain) and was reduced to 26.4 dB by utilizing the non-iterative SSBI E&C. As discussed in Section 5.1, the single-stage linearization filter introduces extra unwanted beating interference, thus its compensation performance is limited. On the other hand, by combining it with the single-stage linearization filter, the non-iterative SSBI E&C offers the same performance as the iterative scheme without the requirement for multiple demodulation and modulation operations, and its digital circuit design is therefore significantly simpler. In addition, due to improved approximation of the signal-signal beating terms, the SSBI E&C schemes provide the best compensation performance at high OSNRs, although its performance is degraded at lower OSNR levels due to the increased number of inaccurate symbol decisions.

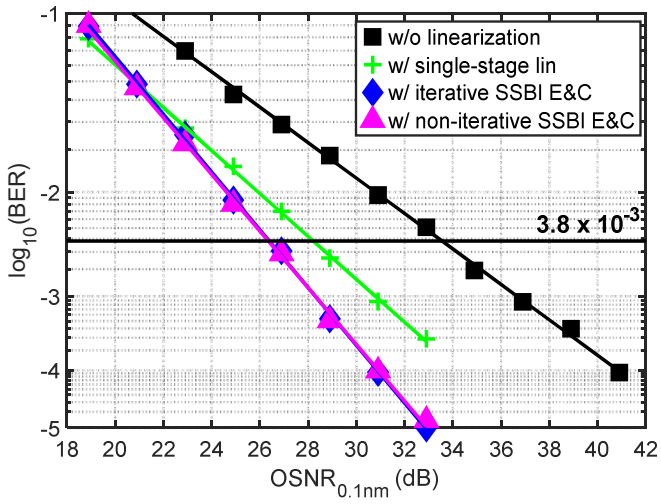

Fig. 5.6: BER versus OSNR without and with receiver-based digital single-stage linearization filter, iterative and non-iterative SSBI E&C schemes.

5.2.2 WDM Transmission Performance Evaluation

WDM transmission evaluations were also carried out. BER versus optical launch power per channel over 240 km WDM transmission was plotted in Fig. 5.7. It can be seen that the system performance was improved at all optical launch powers and the optimum launch power was reduced by approximately 1 dB by applying these linearization schemes. The optimum CSPR was 10 dB with the single-stage linearization filter and 9 dB with the non-iterative SSBI E&C approach, which corresponded to reductions of 2 dB and 3 dB compared to the uncompensated case respectively.

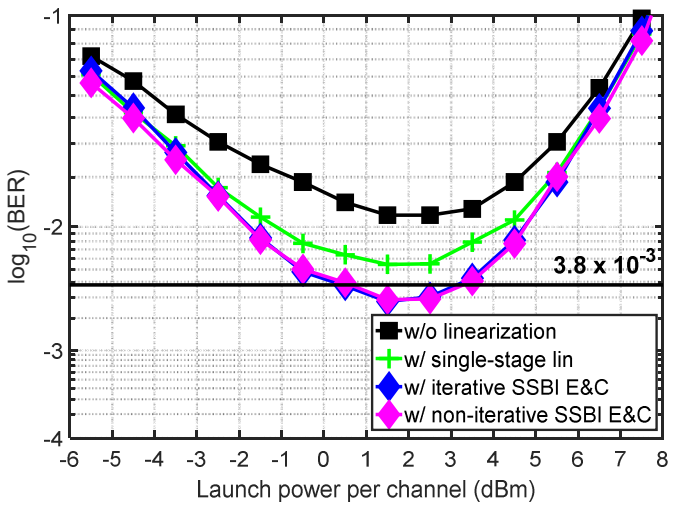

Fig. 5.7: BER versus optical launch power per channel without and with digital single-stage linearization filter, iterative and non-iterative SSBI E&C schemes over 240 km WDM transmission.

Furthermore, the BER was plotted versus the number of iterations employed in the compensation DSP for WDM transmission over 240 km in Fig. 5.8 for the cases with these three approaches. It can be seen that, the non-iterative SSBI E&C scheme offered better performance than the single-stage linearization filter and similar performance to that of the iterative approach whilst the need to perform multiple (approximately four times in the figure) iterations was avoided.

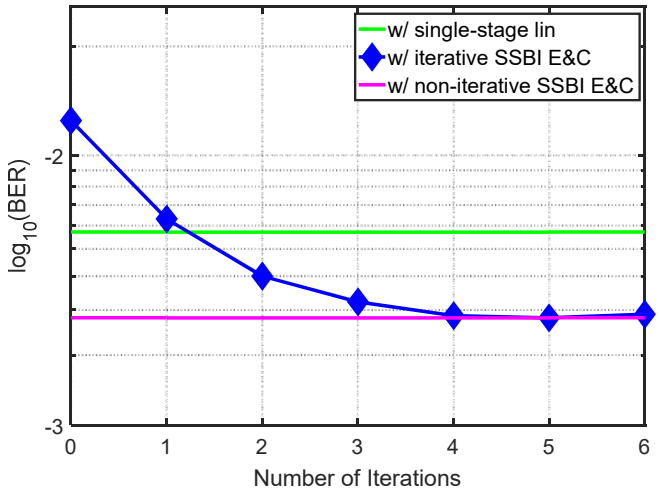

Fig. 5.8: BER versus receiver iteration numbers with digital single-stage linearization filter, iterative and non-iterative SSBI E&C schemes over 240 km WDM transmission.

In addition, the BER (at the optimum launch power and CSPR) versus transmission distance was plotted in Fig. 5.9. It can be observed that both the single-stage linearization filter and the non-iterative SSBI E&C scheme improved the system performance at all transmission distances from 80 km to 240 km. The non-iterative SSBI E&C scheme exhibited better compensation performance (BER of 3.0×10^{-3} over 240 km transmission) than single-stage linearization filter (BER = 5.8×10^{-3}), and similar compensation performance with the iterative scheme.

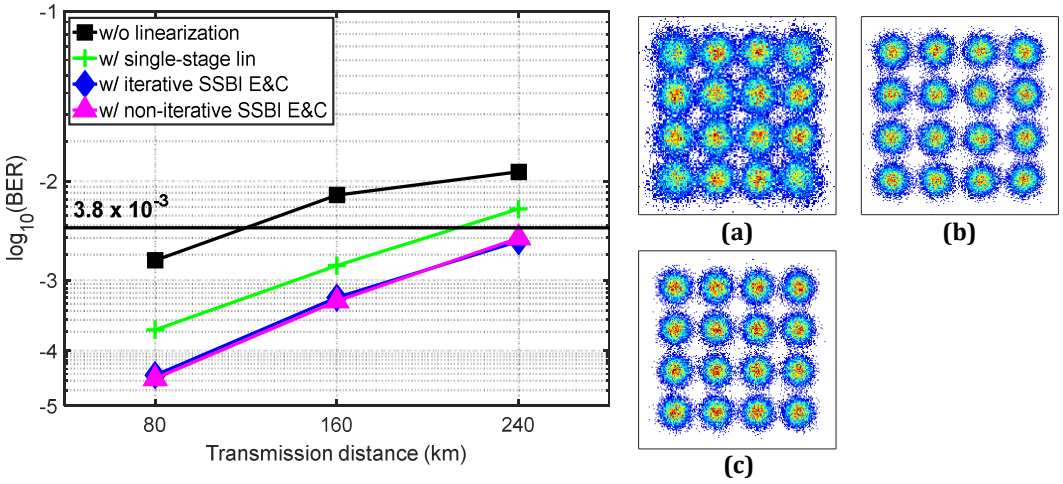

Fig. 5.9: BER versus transmission distance without and with digital single-stage linearization filter, iterative and non-iterative SSBI E&C schemes. Insets: Received constellation diagrams over 240 km WDM transmission, (a) without (21.2%), (b) with sinlge-stage linearization filter (17.4%), (c) with non-iterative SSBI E&C scheme (17.1%).

Fig. 5.10 showed all four WDM channels' performance at the optimum optical launch power at a distance of 240 km. Since the two centre channels suffer from higher FWM, as they each have two direct neighbouring channels, the BERs for these channels are relatively higher than those for the remaining two channels. The average BER for all the channels was reduced to 5.1×10^{-3} using the single-stage linearization filter and was further reduced to 2.6×10^{-3} using the non-iterative SSBI E&C, similar to that of the iterative approach. According to the theoretical hard-decision decoding bound, the achieved maximum net optical ISDs were 3.05 (b/s)/Hz and 3.11 (b/s)/Hz respectively.

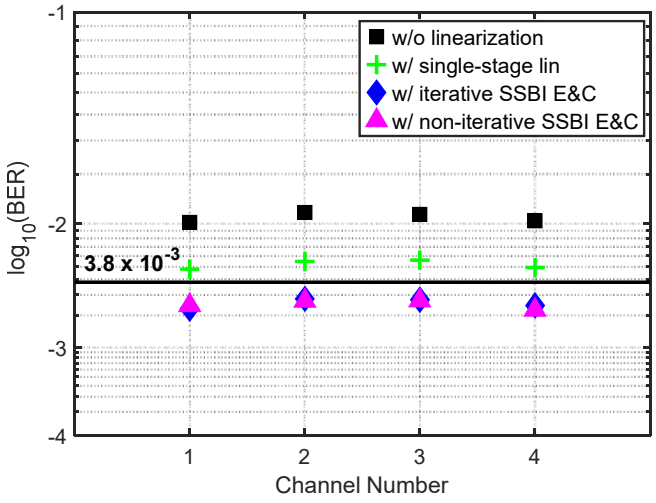

Fig. 5.10: BERs for each WDM channel without and with digital single-stage linearization filter, iterative and non-iterative SSBI E&C schemes over 240 km transmission.

5.3 Summary

This chapter focused on the receiver-based digital single-stage linearization filter and its application to avoid the requirement for multiple iterations in the SSBI E&C scheme. The working principles were mathematically described, followed by experimental evaluations of a dispersion

pre-compensated 35 GHz-spaced 112 Gb/s per channel spectrally-efficient WDM SSB 16-QAM Nyquist-SCM DD system transmitting over SSMF links of up to 240 km. Both the theoretical analysis and the experimental results indicated that the single-stage linearization filter can partially compensate the SSBI with a very simple DSP structure. However, as this technique itself introduces extra beating interference, its compensation performance is limited. On the other hand, a non-iterative SSBI E&C scheme was also proposed and demonstrated by combining it with the single-stage linearization filter. This scheme offers compensation performance similar to the iterative SSBI E&C technique and avoids the requirement for multiple (typically more than four) symbol decision-based SSBI reconstruction processes. Therefore, it offers significantly reduced DSP complexity in contrast to the iterative SSBI E&C. Since the non-iterative SSBI E&C is still symbol decision-based, its compensation performance is noticeably degraded at lower OSNR values.

References

[1] S. Randel, D. Pilori, S. Chandrasekhar, G. Raybon, and P. Winzer, "100-Gb/s discrete-multitone transmission over 80-km SSMF using single-sideband modulation with novel interference-cancellation scheme," in European Conference and Exhibition on Optical Communication (ECOC 2015), paper Mo.4.5.2.

[2] Z. Li, M. S. Erkilinc, R. Maher, L. Galdino, K. Shi, B. C. Thomsen, P. Bayvel, and R. I. Killey, "Two-stage linearization filter for direct-detection subcarrier modulation", IEEE Photon. Technol. Lett. 28(24), 2838-2841 (2016).

[3] W. Peng, X. Wu, K. Feng, V.R. Arbab, B. Shamee, J. Yang, L.C. Christen, A.E. Willner, and S. Chi, "Spectrally efficient direct-detected OFDM transmission employing an iterative estimation and cancellation technique," Opt. Express 17(11) 9099-9111 (2009).

[4] J.-H. Yan, Y.-W. Chen, B.-C. Tsai, and K.-M. Feng, "A multiband DDO-OFDM System with spectral efficient iterative SSBI reduction DSP," IEEE Photon. Technol. Lett. 28(2), 119-122 (2016).

[5] Z. Li, M. S. Erkılınç, S. Pachnicke, H. Griesser, R. Bouziane, B.C. Thomsen, P. Bayvel, and R.I. Killey, "Signal-signal beat interference cancellation in spectrally-efficient WDM direct-detection Nyquist-pulse-shaped 16-QAM subcarrier modulation," Opt. Express 23(18), 23694-23709 (2015).

[6] Z. Li, M. S. Erkilinc, R. Maher, L. Galdino, K. Shi, B. C. Thomsen, P. Bayvel, and R. I. Killey, "Reach enhancement for WDM direct-detection subcarrier modulation using low-complexity two-stage signal-signal beat interference cancellation", in European Conference and Exhibition on Optical Communication (ECOC 2016), paper M 2.B.1.

CHAPTER 6

RECEIVER-BASED DIGITAL TWO-STAGE LINEARIZATION FILTER

As mentioned in Chapter 5, in the single-stage linearization filter [1], inaccuracies in the approximation of SSBI terms occur due to the inclusion of the SSBI terms in the detected signal, $V_{SF1}(n)$, the compensation effectiveness of the single-stage linearization filter being limited by the resulting additional beating interference. In order to achieve improved compensation performance, one solution is to iteratively repeat the single-stage linearization filtering process, using an iterative linearization filter [2, 3]. Its DSP design can be found in Chapter 3, Section 3.2. This technique improves the performance of the single-stage linearization filter by using the stored received signal waveform and iteratively repeating the SSBI estimation. However, as discussed in Chapter 4, the DSP complexity is directly related to the number of iterations used because it is impossible to reuse the same digital hardware in the iteration for continuous transmitted data. Carrying out multiple (more than four) iterations leads to its DSP complexity being significantly increased [4].

This chapter focuses on an alternative method to enhance the performance of the single-stage linearization filter, through the use of a two-stage linearization filter. This technique has been shown to offer similar performance to the iterative linearization filter and at the same time does not require the implementation of a complex iterative compensation process, thus offering a good tradeoff between the compensation effectiveness and the digital circuit design complexity. Its working principle is first described mathematically in Section 6.1. Section 6.2 presents the obtained experimental results on the dispersion pre-compensated 35 GHz-spaced 112 Gb/s per channel spectrally-efficient WDM SSB 16-QAM Nyquist-SCM DD system in transmission over SSMF links of up to 240 km and Section 6.3 concludes this chapter.

6.1 Principle of Operation

The two-stage linearization filter was proposed for SSB Nyquist-SCM DD systems in [5-7]. Its working principle is explained in detail in this section.

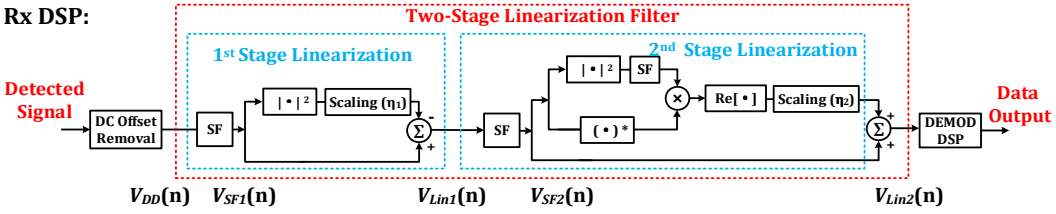

Fig. 6.1: Receiver DSP design with the two-stage linearization filter. SF: sideband filter. DEMOD DSP: SSB SCM signal demodulation.

The receiver DSP design with the two-stage linearization filter is shown in Fig. 6.1. A second linearization stage is applied to remove the majority of the unwanted beating interference introduced by the first stage. The operation principle can be described as follows: In the first linearization stage, which is the same as the single-stage linearization filter described in Chapter 5, with optimum adjustment of η_1, the SSBI penalty is removed and the remaining terms are the

signal-SSBI (fourth term) and SSBI-SSBI (fifth) beating terms, as described in Eq. 5.2. Following this, the output signal passes through the second linearization stage to compensate the signal-SSBI beating interference introduced by the first stage, as follows:

$$V_{SF2}(n) = \alpha \cdot E_0(n) - 2\alpha\eta_1 \cdot \Lambda\left[Re\left[E_0^*(n) \cdot \Lambda[|E_0(n)|^2]\right]\right] - \eta_1 \cdot \Lambda[|\Lambda[|E_0(n)|^2]|^2] \tag{6.1}$$

$$V_{Lin2}(n) = V_{SF2}(n) + \eta_2 \cdot Re\left[V_{SF2}^*(n) \cdot \Lambda[|V_{SF2}(n)|^2]\right] \tag{6.2}$$

where $V_{SF2}(n)$ is the filtered SSB signal, and $V_{Lin2}(n)$ is the output of the second linearization stage. The scaling factor η_2 can be optimized to achieve the maximum compensation gain. Since the input of the second linearization stage $V_{Lin2}(n)$ is mainly the desired CSBP, the estimation of the signal-SSBI beating is significantly improved and the majority of the signal-SSBI beating interference can be compensated in this stage, thus further enhancing the compensation performance. It is worth noting that, since the SSBI-SSBI beating term results in a very small penalty in contrast to the signal-SSBI beating term, it is left uncompensated in order to keep the DSP simple. Note that DC offset removal is performed to ensure the re-generation of only the signal-signal beating products.

In contrast to the single-stage linearization filter, the two-stage linearization filter offers the advantage of enhanced compensation performance. Compared with the other digital SSBI compensation schemes such as the above-mentioned iterative linearization filter or the SSBI estimation and cancellation schemes [8-11] described in Chapter 4, this technique avoids the requirement for multiple iterations or multiple modulation and demodulation DSP operations. Hence, although the DSP complexity is more than twice that of the single-stage linearization filter, it is still relatively low compared to the iterative linearization filter and the SSBI E&C schemes.

6.2 Experimental Results

The performance of both WDM optical back-to-back and transmission implementing the two-stage linearization filter was assessed using the experimental test-bed described in Chapter 4, Section 4.2. Its performance was compared with the single-stage linearization filter and non-iterative SSBI E&C.

6.2.1 WDM Back-to-Back Performance Evaluation

BER versus carrier to signal power ratio (CSPR) at an OSNR of 31 dB was plotted in Fig. 6.2 to show the sensitivity of the systems to the applied CSPR value. Compared with the system without linearization, the optimum CSPR value was reduced by approximately 3 dB after utilizing the two-stage linearization filter, which was 1 dB higher than the case with the single-stage linearization filter. This can be explained by the second linearization stage of the filter eliminating the additional distortion introduced by the first stage, hence achieving enhanced compensation effectiveness compared to the single-stage linearization filter. In addition, the range of the CSPRs at which the BER values are below the HD-FEC threshold for the system with the two-stage linearization filter was approximately 1 dB wider than that with non-iterative SSBI E&C approach.

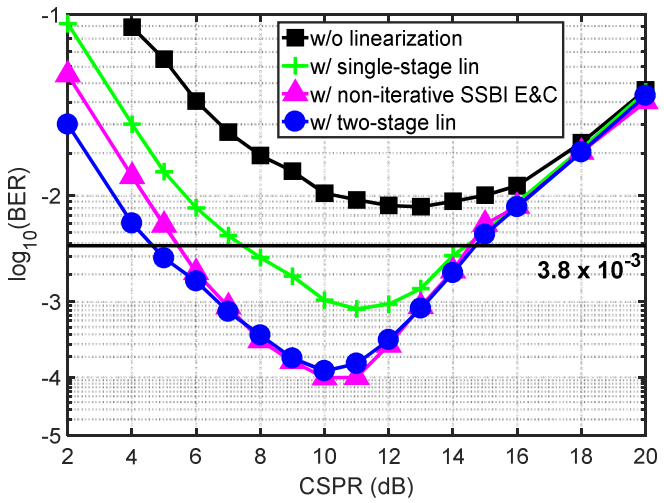

Fig. 6.2: BER versus CSPR without and with receiver-based digital single-stage linearization filter, two-stage linearization filter and non-iterative SSBI E&C scheme at OSNR = 31 dB.

Fig. 6.3 showed the variations of the optimum CSPR values with respect to the OSNRs. It can be observed that, in comparison to the uncompensated case, the optimum CSPR values needed to be reduced by 3 dB at all values of OSNR when using the two-stage linearization filter, which was 1 dB higher than that achieved using the single-stage linearization filter. In contrast to the non-iterative SSBI E&C approach, this optimum CSPR reduction was up to 1.5 dB higher for low OSNRs ($\leq$ 21 dB), and gradually became the same for high OSNRs ($\geq$ 27 dB).

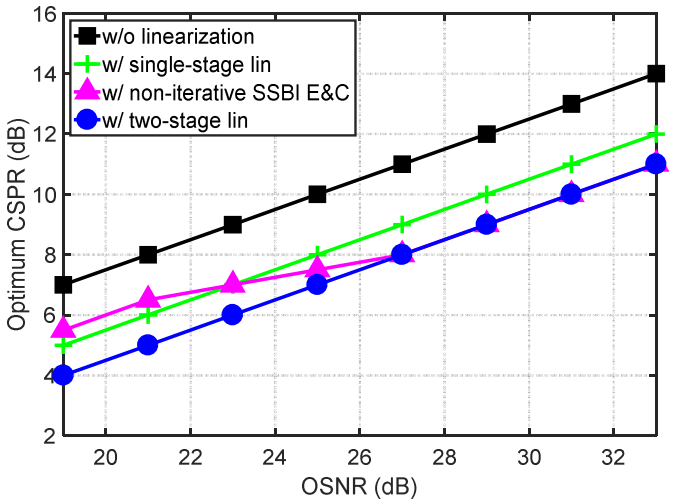

Fig. 6.3: Optimum CSPR versus OSNR without and with receiver-based digital single-stage linearization filter, two-stage linearization filter and non-iterative SSBI E&C scheme in back-to-back operation.

As shown in Fig. 6.1, there are two amplitude scaling processes in the DSP design of the two-stage linearization filter. It is therefore crucial to optimize these two applied scaling factors to achieve the maximum compensation gain. Fig. 6.4 showed the BER versus applied amplitude scaling factors (η_1 and η_2) at 31 dB OSNR and 10 dB CSPR. The BER was initially reduced by optimum adjustment of the scaling factor η_1 (with η_2 set to zero), following which it was further decreased by optimizing η_2. The plot showed the sensitivity of the system to the scaling factor values. The optimum value of η_1 (-10 dB) was found to be 2 dB lower than η_2 (-8 dB). Note that,

the values of the scaling factors are inversely proportional to the utilized CSPR, and do not change with the optical signal power.

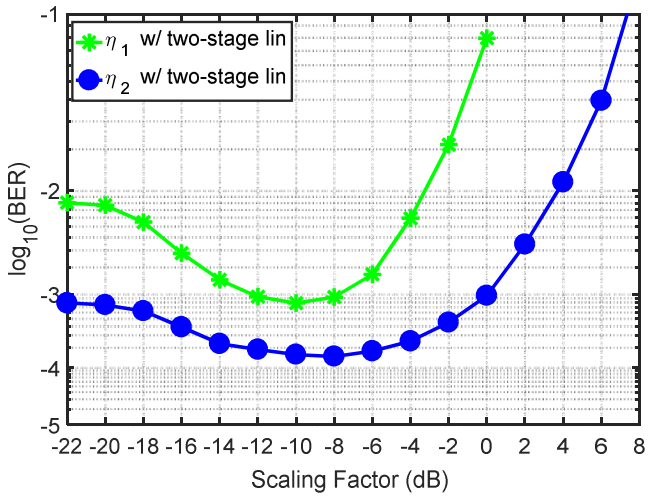

Fig. 6.4: BER versus scaling factor (η_1 and η_2) with digital two-stage linearization filter at OSNR = 31 dB, CSPR = 10 dB.

Furthermore, the BER with respect to OSNR for the cases without and with single-stage linearization filter, two-stage linearization filter and non-iterative SSBI E&C scheme was plotted in Fig. 6.5. It can be seen that, by implementing the two-stage linearization filter, the required OSNR at HD-FEC threshold, assumed to be BER = 3.8×10^{-3}, was reduced to 25.9 dB. In contrast to the case without linearization, the achieved compensation gain was 7.6 dB, which is higher than the 5.4 dB and 7.1 dB using the single-stage linearization filter and non-iterative SSBI E&C approach, respectively. Furthermore, it can also be observed that, the two-stage linearization filter offered noticeably better compensation gain than the non-iterative SSBI E&C approach at low OSNR levels (< 25 dB), because the performance of this technique does not rely on the accuracy of the symbol decision making.

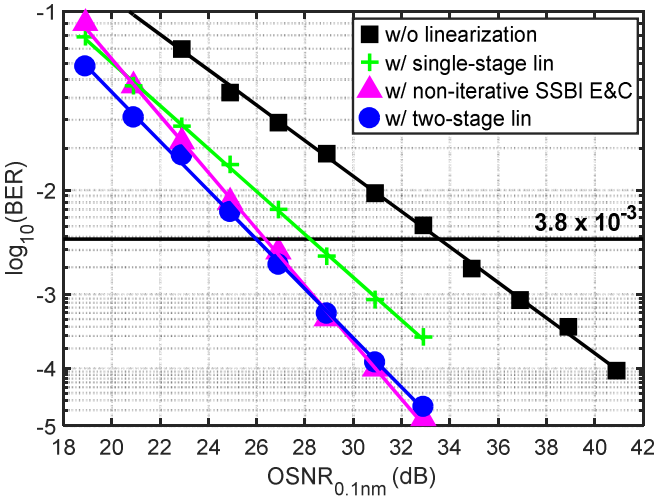

Fig. 6.5: BER versus OSNR without and with receiver-based digital single-stage linearization filter, two-stage linearization filter and non-iterative SSBI E&C scheme.

6.2.2 WDM Transmission Performance Evaluation

Following the WDM optical back-to-back assessment, the WDM transmission experiments were carried out. BER versus optical launch power per channel over 240 km WDM transmission without and with the single-stage linearization, the two-stage linearization filter and the non-iterative SSBI E&C scheme was plotted in Fig. 6.6. It can be seen that the two-stage linearization filter offered the widest range of optical launch powers at which the BER is below the FEC threshold, and a 1 dB reduction of the optimum launch power can be observed. The optimum CSPR was 9 dB (a 3 dB reduction in comparison to the uncompensated case) when using the two-stage linearization filter.

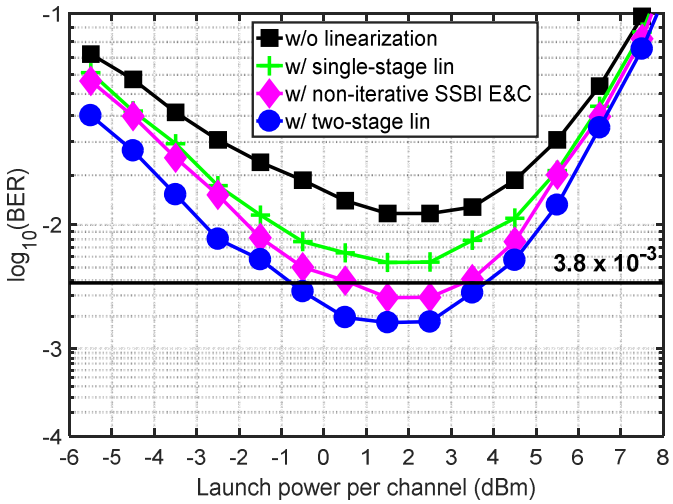

Fig. 6.6: BER versus optical launch power per channel without and with receiver-based digital single-stage linearization filter, two-stage linearization filter and non-iterative SSBI E&C scheme over 240 km WDM transmission.

Following this, the BER (at the optimum launch power and CSPR) versus transmission distance was plotted in Figs. 6.7. The BER at 240 km transmission was 1.8×10^{-3} with the two-stage linearization filter, which achieved better transmission performance than both the single-stage linearization filter and the non-iterative SSBI E&C scheme. Insets (a-d) showed the received signal constellation diagrams with corresponding EVM values following transmission over 240 km.

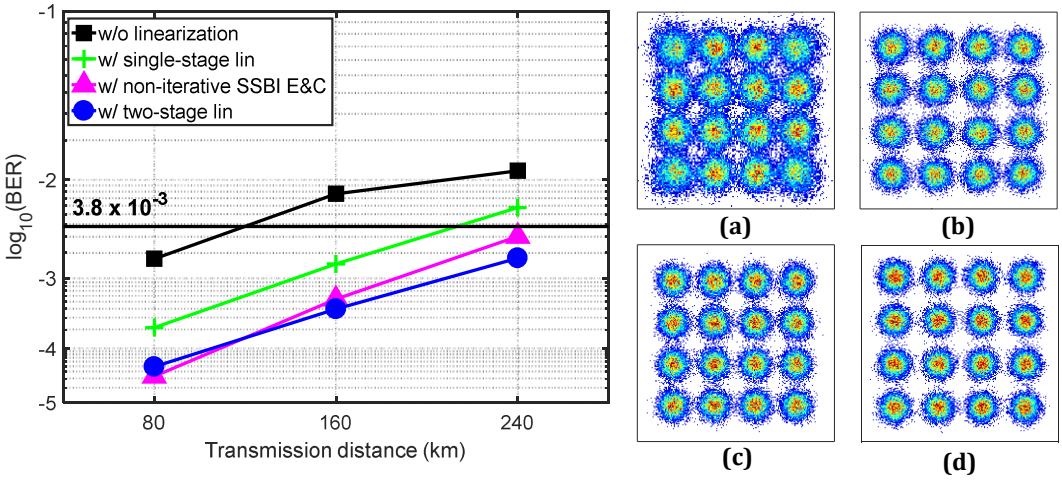

Fig. 6.7: BER versus transmission distance without and with receiver-based digital single-stage linearization filter, two-stage linearization filter and non-iterative SSBI E&C scheme. Insets: Received constellation diagrams over 240 km WDM transmission, (a) without (21.2%), (b) with single-stage linearization filter (17.4%), (c) with non-iterative SSBI E&C scheme (17.1%) and (d) with two-stage linearization filter (15.8%).

Finally, the performance of all four WDM channels at the optimum launch power after transmission over 240 km was plotted in Fig. 6.8. The average BER value with two-stage linearization filter was found to be 1.6×10^{-3} and the achieved maximum net optical ISD was 3.15 (b/s)/Hz.

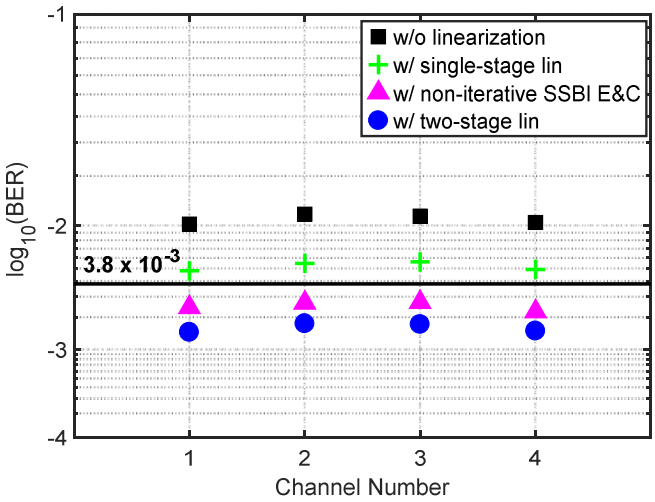

Fig. 6.8: BERs for each WDM channel without and with receiver-based digital single-stage linearization filter, two-stage linearization filter and non-iterative SSBI E&C scheme over 240 km transmission.

6.3 Summary

The receiver-based digital two-stage linearization filtering scheme was described and demonstrated in this chapter. The working principles were first described mathematically, and its performance in a dispersion pre-compensated 35 GHz-spaced 112 Gb/s per channel spectrally-efficient WDM SSB 16-QAM Nyquist-SCM DD system transmitting over up to 240 km of SSMF was experimentally assessed. The results suggest that the two-stage linearization filter enhances the compensation performance of the single-stage linearization by adding one additional

linearization stage to eliminate the majority of the unwanted extra beating interference introduced by the single-stage linearization filter. In contrast to the iterative compensation approaches, this technique avoids the requirement for multiple compensation processes, and the DSP therefore has significantly reduced complexity. Furthermore, since the two-stage linearization filter does not reply on the accuracy of the symbol decision making, this technique offers noticeably better compensation performance than the non-iterative SSBI E&C scheme at the lower OSNR levels.

References

[1] S. Randel, D. Pilori, S. Chandrasekhar, G. Raybon, and P. Winzer, "100-Gb/s discrete-multitone transmission over 80-km SSMF using single-sideband modulation with novel interference-cancellation scheme," in European Conference and Exhibition on Optical Communication (ECOC 2015), paper Mo.4.5.2.

[2] K. Zou, Y. Zhu, F. Zhang and Z. Chen, "Spectrally efficient terabit optical transmission with Nyquist 64-QAM half-cycle subcarrier modulation and direct-detection," Opt. Lett. 41(12), 2767-2770 (2016).

[3] K. Zou, Y. Zhu, and F. Zhang, "800Gb/s (8×100Gb/s) Nyquist half-cycle single sideband modulation direct detection transmission over 320km SSMF at C-band," J. Lightw. Technol., 35(10), 1900-1905 (2017).

[4] Z. Li, M. S. Erkilinc, L. Galdino, K. Shi, B. C. Thomsen, P. Bayvel, and R. I. Killey, " Comparison of Digital Signal-Signal Beat Interference Compensation Techniques in Direct-Detection Subcarrier Modulation Systems", Opt. Express, 24(25), 29176-29189 (2016).

[5] Z. Li, M. S. Erkilinc, R. Maher, L. Galdino, K. Shi, B. C. Thomsen, P. Bayvel, and R. I. Killey, "Two-stage linearization filter for direct-detection subcarrier modulation", IEEE Photon. Technol. Lett. 28(24), 2838-2841 (2016).

[6] Z. Li, M.S. Erkılınç, K. Shi, E. Sillekens, L. Galdino, B.C. Thomsen, P. Bayvel, and R.I. Killey, "112 Gb/s/λ WDM direct-detection Nyquist-SCM transmission at 3.15 (b/s)/Hz over 240 km SSMF enabled by novel beating interference compensation", in Optical Fiber Communication Conference, OSA Technical Digest Series (CD) (Optical Society of America, 2017), paper Tu3I.4.

[7] Z. Li, M.S. Erkılınç, K. Shi, E. Sillekens, L. Galdino, B.C. Thomsen, P. Bayvel, and R.I. Killey, "Improvement of digital chromatic dispersion post-compensation by utilizing beating interference mitigation for direct-detection SSB Nyquist-SCM", in Optical Fiber Communication Conference, OSA Technical Digest Series (CD) (Optical Society of America, 2017), paper Th3D.2.

[8] Z. Li, M. S. Erkilinc, L. Galdino, K. Shi, B. C. Thomsen, P. Bayvel, and R. I. Killey, " Comparison of digital signal-signal beat interference compensation techniques in direct-detection subcarrier modulation systems", Opt. Express, 24(25), 29176-29189, (2016).

[9] W. Peng, X. Wu, K. Feng, V.R. Arbab, B. Shamee, J. Yang, L.C. Christen, A.E. Willner, and S. Chi, "Spectrally efficient direct-detected OFDM transmission employing an iterative estimation and cancellation technique," Opt. Express 17(11) 9099-9111 (2009).

[10] J.-H. Yan, Y.-W. Chen, B.-C. Tsai, and K.-M. Feng, "A multiband DDO-OFDM System with spectral efficient iterative SSBI reduction DSP," IEEE Photon. Technol. Lett. 28(2), 119-122 (2016).

[11] Z. Li, M. S. Erkilinc, R. Maher, L. Galdino, K. Shi, B. C. Thomsen, P. Bayvel, and R. I. Killey, "Reach enhancement for WDM direct-detection subcarrier modulation using low-complexity two-stage signal-signal beat interference cancellation", in European Conference and Exhibition on Optical Communication (ECOC 2016), paper M 2.B.1.

CHAPTER 7

RECEIVER-BASED DIGITAL KRAMERS-KRONIG SCHEME

As described in Chapters 4, 5 and 6, the techniques including digital SSBI E&C schemes, single-stage and two-stage linearization filters treat the signal-signal beating terms as a perturbation to the signal. The compensation process works by calculating these terms and subtracting them from the detected signal. However, due to the inaccuracy of the SSBI approximation (either caused by inaccurate symbol decision making in the SSBI E&C approaches or the introduction of additional distortion by the linearization filters), these techniques all have the drawback of limited effectiveness. This chapter focuses on the technical details and performance evaluations of a recently proposed receiver-based digital compensation techniques, termed the Kramer-Kronig (KK) scheme, and demonstrates its superior performance compared to the other digital linearization schemes. Section 7.1 explains the principles of its operation, including a mathematical model of the scheme. Section 7.2 presents the results of experimental evaluations on a dispersion pre-compensated 4 × 112 Gb/s spectrally-efficient WDM SSB 16-QAM Nyquist-SCM DD system transmitting over uncompensated SSMF links of up to 240 km. Section 7.3 summarises the work in this chapter.

7.1 Principle of Operation

The digital Kramers-Kronig scheme has been demonstrated for SSB DD systems through numerical simulations [1, 2] and experiments [3, 4], confirming its potential superiority in minimising the nonlinear penalty compared to the other digital linearization schemes. As discussed in Chapter 3, if the transmitted signal is single-sideband and fulfils the condition of minimum phase, the KK scheme enables the optical phase to be reconstructed digitally from the measurement of the optical signal's envelope (making the assumption that the optical signal is single-sideband). To fulfil the minimum phase condition, the optical carrier is required to have an amplitude larger than that of the signal. Fig. 7.1 shows the receiver DSP design including the KK scheme.

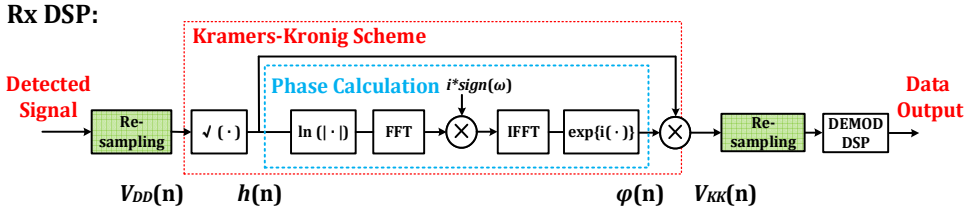

Fig. 7.1: Receiver DSP design with the Kramers-Kronig scheme.

Based on the Kramers-Kronig relation, the phase of the transmitted SSB signal is linked to its intensity [5], and therefore, following direct detection of the total field intensity, the complex-valued electric field of the SSB signal can be extracted from the measured photocurrent. The KK scheme being utilized to recover the complex waveform of the optical signal can be written as:

$$h(n) = \sqrt{V_{DD}(n)} \tag{7.1}$$

$$\varphi(n) = \mathcal{F}^{-1}\{i \cdot sign(\omega)\mathcal{F}\{ln[|h(n)|]\}\} \tag{7.2}$$

$$V_{KK}(n) = h(n) \cdot exp\{i\varphi(n)\} \tag{7.3}$$

where $V_{DD}(n)$ is the DSB real-valued signal obtained after direct detection of the optical SSB signal, Eq. 7.2 is the frequency domain implementation of the KK relation given by Eq. 3.2, $sign(\omega)$ is the sign function, which is equal to 1 for $\omega > 0$, to 0 for $\omega = 0$, and to -1 for $\omega < 0$, and $\mathcal{F}^{-1}\{\cdot\}$ and $\mathcal{F}\{\cdot\}$ are the inverse Fourier and Fourier transform operators. In addition, since the nonlinear operations (*i.e.* square-root and logarithm ($ln(|h(n)|)$)) in the KK scheme introduces signal bandwidth broadening, it is necessary to utilize a relatively high oversampling rate (typically more than 4 samples per symbol) in the KK scheme's DSP. With a sufficiently high oversampling rate, the KK scheme allows the accurate reconstruction of the transmitted SSB signal, which avoids the nonlinear penalties caused by square-law detection. Additionally, similarly to the EDC techniques, the KK scheme's real time implementation can be potentially implemented in the frequency domain using FFTs and the overlap-and-save method, although the performance and complexity of this solution is yet to be evaluated.

7.2 Experimental Results

Experimental assessments of the system performance with the KK scheme were carried out using the transmission test-bed described in Chapter 4, Section 4.2. The joint optimization of CSPR value utilized at the transmitter and the resampling rate in the KK scheme's DSP was first discussed. Following this, the performance of the KK scheme was compared with that of the previously investigated digital linearization techniques, including the single-stage linearization filter [6] and the two-stage linearization filter [7, 8].

7.2.1 WDM Back-to-Back Performance Evaluation

In the WDM optical back-to-back operation, the required OSNR at the HD-FEC BER threshold of 3.8×10^{-3} versus CSPR at different resampling rates (varying from 2 Sa/symbol to 7 Sa/symbol) was plotted in Fig. 7.2. At a fixed resampling rate, a trade-off between the system penalties can be clearly observed. Signals operating at lower CSPR values suffered from large nonlinear penalty, since the minimum phase condition was not met, while high CSPR values led to higher required OSNR, due to the inclusion of excessive optical carrier power, which is included in the numerator of the OSNR calculation. On the other hand, the required OSNR values increased at lower resampling rates, especially at those less than 4 Sa/symbol, due to their failure to meet the Nyquist criterion for the spectrally broadened signals generated within the KK algorithm. The optimum CSPR shifted to higher values at lower sampling rates [9].

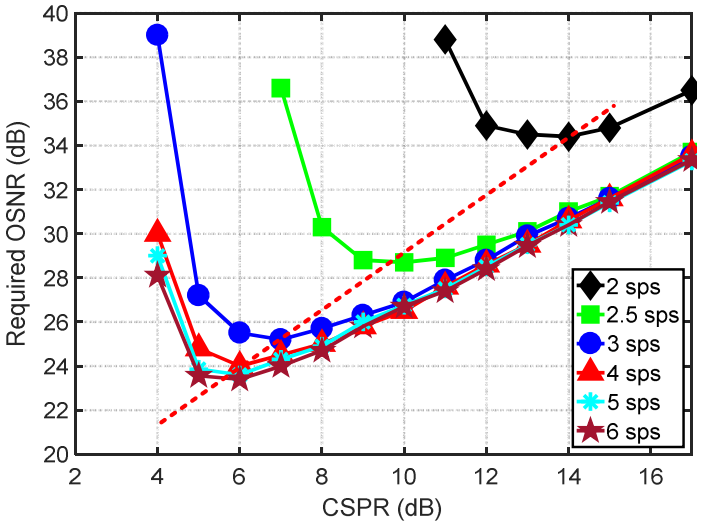

Fig. 7.2: Required OSNR at BER = 3.8×10^{-3} versus CSPR with different KK scheme resampling rate.

The required OSNR values at the optimum CSPR values over a range of resampling rates were plotted in Fig. 7.3. When the resampling rate was lower than 4 Sa/symbol (112 GSa/s), a significant increase in the required OSNR (from 24 dB at 4 Sa/symbol to 34.4 dB at 2 Sa/symbol) can be observed; the performance converged asymptotically to a required OSNR of 23.4 dB when utilizing 6 Sa/symbol (168 GSa/s) or more.

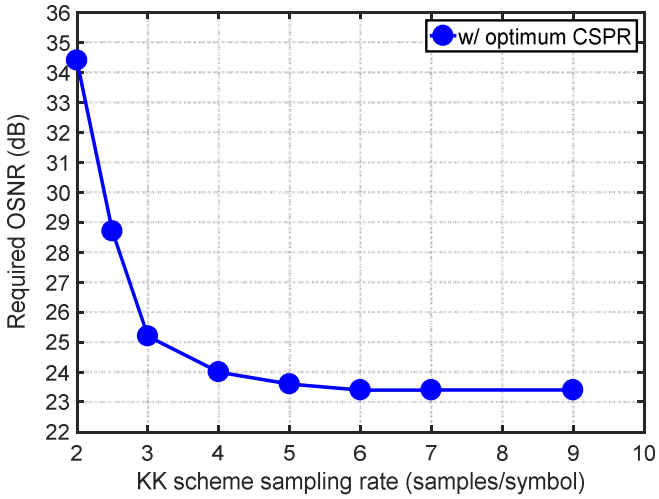

Fig. 7.3: Required OSNR at the optimum CSPR value versus KK scheme resampling rate.

The BER versus OSNR without and with the KK scheme at different resampling rates was plotted in Fig. 7.4. The required OSNR at the 3.8×10^{-3} BER threshold was found to be 33.5 dB without using receiver linearization scheme, reducing by 10.1 dB to 23.4 dB with the KK scheme operating at 6 Sa/symbol.

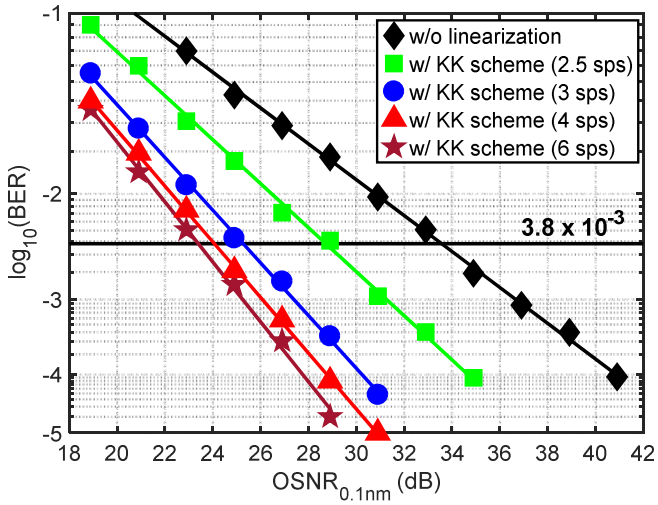

Fig. 7.4: BER versus OSNR with different KK scheme resampling rate.

In order to compare the KK scheme with other digital linearization techniques, Fig. 7.5 showed the optimum CSPR versus OSNR. It can be seen that, for the KK receiver, the optimum CSPR value was 5 dB lower than that for the case without linearization, for OSNRs above 23 dB (*c.f.* 2 dB lower with single-stage linearization filter and 3 dB with two-stage linearization filter). This is because the KK scheme has the strongest capability in suppressing the nonlinearities caused by square law detection. However, the optimum CSPR value was fixed at 4 dB for OSNR levels between 19 dB and 23 dB, since with lower CSPR values, the minimum phase condition was not fulfilled. Note that 6 Sa/symbol was utilized in the KK scheme to achieve the maximum effectiveness.

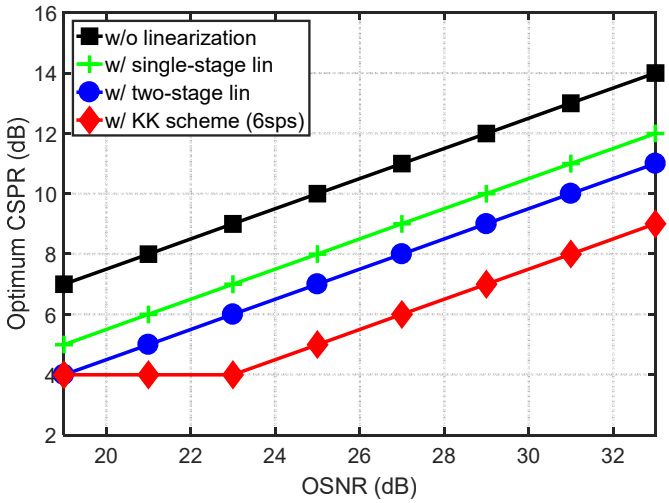

Fig. 7.5: Optimum CSPR versus OSNR without and with receiver-based digital single-stage linearization filter, two-stage linearization filter and KK scheme in back-to-back operation.

Fig. 7.6 plotted the optical back-to-back BER performance of systems without linearization and with single-stage linearization filter, two-stage linearization filter and with KK scheme. It can be observed that the KK scheme provided the best performance of all the techniques in the back-to-back operation.

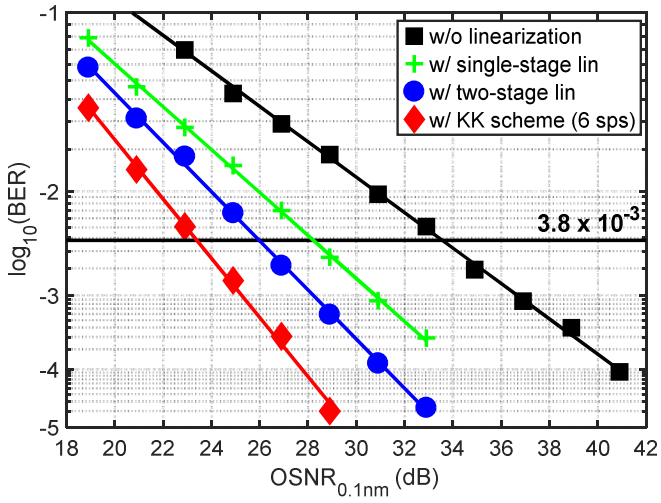

Fig. 7.6: BER versus OSNR without and with receiver-based digital single-stage linearization filter, two-stage linearization filter and KK scheme.

7.2.2 WDM Transmission Performance Evaluation

Next, the WDM transmission performance was assessed. Fig. 7.7 presented the BER at the optimum launch power (1.5 dBm) versus CSPR following transmission over 240 km. A trade-off between the system penalties can still be observed. With the lower resampling rates, the KK scheme's performance was degraded and the optimum CSPR values was increased. In contrast to the back-to-back operation in Fig. 7.2, the optimum CSPR was increased by approximately 2 dB at 6 Sa/symbol, this was because lower noise levels (BER < 10^{-3}) led to the high required CSPR.

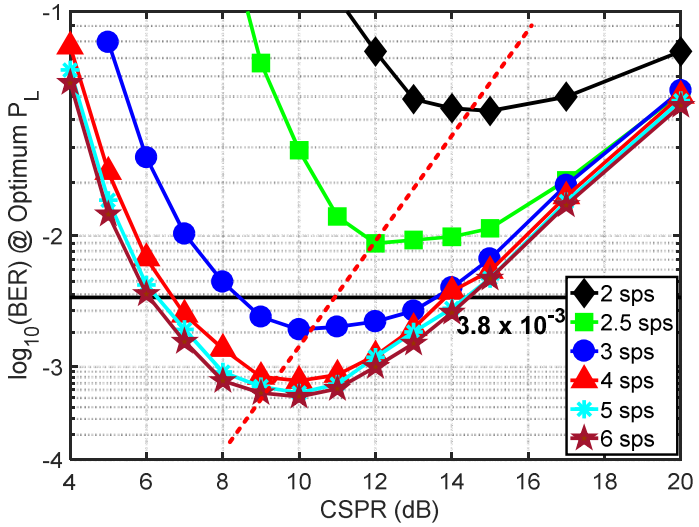

Fig. 7.7: BER at the optimum optical launch power versus CSPR with different KK scheme resampling rate in WDM transmission over 240 km.

Fig. 7.8 showed the BER (at the optimum launch power and CSPR value) versus the utilized resampling rate at transmission distances of 80, 160 and 240 km. The BERs were significantly decreased when resampling rates were increased from 2 Sa/symbol to 4 Sa/symbol, and converged for rates of 6 Sa/symbols and above, with the minimum BERs found to be 1.5×10^{-5}, 9.9×10^{-5} and 5.5×10^{-4} at 80 km, 160 km and 240 km respectively. Since the tradeoff between the ASE-noise and

fibre nonlinearity remained unchanged in multiple span fibre links, the optimum launch power was found to be the same, at 1.5 dBm, for all the transmission distances.

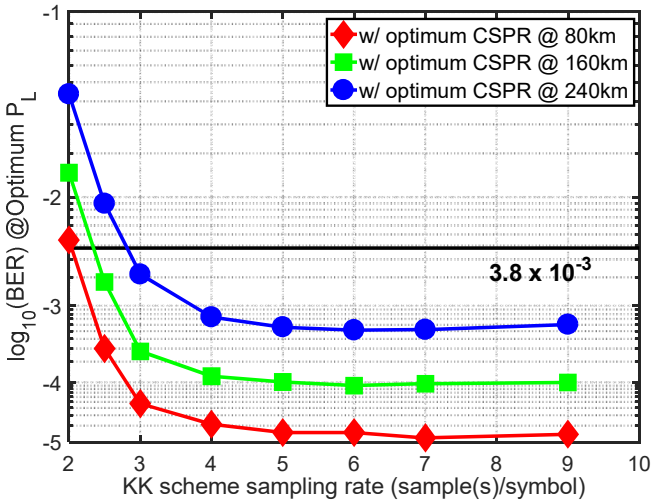

Fig. 7.8: BER at the optimum optical launch power versus KK scheme resampling rate at 80, 160 and 240 km WDM transmisisons.

To compare the performance of different digital linearization techniques, BER versus optical launch power per channel for 240 km WDM transmission and the BER versus transmission distance were plotted in Figs. 7.9 and Fig. 10 respectively. As can be observed in Fig. 7.9, the KK scheme (operating at 6 Sa/symbol) offered the best performance at all optical launch powers. Note that the optimum CSPR was 7 dB (5 dB reduction in contrast to the uncompensated case) when using the KK scheme with 6 Sa/symbol. Furthermore, in Fig. 7.10, it can be seen that the KK scheme also provided the best performance at all transmission distances. The received constellation diagrams with corresponding EVM values were shown in insets (a-d).

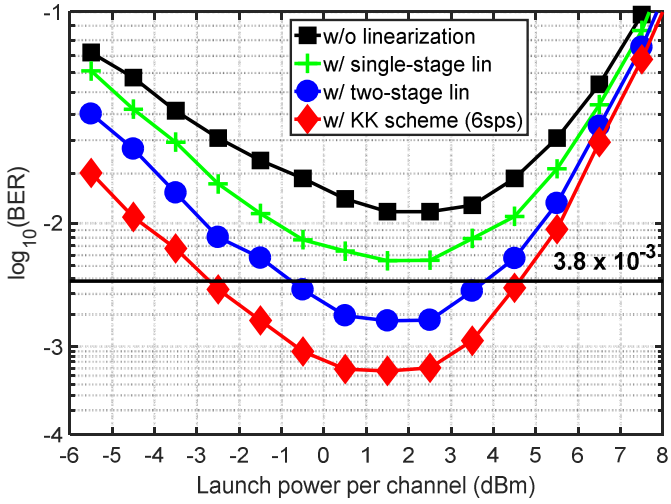

Fig. 7.9: BER versus optical launch power per channel without and with receiver-based digital single-stage linearization filter, two-stage linearization filter and KK scheme over 240 km WDM transmission.

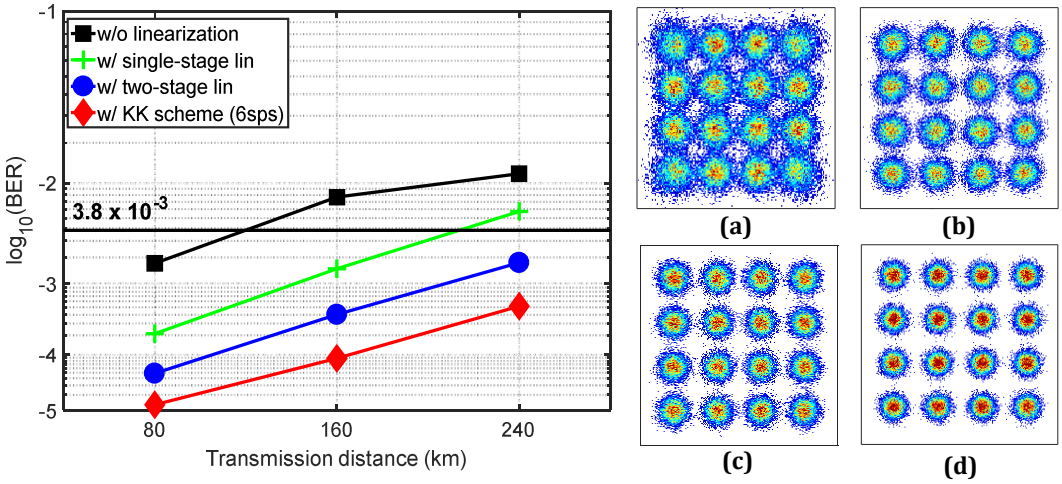

Fig. 7.10: BER versus transmission distance without and with receiver-based digital single-stage linearization filter, two-stage linearization filter and KK scheme. Insets: Received constellation diagrams over 240 km WDM transmission, (a) without (21.2%), (b) with sinlge-stage linearization filter (17.4%), (c) with two-stage linearization filter (15.8%) and (d) with KK scheme (13.6%).

After transmission over 240 km, the BER values for all four WDM channels were measured (Fig. 7.11). The average BER value achieved with the KK scheme was found to be 5.2×10^{-4}, resulting in a net optical SE of 3.18 b/s/Hz based on the theoretical hard-decision decoding bound. This value is currently the highest reported net ISD over this transmission distance at the time of publication.

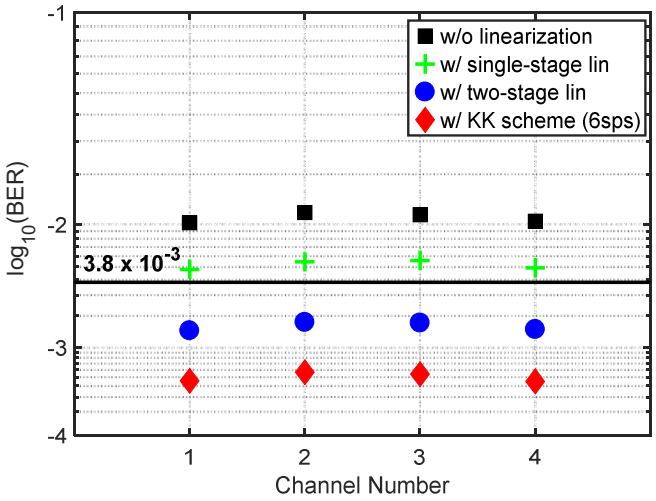

Fig. 7.11: BERs for each WDM channel without and with receiver-based digital single-stage linearization filter, two-stage linearization filter and KK scheme over 240 km transmission.

7.3 Summary

The technical details and performance evaluations of the receiver-based digital Kramers-Kronig scheme were presented in this chapter. Both theoretical analysis and practical experimental assessments indicate that the digital Kramers-Kronig scheme offers the possibility of fully reconstructing the transmitted signal from the detected signal's amplitude, and thus can provide superior linearization effectiveness compared to the other digital linearization techniques studied. In order to deal with the broadened bandwidth resulting from the square-root and logarithm

operations within the KK scheme, it is required to perform digital upsampling prior to the KK scheme, which leads to significantly increased DSP complexity. Good performance is achieved at 4 Sa/symbol, with optimum performance at ≥ 6 Sa/symbol. As high resampling rate leads to increased DSP complexity, the sampling rate utilized in practical implementation of KK scheme may be lower than the theoretical optimum of 6 Sa/symbol.

References

[1] A. Mecozzi, C. Antonelli, and M. Shtaif, "Kramers-Kronig coherent receiver," Optica, 3(11), 1220-1227 (2016).

[2] C. Antonelli, A. Mecozzi, and M. Shtaif, "Kramers-Kronig PAM transceiver," in *Optical Fiber Communication Conference*, OSA Technical Digest Series (CD) (Optical Society of America, 2017), paper Tu3I.5 (2017).

[3] Z. Li, M.S. Erkılınç, K. Shi, E. Sillekens, L. Galdino, B.C. Thomsen, P. Bayvel, and R.I. Killey, "SSBI mitigation and Kramer-Kronig scheme in single-sideband direct-detection transmission with receiver-based electronic dispersion compensation," J. Lightw. Technol., 35(10), 1887-1893 (2017).

[4] X. Chen, C. Antonelli, S. Chandrasekhar, G. Raybon, J. Sinsky, A. Mecozzi, M. Shtaif, and P. Winzer, "218-Gb/s single-wavelength, single-polarization, single-photodiode transmission over 125-km of standard single-mode fiber using Kramers-Kronig detection", in Optical Fiber Communication Conference, OSA Technical Digest Series (CD) (Optical Society of America, 2017), paper Th5B.6 (2017).

[5] H. Voelcker, "Demodulation of single-sideband signals via envelope detection," IEEE Trans. Commun. Technol. 14, 22-30, (1966).

[6] S. Randel, D. Pilori, S. Chandrasekhar, G. Raybon, and P. Winzer, "100-Gb/s discrete-multitone transmission over 80-km SSMF using single-sideband modulation with novel interference-cancellation scheme," in European Conference and Exhibition on Optical Communication (ECOC 2015), paper Mo.4.5.2.

[7] Z. Li, M. S. Erkilinc, R. Maher, L. Galdino, K. Shi, B. C. Thomsen, P. Bayvel, and R. I. Killey, "Two-stage linearization filter for direct-detection subcarrier modulation", IEEE Photon. Technol. Lett. 28(24), 2838-2841 (2016).

[8] Z. Li, M.S. Erkılınç, K. Shi, E. Sillekens, L. Galdino, B.C. Thomsen, P. Bayvel, and R.I. Killey, "112 Gb/s/λ WDM direct-detection Nyquist-SCM transmission at 3.15 (b/s)/Hz over 240 km SSMF enabled by novel beating interference compensation", in Optical Fiber Communication Conference, OSA Technical Digest Series (CD) (Optical Society of America, 2017), paper Tu3I.4.

[9] Z. Li, M.S. Erkılınç, K. Shi, E. Sillekens, L. Galdino, B.C. Thomsen, P. Bayvel, and R.I. Killey, "Joint optimisation of resampling rate and carrier-to-signal power ratio in direct-detection Kramers-Kronig receivers", in European Conference and Exhibition on Optical Communication (ECOC 2017), paper W.2.D.3.

CHAPTER 8

LINEARIZATION TECHNIQUES IN SINGLE-SIDEBAND DIRECT-DETECTION TRANSMISSION WITH RECEIVER-BASED ELELCTRONIC DISPERSION COMPENSATION

For complexity and cost reasons, it is preferable to compensate the accumulated dispersion of the fibre link digitally, a technique referred to as electronic dispersion compensation (EDC), rather than by utilizing optical compensation methods such as the through the use of dispersion compensating fibre (DCF). EDC can be performed at the transmitter (Tx-EDC) using the complex modulator to fully eliminate the accumulated dispersion [1]. However, the nonlinearity introduced by square-law photodetection can significantly impair the performance of direct-detection systems with receiver-based EDC (Rx-EDC). One proposal to overcome this limitation is to use optical single-sideband signalling, with the aim of preserving the optical phase waveform of the signal in the electrical domain after detection, allowing the use of Rx-EDC. This approach was demonstrated with the SSB PAM-2 signal format in [2]. However, even in the case of SSB signalling, the system performance with Rx-EDC is limited by the SSBI caused by square-law detection. In SSB OFDM and SSB Nyquist-SCM demonstrations to date, the dispersion is compensated by either a cyclic prefix (CP) to achieve dispersion tolerance [3-5] or by performing transmitter-based EDC (Tx-EDC) [6, 7]. However, the disadvantages include the reduction in the achievable spectral efficiency due to the CP, or increased complexity of the system operation due to the required knowledge of the link's cumulative dispersion at the transmitter and hence the need for feedback from the receiver. Moreover, the increase of peak-to-average power ratio (the change of the transmitted signal waveform causes peaks in the amplitude due to constructive interference) caused by Tx-EDC may lead to larger quantization noise from the digital-to-analogue converters with limited number of resolution levels and modulation nonlinearities. Thanks to the recent development of digital linearization techniques [8-15], the nonlinear SSBI distortion can be partially compensated or avoided. As suggested in [8], effective linearization techniques offer the possibility of performing the compensation of linear optical effects, such as dispersion, at the receiver with similar performance to systems with pre-compensation.

In this chapter, we assess the performance of Rx- and Tx-EDC schemes, both in theory and experiments, in the presence of the four proposed receiver-based digital linearization techniques described in the previous chapters, namely the single-stage linearization filter and the non-iterative SSBI E&C technique (Chapter 5), the two-stage linearization filter (Chapter 6), and the Kramers-Kronig scheme (Chapter 7). The experimental demonstrations were carried out using a 37.5 GHz-spaced 4 × 112 Gb/s spectrally-efficient WDM SSB 16-QAM Nyquist-SCM DD system over transmission distances of 80 km, 160 km and 240 km. The performance of both Tx- and Rx-EDC schemes were compared for the cases without and with the linearization techniques. Experimental results indicate that the difference in system performance between Tx- and Rx-EDC depends strongly on the performance of the linearization scheme being used, and that they can achieve

similar performance provided an effective linearization technique is performed prior to dispersion compensation at the receiver [16, 17].

8.1 Principle of Operation

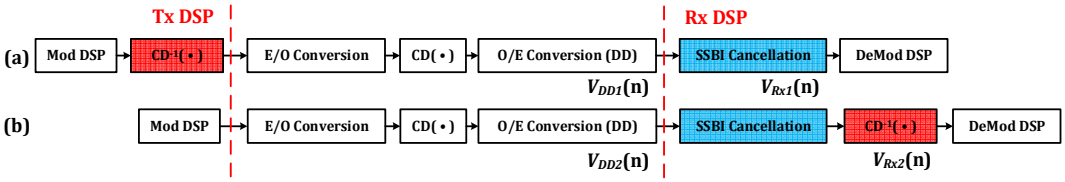

Fig. 8.1: Direct-detection system diagram with (a) Tx-EDC and (b) Rx-EDC combined with SSBI cancellation. Mod & Demod DSP: Modulation and demodulation DSP for SSB Nyquist-SCM signal. O/E conversion consists of an optical band-pass filter follwed by a single-ended photodiode.

In order to assess the effectiveness of Rx- and Tx-EDC combined with linearization techniques, the two DD systems shown in Figs. 8.1(a) and 8.1(b) are considered. For the first configuration (Fig. 8.1(a)), the SSB QAM SCM signal $E_0(n)$ is generated at the transmitter, following the modulation DSP. Tx-EDC, denoted as $(H_{CD}^{-1}(\bullet))$, is performed by pre-distorting the signal with the inverse of the linear lossless channel response due to chromatic dispersion in the frequency domain, as proposed in [1], and details of EDC operation can be found in Section 2.3.2. Following this, the optical carrier, $E_{carrier}(n)$ is added during the electrical-to-optical conversion using an IQ-modulator. After the transmission and square-law detection, the normalized detected double-sideband (DSB) signal, $V_{DD}(n)$ can be written as:

$$\begin{aligned} V_{DD1}(n) &= \left|H_{CD}\left(E_{carrier}(n) + H_{CD}^{-1}\left(E_0(n)\right)\right)\right|^2 \\ &= E_{carrier}^2(n) + 2Re[E_{carrier}(n)\cdot E_0(n)] + |E_0(n)|^2 \end{aligned} \tag{8.1}$$

where $Re[x]$ signifies the real part of x. In the RHS of Eq. 8.1, the first and second terms are the direct current (DC) and the desired carrier-signal beating products (CSBP), the third term is the signal-signal beating term. Assuming that the third term can be completely removed by performing digital receiver linearization, the received signal prior to the demodulation DSP, $V_{Rx1}(n)$ only includes the DC and the desired CSBP terms and can be re-written as follows:

$$V_{Rx1}(n) \approx E_{carrier}^2(n) + 2Re[E_{carrier}(n)\cdot E_0(n)] \tag{8.2}$$

For the second configuration shown in Fig. 8.1(b), if Rx-EDC is used instead of Tx-EDC, the detected signal $V_{DD2}(n)$ is given by:

$$V_{DD2}(n) = E_{carrier}^2(n) + 2Re\left[E_{carrier}(n)\cdot H_{CD}\left(E_0(n)\right)\right] + \left|H_{CD}\left(E_0(n)\right)\right|^2 \tag{8.3}$$

In contrast to Eq. 8.1, it can be seen that the second and third terms become the beating products between the dispersed signal with the optical carrier and with itself, respectively. If Rx-EDC, as proposed in [2], is performed without linearizing the receiver, the frequency-dependent phase rotation of the SSBI terms due to dispersion, denoted as $H_{CD}^{-1}(|H_{CD}(E_0(n))|^2)$, prevents the Rx-EDC from accurately recovering the undispersed signal. Therefore, the performance of Rx-EDC is significantly degraded in comparison to that of Tx-EDC. However, assuming that the third term

can be removed to a large extent by performing digital linearization and Rx-EDC is utilized afterwards, the signal before the demodulation DSP $V_{Rx2}(n)$ becomes:

$$\begin{aligned} V_{Rx2}(n) &\approx H_{CD}^{-1}\left(E_{carrier}^{2}(n) + 2Re\left[E_{carrier}(n) \cdot H_{CD}\left(E_0(n)\right)\right]\right) \\ &\approx E_{carrier}^{2}(n) + 2Re[E_{carrier}(n) \cdot E_0(n)] \end{aligned} \tag{8.4}$$

By comparing Eq. 8.2 and Eq. 8.4, it can be seen that the Rx-EDC can achieve similar performance to Tx-EDC provided the SSBI term is removed. Therefore, it can be concluded that the performance of Rx-EDC depends on the effectiveness of the linearization achieved through the beating interference compensation scheme. It should be noted that, in this study, both Tx- and Rx-EDC is carried out by linear convolution with the inverse of the channel response, as described in Chapter 2.

8.2 Experimental Results

An optical transmission test-bed, shown in Fig. 4.3, Chapter 4, Section 4.2, was used to experimentally assess the performance of the transceiver designs discussed in Section 8.1. Unlike the experimental results shown in Chapters 4 – 7, which utilize a WDM channel spacing of 35 GHz to achieve the maximum achievable optical ISDs, this work was carried out with a 37.5 GHz WDM channel spacing (a potential standard channel spacing for 100 G solution), leading to a gross optical ISD of 3.0 (b/s)/Hz. The performance of the transceiver with Rx-EDC was compared with that using Tx-EDC for the case of no linearization and with different linearization techniques, including the single-stage linearization filter, two-stage linearization filter, non-iterative SSBI E&C and the KK scheme.

8.2.1 Without Receiver Linearization

As discussed in Section 8.1, if Rx-EDC is performed without compensating the beating interference, the introduced additional distortion prevents the receiver from recovering the dispersed signal. A comparison of the performance of Rx-EDC and Tx-EDC without beating interference compensation was plotted in Figs. 8.2 and 8.3. Significant performance differences can be observed between the Rx-EDC and Tx-EDC. As shown in Fig. 8.2, for transmission distances from 80 km to 240 km, the BER ranged from 6.3×10^{-3} to 2.4×10^{-2} for Rx-EDC whereas much lower BER values were obtained with Tx-EDC (from 1.3×10^{-3} to 9.3×10^{-3}), as predicted by the analysis in Section 8.1; the nonlinear beating interference prevented the Rx-EDC from accurately recovering the undispersed signal. Fig. 8.3 showed a comparison of both EDC schemes through plots of BER versus optical launch power per channel. Obvious performance differences between Rx-EDC and Tx-EDC can be observed at all optical launch power values.

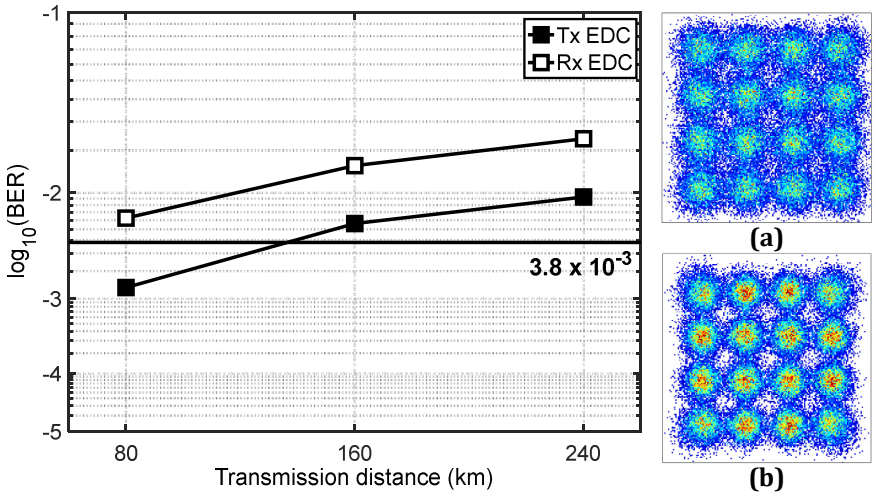

Fig. 8.2: BER vs transmission distance with Tx-EDC and Rx-EDC without beating interference mitigation.Inset: Received constellation with (a) Rx-EDC (EVM = 23.0%) and (b) Tx-EDC (EVM = 20.7%).

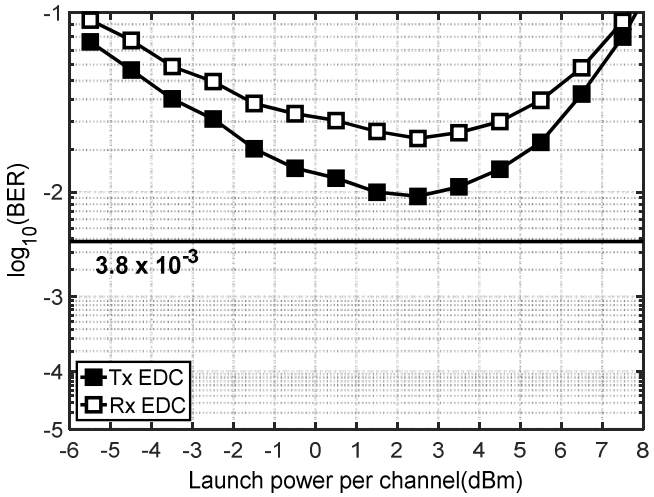

Fig. 8.3: BER vs launch power per channel with Tx-EDC and Rx-EDC at 240 km without beating interference mitigation.

8.2.2 With Single-Stage Linearization Filter

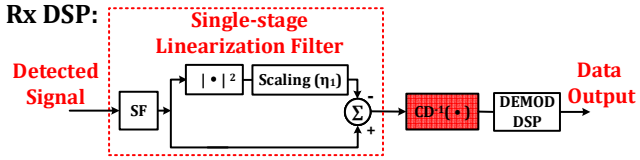

Fig. 8.4: Receiver DSP including single-stage linearization filter and Rx-EDC. Demod DSP: Conventional demodulation DSP for SSB Nyquist-SCM signal. SF: Sideband filter.

Fig. 8.4 showed the Rx DSP design using the single-stage linearization filter followed by Rx-EDC. In the single-stage linearization filter (details of which can be found in Chapter 5), a digital SSB signal is first generated from the detected signal using a sideband filter (SF), and an approximation of the waveform of the signal-signal beating products is calculated based on this SSB signal, which is then subtracted from the signal to partially compensate the SSBI. The advantage of this technique

is its use of a very simple DSP structure. However, as the calculation of signal-signal beating products is based on the received distorted signal, this technique itself introduces extra beating interference, thus limiting the compensation performance. The performance difference between Rx- and Tx-EDC schemes combined with single-stage linearization filter was shown in Figs. 8.5 and 8.6. It can be observed that the BER was reduced and also the performance difference between Rx-EDC and Tx-EDC was reduced. Fig. 8.5 showed that from 80 km to 240 km, BER ranged from 1.9×10^{-4} to 4.0×10^{-3} for Rx-EDC and from 7.5×10^{-5} to 2.1×10^{-3} for Tx-EDC, BERs being approximately halved with the use of Tx-EDC. Furthermore, the transmission performance of both EDC schemes over a range of launch powers was also improved, as plotted in Fig. 8.6.

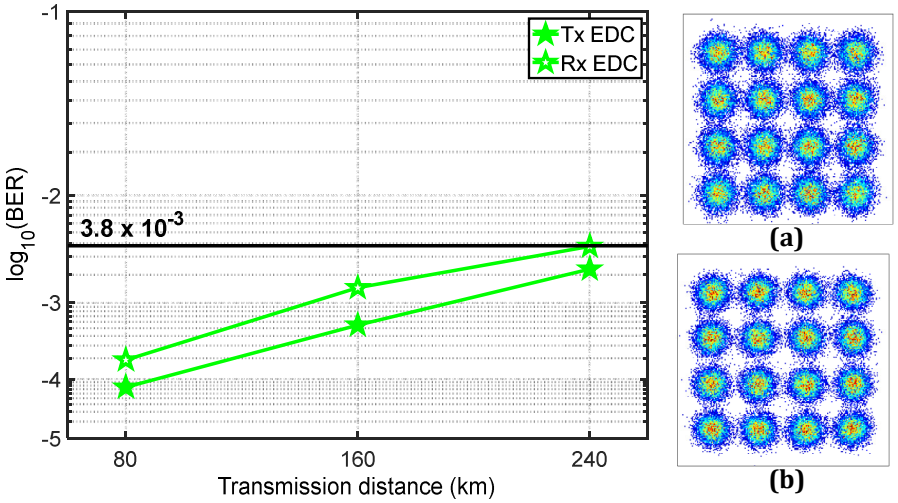

Fig. 8.5: BER vs transmission distance with Tx-EDC and Rx-EDC using the single-stage linearization filter. Inset: Received constellation with (a) Rx-EDC (EVM = 18.5%) and (b) Tx-EDC (EVM = 16.9%).

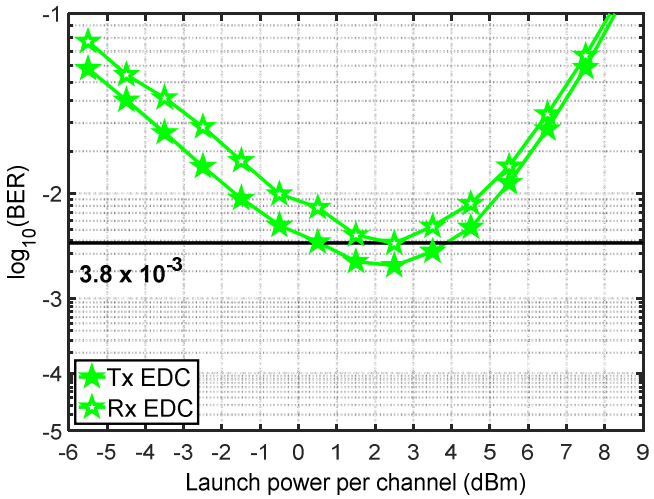

Fig. 8.6: BER vs launch power per channel with Tx-EDC and Rx-EDC at 240 km using the single-stage linearization filter.

8.2.3 With Two-Stage Linearization Filter

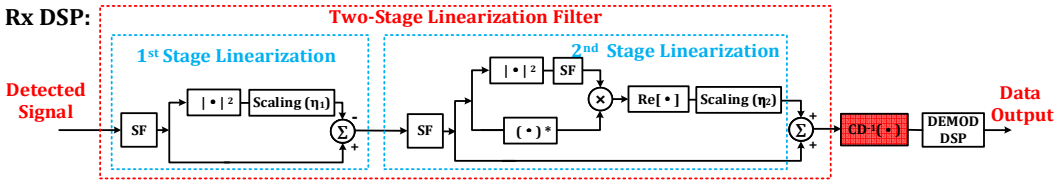

Fig. 8.7: Receiver DSP using the two-stage linearization filter and Rx-EDC. Demod DSP: Conventional demodulation DSP for SSB Nyquist-SCM signal. SF: Sideband filter.

The Rx DSP design using the two-stage linearization filter followed by Rx-EDC was shown in Fig. 8.7. In the two-stage linearization filter (Chapter 6), a second linearization stage is applied to remove the majority of the unwanted beating interference (mainly signal-SSBI beating products) introduced by the first linearization stage, the latter being identical to the above-mentioned single-stage linearization filter. Consequently, the second stage further enhances the compensation gain. Comparisons between both EDC schemes utilizing the two-stage linearization filter were shown in Figs. 8.8 and 8.9 respectively. Further improvement of BERs was achieved and Rx-EDC and Tx-EDC offered very similar performance. As can be seen from Fig. 8.8, from 80 km to 240 km, the BER ranged from 4.8×10^{-5} to 1.5×10^{-3} when using Rx-EDC and from 3.4×10^{-5} to 1.2×10^{-3} with Tx-EDC, which was marginally lower. The slight difference in obtained BER values shown in Figs. 8.8 and 8.9 was mainly due to the residual uncompensated beating terms introduced by the second-stage of the linearizing filter.

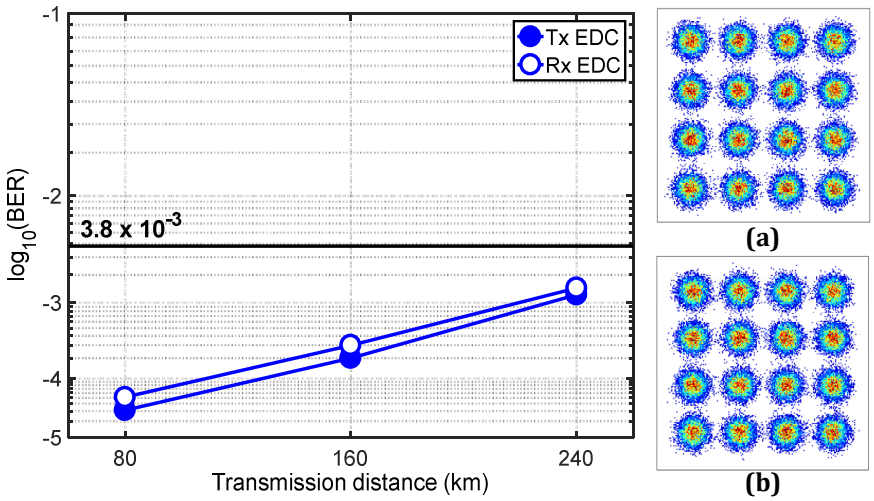

Fig. 8.8: BER vs transmission distance with Tx-EDC and Rx-EDC using the two-stage linearization filter. Inset: Received constellation with (a) Rx-EDC (EVM = 15.7%) and (b) Tx-EDC (EVM = 15.3%).

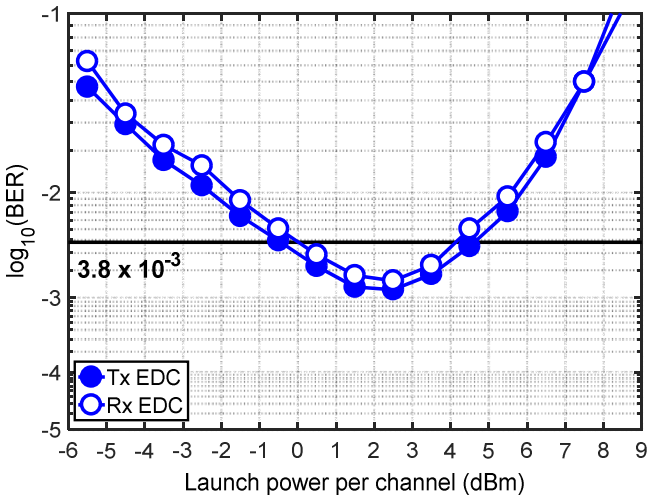

Fig. 8.9: BER vs launch power per channel with Tx-EDC and Rx-EDC at 240 km using the two-stage linearization filter.

8.2.4 With Non-iterative SSBI Estimation and Cancellation

Rx DSP:

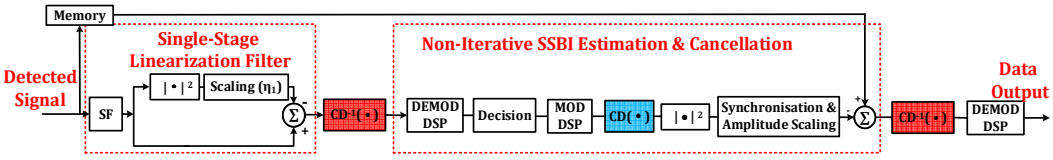

Fig. 8.10: Receiver DSP using the non-iterative SSBI estimation and cancellation and Rx-EDC. Mod & Demod DSP: Conventional modulation and demodulation DSP for SSB Nyquist-SCM signal. SF: Sideband filter.

The Rx DSP including the non-iterative SSBI E&C technique and Rx-EDC was shown in Fig. 8.10. The non-iterative SSBI E&C technique (Chapter 5) is an updated version of the previously proposed iterative SSBI E&C scheme (Chapter 4); it offers compensation performance similar to the iterative SSBI E&C technique and avoids the requirement for multiple (typically three or four) symbol decision-based SSBI reconstruction processes, which requires multiple IFFT/FFT pairs (the same digital hardware in the iteration cannot be reused for continuous transmitted data, thus each iteration requires its own dedicated DSP hardware). Unlike the linearization filtering schemes, this technique does not introduce additional unwanted beating products, and thus it offers potentially better compensation gain especially at higher OSNR levels. However, the limitation of this technique is its dependency on the accuracy of the symbol decision making, which noticeably degrades its performance at lower OSNR values. Performance comparisons between both EDC schemes with the non-iterative SSBI E&C technique were carried out (Figs. 8.11 and 8.12). Again, very similar performance can be observed. Fig. 8.11 showed that from 80 km to 240 km, BER ranged from 1.9×10^{-5} to 2.4×10^{-3} for Rx-EDC and from 2.2×10^{-5} to 2.2×10^{-3} for Tx-EDC. Similar performance was also observed over a range of optical launch powers at 240 km transmission, as shown in Fig. 8.12. It should be mentioned that, in contrast to the case of Tx-EDC, if Rx-EDC is performed, it is required to apply chromatic dispersion to the reconstructed signal-signal beating terms in the non-iterative SSBI E&C process, because the transmitted signal prior to the square-law detection has been chromatically dispersed.

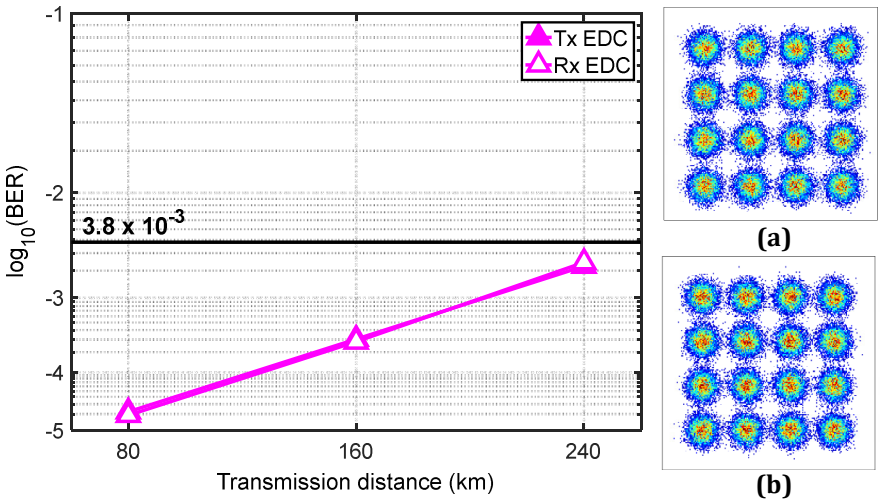

Fig. 8.11: BER vs transmission distance with Tx-EDC and Rx-EDC using the non-iterative SSBI estimation and cancellation. Inset: Received constellation with (a) Rx-EDC (EVM = 17.2%) and (b) Tx-EDC (EVM = 16.8%).

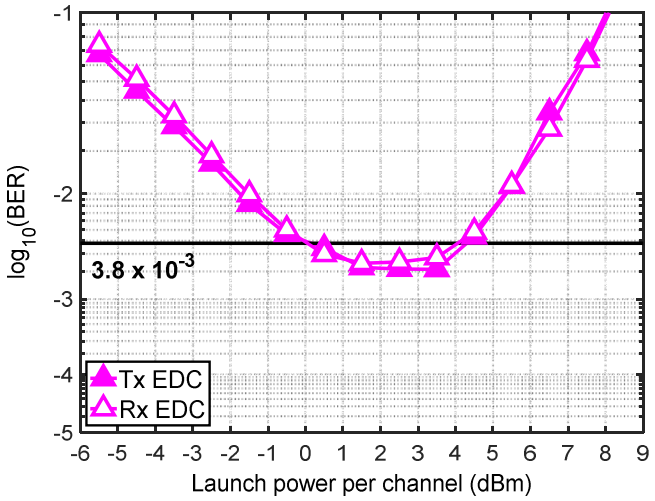

Fig. 8.12: BER vs launch power per channel at 240 km with Tx-EDC and Rx-EDC with non-iterative SSBI estimation and cancellation.

8.2.5 With Kramers-Kronig Scheme

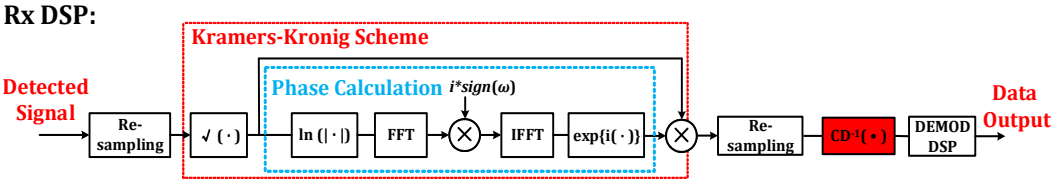

Fig. 8.13: Receiver DSP using the Kramers-Kronig algorithm and Rx-EDC. Mod & Demod DSP: Conventional modulation and demodulation DSP for SSB Nyquist-SCM signal. SF: Sideband filter.

The recently-proposed Kramers-Kronig scheme (Chapter 7) was also tested with Rx-EDC in the experiment. Fig. 8.13 showed the corresponding Rx DSP. When the KK algorithm was applied in system, Tx- and Rx-EDC schemes were found to achieve the same performance while, at the same time, the achieved BER was lower than all other linearization schemes. As shown in Figs. 8.14 and 8.15, the BER ranged from 1.0×10^{-5} to 3.6×10^{-4} for Rx-EDC and from 1.4×10^{-5} to 4.0×10^{-4} for Tx-

EDC, and both EDC schemes offered the same performance over the investigated range of launch powers. Note that, a relatively high oversampling rate (4 Sa/symbol) was used in the KK DSP to achieve good compensation performance. However, as discussed in Chapter 7, more than 6 Sa/symbol are needed for the optimum performance.

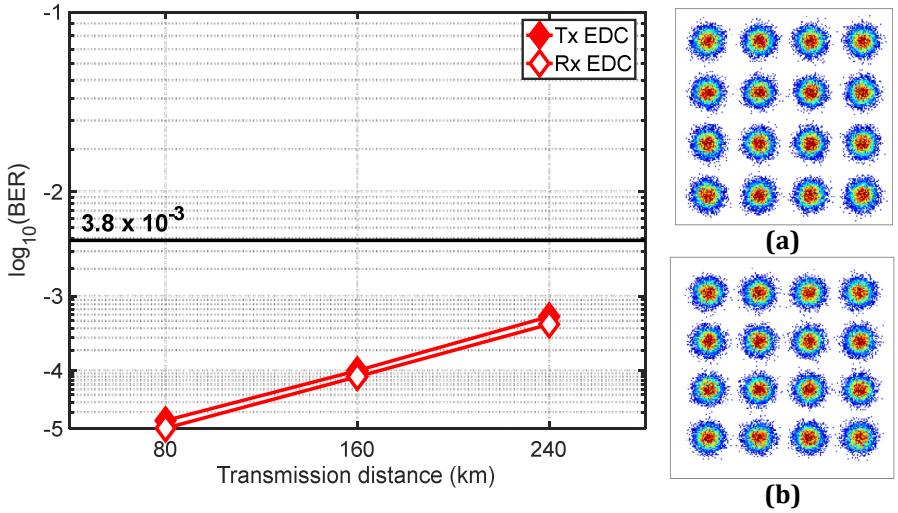

Fig. 8.14: BER vs transmission distance with Tx-EDC and Rx-EDC using the Kramers-Kronig algorithm. Inset: Received constellation with (a) Rx-EDC (EVM = 13.2%) and (b) Tx-EDC (EVM = 13.3%).

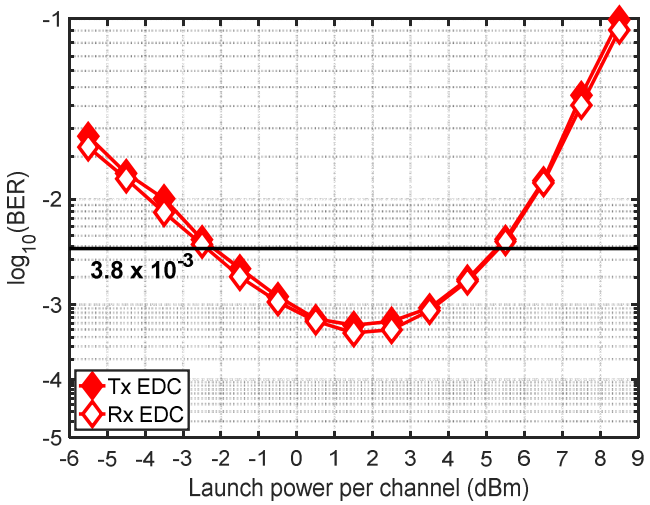

Fig. 8.15: BER vs launch power per channel at 240 km with Tx-EDC and Rx-EDC with KK scheme.

8.2.6 Comparsion of Different Schemes

Finally, all four WDM channels were tested with Rx-EDC over a transmission distance of 240 km, with similar performance across all channels being observed (Fig. 8.16). Assuming a HD-FEC overhead of 7%, allowing a pre-FEC BER = 3.8×10^{-3}, the net information spectral density of the WDM signal was calculated to be 2.8 b/s/Hz.

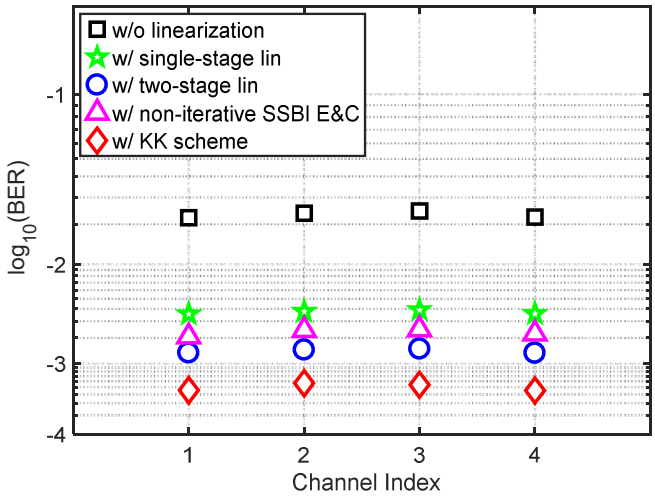

Fig. 8.16: BER versus WDM channel index with Rx-EDC in case of without beating interference compensation, and by applying different linearization techniques after 240 km transmission.

8.3 Summary

In this chapter, both theoretical and experimental studies were presented, analysing the effectiveness of performing electronic dispersion compensation (EDC) either at the transmitter (Tx-EDC) or at the receiver (Rx-EDC) in SSB SCM DD transceivers combined with different receiver linearization techniques. The four different digital linearization techniques described in the previous chapters, including the single-stage linearization filter, the two-stage linearization filter, the non-iterative SSBI E&C technique and the Kramers-Kronig scheme all operating with either Tx- or Rx-EDC were assessed. The performance of the EDC schemes was experimentally evaluated in a 37.5 GHz-spaced 4×112 Gb/s spectrally-efficient (2.8 b/s/Hz net ISD) WDM direct-detection single-sideband 16-QAM Nyquist-SCM DD system over reaches of up to 240 km of uncompensated SSMF. The experimental results indicate that the performance difference of Tx and Rx-EDC depends on the effectiveness of the linearization scheme that is used, and that they can achieve similar performance provided the beating interference is effectively suppressed. Therefore, it becomes possible to perform the EDC at the receiver rather than at the transmitter, which simplifies the system operation since knowledge of link dispersion is not required at the transmitter. Due to the reduction in complexity, the proposed solution increases the suitability of WDM DD SSB SCM signalling for short- and medium-reach applications such as metro networks, back-haul, access and inter-data centre links.

References

[1] R.I. Killey, P.M. Watts, V. Mikhailov, M. Glick, and P. Bayvel, "Electronic dispersion compensation by signal predistortion using digital processing and a dual-drive Mach-Zehnder modulator," IEEE Photon. Technol. Lett., 17(3), 714-716 (2005).

[2] M. Sieben, J. Conradi, and D.E. Dodds, "Optical single sideband transmission at 10 Gb/s using only electrical dispersion compensation" J. Lightw. Technol., 17(10), 1742-1749 (1999).

[3] Q. Zhang, Y. Fang, E. Zhou, T. Zuo, L. Zhang, G.N. Liu and X. Xu, "C-band 56Gbps transmission over 80-km single mode fiber without chromatic dispersion compensation by using intensity-modulation direct-detection," in *European Conference and Exhibition on Optical Communication* (ECOC 2014), paper P.5.19.

[4] L. Zhang, T. Zuo, Y. Mao, Q. Zhang, E. Zhou, G.N. Liu, and X. Xu. "Beyond 100-Gb/s transmission over 80-km SMF using direct-detection SSB-DMT at C-band." J. Lightw. Technol., 34(2), 723-729 (2016).

[5] S. Randel, D. Pilori, S. Chandrasekhar, G. Raybon, and P. Winzer, "100-Gb/s discrete-multitone transmission over 80-km SSMF using single-sideband modulation with novel interference-cancellation scheme," in *European Conference and Exhibition on Optical Communication* (ECOC 2015), paper Mo.4.5.2.

[6] M.S. Erkılınç, Z. Li, S. Pachnicke, H. Griesser, B.C. Thomsen, P. Bayvel, and R.I. Killey, "Spectrally-efficient WDM Nyquist-pulse-shaped 16-QAM subcarrier modulation transmission with direct detection," J. Lightw. Technol., 33(15), 3147-3155 (2015).

[7] K. Zou, Y. Zhu, F. Zhang and Z. Chen, "Spectrally efficient terabit optical transmission with Nyquist 64-QAM half-cycle subcarrier modulation and direct-detection," Opt. Lett., 41(12), 2767-2770 (2016).

[8] A. Mecozzi, C. Antonelli, and M. Shtaif, "Kramers-Kronig coherent receiver," Optica, 3(11), 1220-1227 (2016).

[9] Z. Li, M. S. Erkilinc, R. Maher, L. Galdino, K. Shi, B. C. Thomsen, P. Bayvel, and R. I. Killey, "Two-stage linearization filter for direct-detection subcarrier modulation," IEEE Photon. Technol. Lett., 28(24), 2838-2841 (2016).

[10] Z. Li, M. S. Erkilinc, R. Maher, L. Galdino, K. Shi, B. C. Thomsen, P. Bayvel, and R. I. Killey, "Reach enhancement for WDM direct-detection subcarrier modulation using low-complexity two-stage signal-signal beat interference cancellation", in *European Conference and Exhibition on Optical Communication* (ECOC 2016), paper M.2.B.1.

[11] W.R. Peng, X. Wu, K. Feng, V.R. Arbab, B. Shamee, J. Yang, L. C. Christen, A. E. Willner, and S. Chi, "Spectrally efficient direct-detected OFDM transmission employing an iterative estimation and cancellation technique," Opt. Express, 17(11), 9099-9111 (2009).

[12] Z. Li, M. S. Erkılınç, S. Pachnicke, H. Griesser, R. Bouziane, B.C. Thomsen, P. Bayvel, and R.I. Killey, "Signal-signal beat interference cancellation in spectrally-efficient WDM direct-detection Nyquist-pulse-shaped 16-QAM subcarrier modulation," Opt. Express, 23(18), 23694-23709 (2015).

[13] C. Sánchez, B. Ortega, and J. Capmany, "System performance enhancement with pre-distorted OOFDM signal waveforms in IM/DD systems," Opt. Express, 22(6), 7269-7283 (2014).

[14] C. Ju, N. Liu, X. Chen, and Z. Zhang, "SSBI mitigation in a RF-tone-based VSSB-OFDM system with a frequency-domain Volterra series equalizer" J. Lightw. Technol., 33(23), 4997-5006 (2015).

[15] Z. Li, M.S. Erkilinc, L. Galdino, K. Shi, B.C. Thomsen, P. Bayvel, and R.I. Killey, "Comparison of digital signal-signal beat interference compensation techniques in direct-detection subcarrier modulation systems," Opt. Express, 24(25), 29176-29189 (2016).

[16] Z. Li, M.S. Erkılınç, K. Shi, E. Sillekens, L. Galdino, B.C. Thomsen, P. Bayvel, and R.I. Killey, "SSBI mitigation and Kramer-Kronig scheme in single-sideband direct-detection transmission with receiver-based electronic dispersion compensation," J. Lightw. Technol., 35(10), 1887-1893 (2017).

[17] Z. Li, M.S. Erkılınç, K. Shi, E. Sillekens, L. Galdino, B.C. Thomsen, P. Bayvel, and R.I. Killey, "Improvement of digital chromatic dispersion post-compensation by utilizing beating interference mitigation for direct-detection SSB Nyquist-SCM", in Optical Fiber Communication Conference, OSA Technical Digest Series (CD) (Optical Society of America, 2017), paper Th3D.2.

CHAPTER 9

FUNDEMENTAL PERFORMANCE LIMIT OF 100G TRANSCEIVERS AND FURTHER DEVELOPMENTS

As mentioned in the previous chapters, it may be favourable to utilize direct detection systems for metro applications because of the lower-cost optical hardware structure [1, 2]. However, the performance of the DD systems is severely degraded because of SSBI. Recently, a beating interference cancellation balanced receiver (BICBRx) has been proposed to offer superior performance to overcome the SSBI penalty [3, 4], but its receiver optical hardware complexity is significantly increased due to the requirement for two single-ended photodiodes and a very narrow optical filter (<1 GHz) to suppress the optical carrier. On the other hand, since the SSBI products fall over a bandwidth equal to that of the original subcarrier signal (B_{sc}), an alternative solution to avoid the SSBI penalty is to leave a sufficient spectral guard-band ($B_{gap} \geq B_{sc}$) between the optical carrier and the subcarrier signal [5, 6]. However, drawbacks such as halving the achievable optical ISD and wasting of approximately 50% of the electrical and optical components' bandwidths make it very challenging to achieve high ISD ($\geq$ 3 (b/s)/Hz) with this approach. Fortunately, as described in Chapters 4-7, recently demonstrated digital SSBI compensation techniques have been shown to be an effective approach, allowing the use of narrow or even no guard-band without requiring a change to the optical hardware design [7-17].

In this chapter, we first present a theoretical assessment of different 112 Gb/s per channel system architectures through numerical simulations. The transceivers being studied include the coherent (homodyne and heterodyne) and DD systems without and with different optical or digital linearization techniques. Following this, in Section 9.2, some further developments of this work are described. We explore the optical ISD limits of the SSB SCM DD transceiver, through experiments with higher-order QAM modulation format. We successfully transmitted four WDM channels with 35 GHz channel spacing to achieve a record net ISD of 4.54 b/s/Hz over 80 km (exceeding the previous record of 3.58 b/s/Hz for this distance [21]) using 168 Gb/s per channel SSB 64-QAM Nyquist-SCM.

9.1 Performance Assessment of Different 100 G Transceiver Structures

This section presents the theoretical performance comparisons of different 112 Gb/s/λ coherent and direct-detection transceiver structures based on simulations of ideal transceivers. Fig. 9.1 shows a schematic diagram of the different receiver architectures. The coherent receivers considered include conventional homodyne and heterodyne structures [18, 19] (shown in Figs. 9.1(a) and 9.1(b)), while the direct-detection receiver structures include a balanced receiver-based BICBRx (Fig. 8.1(c)) [3, 4], a single-ended photodiode-based system with a guard-band

sufficiently large to avoid SSBI [5, 6] (Fig. 9.1(d)), and systems without guard-band but with digital receiver linearization techniques (Fig. 9.1(e)) [7, 8, 17].

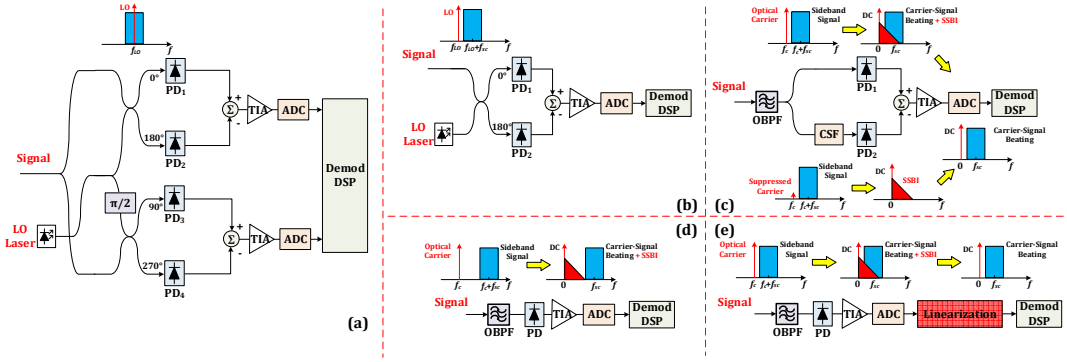

Fig. 9.1: Schematic diagrams of different 100G receiver architectures. (a) Coherent homodyne, (b) coherent heterodyne, (c) beating interference cancellation balanced receiver (BICBRx), (d) DD with guard-band and (e) DD without guard-band and with digital linearization technique: OBPF: Optical band-pass filter, PC: Polarization controller, LO: Local oscillator, CSF: Carrier suppression filter, PD: Photodiode, TIA: Transimpedance amplifier, ADC: Analogue-to-digital converter, DEMOD DSP: Demodulation DSP for baseband Nyquist (coherent homodyne systems) signal or SSB Nyquist-SCM signal (coherent heterodyne and DD systems).

In order to assess the performance difference between these transceiver architectures, simulations of ideal systems were carried out. Practical limiting parameters such as digital-to-analogue converter (DAC)/analogue-to-digital convertor (ADC) quantization noise and electrical low-pass filtering effects were neglected. Moreover, an ideal rectangular ("brickwall-shaped") optical band-pass filter was assumed, and the carrier suppression filter (CSF) used in the BICRx had a 1MHz 3-dB bandwidth to remove the optical carrier completely. The modulation formats being used in all cases were 112 Gb/s baseband 16QAM Nyquist signals for coherent systems and SSB 0.51×cycle (nearly half-cycle) 16QAM Nyquist-SCM for DD systems, generated using root-raised cosine (RRC) filters with a roll-off parameter of 0.01. The reason for using SSB half-cycle QAM Nyquist-SCM modulation format for DD system was that the QAM signalling, SSB, Nyquist pulse shaping, and no spectral guard-band increase the achievable ISD whilst Nyquist-SCM exhibits lower peak-to-average power ratio (PAPR in the range of 7 dB) than that of orthogonal frequency division multiplexing (OFDM) due to a single subcarrier being utilized. The digital receiver linearization techniques being used were single-stage, two-stage linearization filters and the Kramers-Kronig scheme, due to their performance and implementation advantages over the other compensation schemes, as discussed in Chapters 4-7.

The back-to-back system performance was evaluated by amplified spontaneous emission (ASE) noise loading, and bit error ratio (BER) as a function of optical signal-to-noise ratio (OSNR at a resolution of 0.1 nm) was plotted in Fig. 9.2. Note that, since an optical carrier is added at the transmitter to recover the signal from the carrier-signal beating products in the case of the direct detection systems, it is important to optimize the optical CSPR value at each OSNR for the DD systems. The coherent homodyne results shown in this figure were based on simulations of a single-polarization 112 Gb/s homodyne coherent transceiver. For polarization multiplexed 112 Gb/s (2 × 56 Gb/s) homodyne coherent transceiver, the required OSNR would be the same but with doubled spectral efficiency.

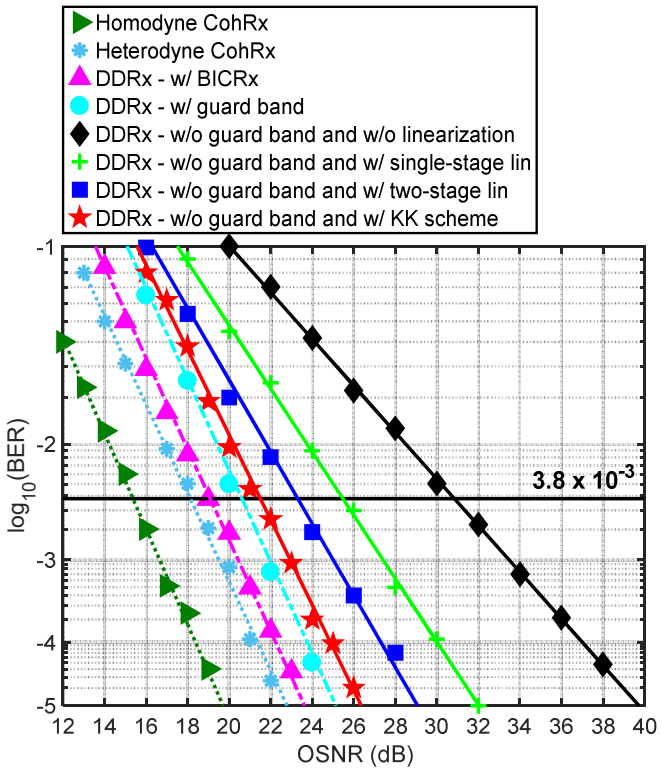

Fig. 9.2: Theoretical BER versus OSNR with different coherent and DD transceiver architectures.

It can be seen that there was an approximately 15.7 dB (from 15.3 dB to 31.0 dB) difference in the required OSNR at the HD-FEC threshold (BER = 3.8×10^{-3}) between the homodyne coherent system and the DD system with no guard-band and no linearization applied. The required OSNR was reduced to 25.6 dB (5.4 dB gain) and 23.3 dB (7.7 dB gain) by applying a single-stage linearization filter (further details can be found in Chapter 5) and a two-stage linearization filter (Chapter 6), respectively. Moreover, by utilizing the Kramers-Kronig scheme (Chapter 7), the required OSNR was found to be 21.5 dB (9.5 dB gain), which was only 0.8 dB higher than that for the case of DD with sufficient guard-band (1.5 × cycle). Finally, with the use of an optical method to mitigate the SSBI (BICBRx), the required OSNR was 19.1 dB, which was 0.9 dB worse than the case with heterodyne coherent detection, due to the utilization of a low power optical carrier. This can be explained by the presence of the optical carrier with the BICRx, which is not needed in the case of coherent detection. The optical CSPR was swept, and the optimum value, for the BICRx, was found to be -6 dB at all values of OSNR. Since the system noise level is halved by using the coherent homodyne detection, the required OSNR of the coherent homodyne system is approximately 3 dB less than that of the coherent heterodyne system. It can be observed that the performance difference between the coherent and DD systems is significantly reduced if effective optical and digital receiver linearization schemes are utilized. However, as shown in Fig. 9.1, although the direct-detection system with BICBRx had potentially only a 3.8 dB higher required OSNR than the coherent homodyne system, the optical hardware complexity is significantly higher compared to the other direct-detection approaches due to the requirement for a balanced receiver and an optical carrier suppression filter (CSF). On the other hand, if only a single-ended photodiode was utilized, the DD system with sufficient guard-band offered similar performance to the BICRx scheme, but is wasteful of spectrum. The difference in the required OSNR between the heterodyne

coherent receiver and the DD receiver employing the digital Kramers-Kronig scheme without guard-band was only 3.3 dB.

Since the optimization of the CSPR value is crucial to achieve the optimum performance of DD systems, further analysis of CSPR optimization and its impact on system performance was carried out by plotting optimum CSPR versus OSNR and required OSNR (assuming BER = 3.8×10^{-3}) versus CSPR, as shown in Figs. 9.3 and 9.4 respectively.

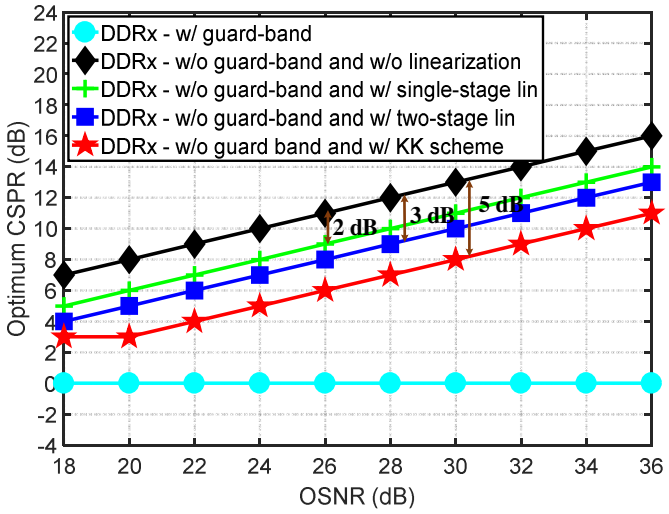

Fig. 9.3: Theoretical optimum CSPR versus OSNR with different DD transceiver architectures.

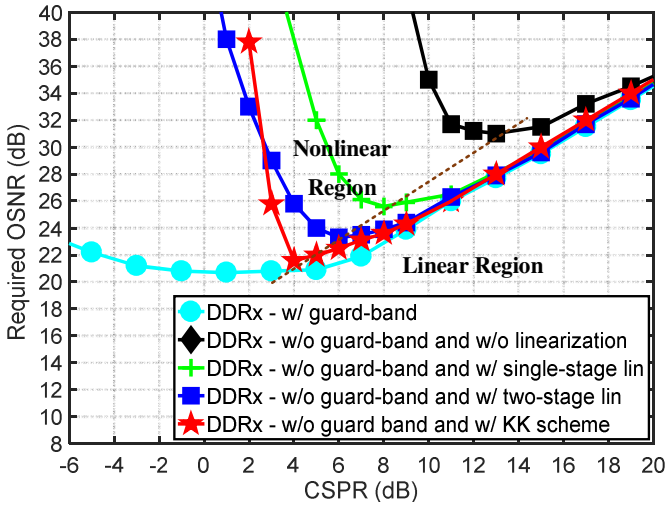

Fig. 9.4: Theoretical required OSNR (assuming BER = 3.8×10^{-3}) versus CSPR with different DD transceiver architectures.

Fig. 9.3 showed the optimum CSPR value as a function of OSNR for each DD system. For the DD system with no guard-band and no linearization technique, it can be seen that the optimum CSPR value increased with OSNR; every 2 dB increase in OSNR corresponded to an approximately 1 dB increase in the optimum CSPR value. The optimum CSPR increased from 7 dB to 16 dB over the OSNR range 18 dB to 36 dB. Moreover, for each value of OSNR, the optimum CSPR value was reduced by 2 dB to obtain the maximum compensation gain with the single-stage linearization filter and by 3 dB with the two-stage linearization filter. For the case with the Kramers-Kronig scheme, the optimum CSPR value was reduced by 5 dB over the OSNR range 20

dB to 36 dB and was fixed to 3 dB to fulfil the requirement of the signal being a minimum phase one [17]. In the case of the DD system with sufficient guard-band, the optimum CSPR remained at 0 dB for all the OSNR levels, which matches with the description in [20]. The sensitivity of the system performance to CSPR optimization and the CSPR reductions after implementing different SSBI compensation schemes were further presented in Fig. 9.4. It can be observed that there was a tradeoff between the SSBI and the optical carrier power. Signals operating at lower CSPR values suffered from large SSBI effect (nonlinear region), while higher CSPR value led to high required OSNR due to the high power in the carrier (linear region). Since utilization of the linearization techniques significantly reduced the nonlinear SSBI effect, the tradeoff was changed, and therefore, the optimum CSPR value was reduced to a lower value. Due to the different capabilities in suppressing the SSBI, the two-stage linearization filter provided further reduction in the optimum CSPR compared with the single-stage linearization filter. The KK scheme achieved the biggest reduction in the optimum CSPR, but its performance was dramatically degraded at lower CSPR values (< 4 dB) because the minimum phase condition was not met.

9.2 168 Gb/s/λ Single-sideband Subcarrier Modulation Direct-Detection Transmission System

To assess the performance of direct detection transmission system at data rates beyond 100 Gb/s, the performance of 4 × 168 Gb/s SSB 64-QAM Nyquist-SCM DD system was assessed with the experimental test-bed described in Chapter 4, Section 4.2. In the transmitter DSP, 28 Gbaud (168 Gb/s) 0.51 cycle SSB 64-QAM Nyquist-SCM signal was generated. Four WDM channels were transmitted, with the channel spacing set to 35 GHz, giving a gross optical ISD of 4.8 b/s/Hz. Transmission experiments were carried out by utilizing an 80-km single-span SSMF. The channel of interest was demultiplexed and detected with a single PIN photodiode. In the receiver DSP, digital linearization was first implemented. The two-stage linearization filter [8, 22] and the Kramers-Kronig scheme [17, 23-25] (operating at 6 Sa/symbol) were utilized due to their strong capabilities in suppressing the SSBI penalty, in comparison with the single-stage linearization filter, as discussed in Chapters 6 and 7. Technical details of such linearization schemes can be found in Chapter 6 and Chapter 7 respectively. Moreover, as demonstrated in Chapter 8, both Tx-EDC and Rx-EDC offer similar performance when combined with these two linearization approaches, and Rx-EDC was therefore carried out for simplification of the system operations.

Both the WDM back-to-back and transmission performance were plotted in Figs. 9.5 to 9.7. As shown in Fig. 9.5, the optical back-to-back performance was evaluated by measuring BER versus OSNR using ASE-noise loading at the receiver for WDM without and with receiver linearization. The results were compared with those of simulations using the KK scheme, assuming ideal transceivers using ideal electrical and optical components, *i.e.* no quantization or other electrical noise, no phase noise, a linear modulator and an ideal 'rectangular' shaped OBPF. The optimum system performance was achieved by sweeping the CSPR and setting it at the optimum value at each OSNR level. In all WDM back-to-back and transmission experiments, compared with the system without linearization, the optimum CSPR values were found to be approximately 3 dB and 5 dB lower for the cases with the two-stage linearization filter and the KK scheme respectively. It can be seen that, compared to the ideal system simulations (shown as 'Theory' in Fig. 9.5), the 64-

QAM system is sensitive to implementation penalties such as transceiver noise and crosstalk from neighbouring WDM channels. Such implementation penalties also causes the difference in the slopes of the theoretical and practical curves. The BER at 36 dB OSNR was decreased from 2.5×10^{-2} to 7.1×10^{-3} and 2.2×10^{-3}, and the corresponding optimum CSPR value was reduced from 14 dB to 11 dB and 9 dB using the two-stage linearization filter and the KK scheme respectively.

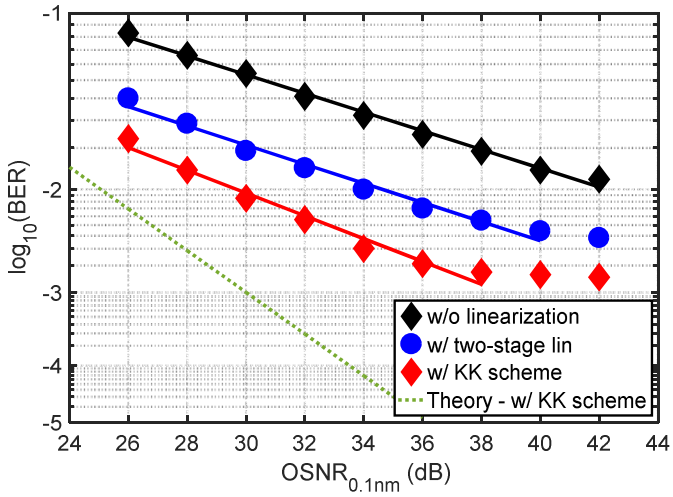

Fig. 9.5: BER versus OSNR without and with receiver-based digital two-stage linearization filter and KK scheme.

As shown in Fig. 9.6, in WDM transmission over 80 km SSMF, system performance was improved at all optical launch powers after applying linearization. The BER at the optimum launch power was reduced from 3.2×10^{-2} to 1.1×10^{-2} and 6.9×10^{-3} with the optimum launch power reduced by 0.5 dB and by 2 dB with the two-stage linearization filter and KK scheme respectively. The received constellation diagrams, without linearization and with the KK scheme over 80 km were plotted in the insets (a) and (b). Significantly less distortion can be observed after applying the KK scheme. The EVM was decreased from 23.1% to 13.8%.

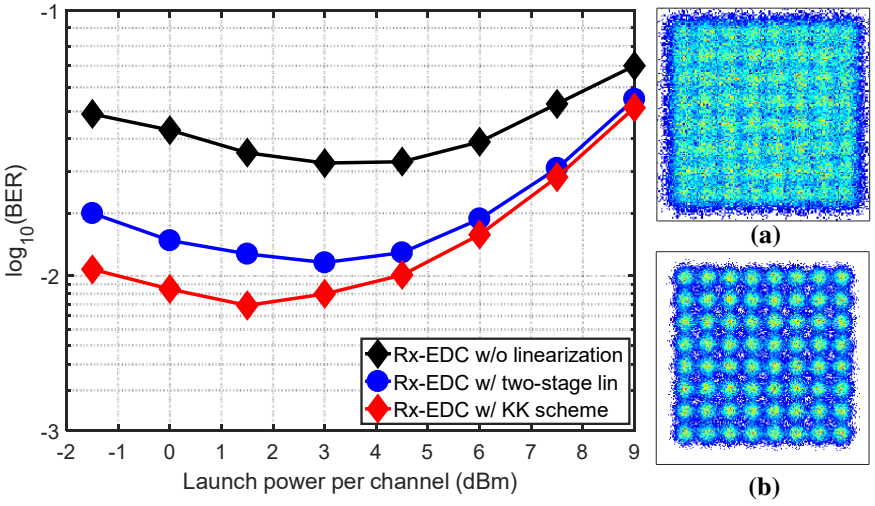

Fig. 9.6: BER versus optical launch power per channel without and with receiver-based digital two-stage linearization filter and KK scheme over 80 km WDM transmission. Insets: Received constellations (a) without receiver linearization (EVM = 23.1%) and (b) with KK scheme (EVM = 13.8%).

The BER of all four WDM channels after 80 km transmission was plotted in Fig. 9.7. The average BER across the channels was decreased from 3.1×10^{-2} to 6.1×10^{-3} giving an achieved net

optical information spectral density (based on the theoretical hard-decision decoding bound) of 4.54 b/s/Hz, to the best of our knowledge, the highest reported net optical ISD for a single-polarization single-photodiode based DD transceiver for metro reach transmission at the time of publication.

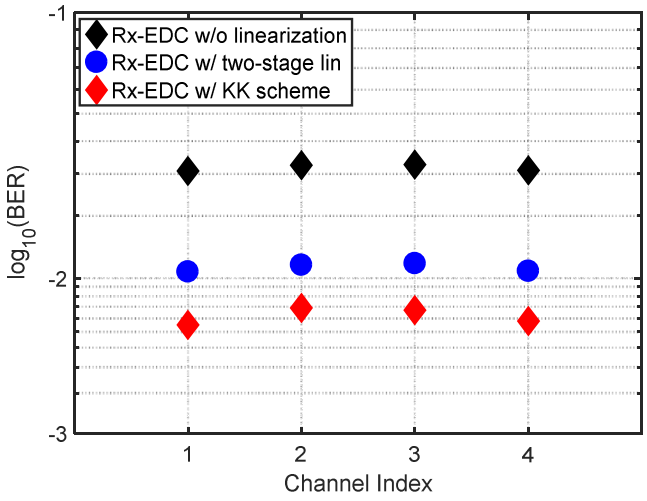

Fig. 9.7: BERs for each WDM channel without and with receiver-based digital two-stage linearization filter and KK scheme over 80 km transmission.

9.3 Summary

This chapter first presented a theoretical assessment of different 112 Gb/s per channel transceiver designs including the coherent (homodyne and heterodyne) and DD systems without and with different optical or digital linearization techniques through ideal simulations. The results show that the single-ended photodiode based 16-QAM DD transceiver can achieve a required OSNR at the HD-FEC threshold (BER = 3.8×10^{-3}) only 5.4 dB higher than the homodyne coherent system if a sufficient spectral guard-band is utilized to avoid SSBI penalty. However, this leads to a halving in the ISD. The recently-proposed digital linearization schemes avoid the requirement for the spectral guard-band, and achieve a required OSNR increase by 6.2 dB (relative to the homodyne coherent system) whilst avoiding the reduction in the achievable optical ISD. Following this, the optical ISD limit of the SSB SCM DD transceiver was explored with higher QAM modulation format by experiments. 4 × 168 Gb/s WDM SSB 64-QAM Nyquist-SCM signals was successfully transmitted over 80 km at a record net ISD of 4.54 b/s/Hz.

References

[1] D. Che, Q. Hu, and W. Shieh, "Linearization of direct detection optical channels using self-coherent subsystems," J. Lightw. Technol. 34(2) 516-524 (2016).

[2] R.I. Killey, M.S. Erkılınç, Z. Li, S. Pachnicke, H. Griesser, R. Bouziane, B.C. Thomsen, and P. Bayvel, "Spectrally-efficient direct-detection WDM transmission system," in *International Conference on Transparent Optical Networks* (ICTON 2015), paper We.B.3.2.

[3] W.R. Peng, I. Morita, and H. Tanaka, "Enabling high capacity direct-detection optical OFDM transmissions using beat interference cancellation receiver," in *European Conference and Exhibition on Optical Communication* (ECOC 2010), paper Tu.4.A.2.

[4] S.A. Nezamalhosseini, L.R. Chen, Q. Zhuge, M. Malekiha, F. Marvasti, and D.V. Plant, “Theoretical and experimental investigation of direct detection optical OFDM transmission using beat interference cancellation receiver,” Opt. Express 21(13) 15237-15246 (2013).

[5] B.J.C. Schmidt, A.J. Lowery, and L.B. Du, “Low sample rate transmitter for direct-detection optical OFDM,” in *Optical Fiber Communication Conference*, OSA Technical Digest Series (CD) (Optical Society of America, 2009), paper OWM4.

[6] L. Zhang, T. Zuo, Q. Zhang, J. Zhou, E. Zhou and G.N. Liu, “150-Gb/s DMT over 80-km SMF transmission based on spectrally efficient SSBI cancellation using guard-band twin-SSB technique,” in *European Conference and Exhibition on Optical Communication* (ECOC 2016), pp. 1178-1180.

[7] S. Randel, D. Pilori, S. Chandrasekhar, G. Raybon, and P. Winzer, “100-Gb/s discrete-multitone transmission over 80-km SSMF using single-sideband modulation with novel interference-cancellation scheme,” in *European Conference and Exhibition on Optical Communication* (ECOC 2015), paper Mo.4.5.2.

[8] Z. Li, M. S. Erkilinc, R. Maher, L. Galdino, K. Shi, B. C. Thomsen, P. Bayvel, and R. I. Killey, "Two-stage linearization filter for direct-detection subcarrier modulation", IEEE Photon. Technol. Lett. 28(24), 2838-2841 (2016).

[9] Z. Li, M. S. Erkilinc, R. Maher, L. Galdino, K. Shi, B. C. Thomsen, P. Bayvel, and R. I. Killey, "Reach enhancement for WDM direct-detection subcarrier modulation using low-complexity two-stage signal-signal beat interference cancellation", in *European Conference and Exhibition on Optical Communication* (ECOC 2016), paper M 2.B.1.

[10] K. Zou, Y. Zhu, F. Zhang and Z. Chen, “Spectrally efficient terabit optical transmission with Nyquist 64-QAM half-cycle subcarrier modulation and direct-detection,” Opt. Lett. 41(12), 2767-2770 (2016).

[11] W. Peng, X. Wu, K. Feng, V.R. Arbab, B. Shamee, J. Yang, L.C. Christen, A.E. Willner, and S. Chi, “Spectrally efficient direct-detected OFDM transmission employing an iterative estimation and cancellation technique,” Opt. Express 17(11), 9099-9111 (2009).

[12] Z. Li, M. S. Erkılınç, S. Pachnicke, H. Griesser, R. Bouziane, B.C. Thomsen, P. Bayvel, and R.I. Killey, “Signal-signal beat interference cancellation in spectrally-efficient WDM direct-detection Nyquist-pulse-shaped 16-QAM subcarrier modulation,” Opt. Express 23(18), 23694-23709 (2015).

[13] C. Sánchez, B. Ortega, and J. Capmany, “System performance enhancement with pre-distorted OOFDM signal waveforms in IM/DD systems,” Opt. Express 22(6), 7269-7283 (2014).

[14] C. Ju, X. Chen, N. Liu, and L. Wang, “SSII cancellation in 40 Gbps VSB-IMDD OFDM system based on symbol pre-distortion,” in *European Conference and Exhibition on Optical Communication* (ECOC 2014), paper P.7.9.

[15] Z. Li, M. S. Erkilinc, R. Bouziane, B. C. Thomsen, P. Bayvel, and R. I. Killey, "Simplifed DSP-based signal-signal beat interference mitigation technique for direct detection OFDM", J. Lightw. Technol. 34(3), 866-872 (2016).

[16] Z. Li, M.S. Erkilinc, L. Galdino, K. Shi, B.C. Thomsen, P. Bayvel, and R.I. Killey, “Comparison of digital signal-signal beat interference compensation techniques in direct-detection subcarrier modulation systems,” Opt. Express 24(25), 29176-29189 (2016).

[17] A. Mecozzi, C. Antonelli, and M. Shtaif, “Kramers-Kronig coherent receiver,” Optica 3(11), 1220-1227 (2016).

[18] K. Kikuchi, "Fundamentals of coherent optical fiber communications", J. Lightw. Technol. 34(1), 157-179 (2016).

[19] E. Ip, A.P.T. Lau, D.J.F. Barros, and J.M. Kahn, “Coherent detection in optical fiber systems,” Opt. Express 16(2), 753-791 (2008).

[20] A.J. Lowery, L.B. Du, and J. Armstrong, "Performance of optical OFDM in ultralong-haul WDM lightwave systems", J. Lightw. Technol. 25(1), 131-138 (2007).

[21] R. Hirai, N. Kikuchi, and T. Fukui, “High-spectral efficiency DWDM transmission of 100-Gb/s/lamda IM/DD single-sideband-Nyquist-PAM8 signals,” in *Optical Fiber Communication Conference*, OSA Technical Digest Series (CD) (Optical Society of America, 2017), paper Th3D.4 (2017).

[22] Z. Li, M.S. Erkılınç, K. Shi, E. Sillekens, L. Galdino, B.C. Thomsen, P. Bayvel, and R.I. Killey, "112 Gb/s/λ WDM direct-detection Nyquist-SCM transmission at 3.15 (b/s)/Hz over 240 km SSMF enabled by novel beating interference compensation", in *Optical Fiber Communication Conference*, OSA Technical Digest Series (CD) (Optical Society of America, 2017), paper Tu3I.4.

[23] C. Antonelli, A. Mecozzi, and M. Shtaif, “Kramers-Kronig PAM transceiver,” in *Optical Fiber Communication Conference*, OSA Technical Digest Series (CD) (Optical Society of America, 2017), paper Tu3I.5 (2017).

[24] Z. Li, M.S. Erkılınç, K. Shi, E. Sillekens, L. Galdino, B.C. Thomsen, P. Bayvel, and R.I. Killey, “SSBI mitigation and Kramer-Kronig scheme in single-sideband direct-detection transmission with receiver-based electronic dispersion compensation,” J. Lightw. Technol., 35(10), 1887-1893 (2017).

[25] X. Chen, C. Antonelli, S. Chandrasekhar, G. Raybon, J. Sinsky, A. Mecozzi, M. Shtaif, and P. Winzer, "218-Gb/s single-wavelength, single-polarization, single-photodiode transmission over 125-km of standard single-mode fiber using Kramers-Kronig detection", in *Optical Fiber Communication Conference*, OSA Technical Digest Series (CD) (Optical Society of America, 2017), paper Th5B.6 (2017).

CHAPTER 10

CONCLUSIONS AND FUTURE WORK

Single-sideband subcarrier modulation direct-detection transmission systems employing a number of digital linearization techniques to support high data rate (≥ 100 Gb/s per channel) and spectrally-efficient (net ISD > 2 b/s/Hz) WDM transmission covering metropolitan reach scenarios (up to 240 km) have been extensively studied in this thesis. The key results and technical achievements from this study are summarized in Sections 10.1 and 10.2, and topics that can be potentially valuable to investigate in the future are discussed in Section 10.3.

10.1 Summary of Research

Due to their simplicity and relatively low cost, single-polarization direct-detection (DD) transceivers may be an attractive technology for short and medium reach optical fibre transmission systems, for example in metropolitan, back-haul, access and inter-data centre applications.

Considering the ongoing development of complementary metal oxide silicon (CMOS) technology, especially the high-speed digital-to-analogue and analogue-to-digital converters (DACs and ADCs), much of the transceiver complexity can be moved from the optical to the electrical domain. It allows the use of multi-level and multi-dimensional coding in DD links with a single-ended photodiode and without the requirement for delay-line interferometers (DLIs)), and consequently, higher information spectral densities (ISDs) with reasonable receiver sensitivity can be achieved using cost-effective transceiver designs. The single-sideband (SSB) subcarrier modulation (SCM) format which enables the use of M-ary quadrature amplitude modulation (QAM) signalling with minimum Euclidean symbol spacing implemented using a digital signal processing (DSP)-based transceiver architecture with a simple single photodiode is a potentially attractive and practical solution. However, the performance of such transceivers is severely degraded because of a nonlinear effect introduced by the square-law detection, referred to as signal-signal beat interference (SSBI). Therefore, it is essential to develop effective and low-cost linearization techniques for improved system performance.

Chapter 4 described an effective receiver-based digital iterative SSBI estimation and cancellation (E&C) technique and experimentally tested this technique on a dispersion pre-compensated 112 Gb/s per channel spectrally-efficient WDM SSB 16-QAM Nyquist-SCM direct detection system in transmission over a straight-line multiple span (up to 240 km) uncompensated SSMF link. In optical back-to-back operation, the use of this SSBI compensation technique led to reductions of the required OSNR at the hard-decision forward-error-correction (HD-FEC) threshold, and reductions in BER after transmission over uncompensated SSMF. However, although this iterative SSBI post-compensation scheme compensates the SSBI with low receiver optical hardware complexity, the digital hardware complexity of the receiver is very high due to the multiple (more than four) iterations required to achieve the maximum compensation gain. In addition, the performance of this technique depends on the accuracy of the symbol decision making, thus noticeably degrading its effectiveness at lower OSNR levels.

In Chapter 5, a simple structured receiver-based digital single-stage linearization filter was assessed. It enables to compensate the SSBI with very simple DSP structure and its performance does not rely on the accuracy of the decision making. However, as this technique itself introduces extra unwanted beating interference, it cannot achieve the maximum compensation performance. However, this technique can also be applied to upgrade the iterative SSBI E&C into non-iterative SSBI E&C, since the symbol decisions are significantly more accurate due to the preceding linearization filtering stage. Hence, multiple iterations are not required to achieve the maximum compensation gain, thus leading to a significant reduction in DSP complexity. The experimental results indicated that the non-iterative approach achieves similar performance to the iterative E&C approach.

Chapter 6 focused on a receiver-based digital two-stage linearization filter, which enhances the performance of the single-stage linearization filter. A second linearization stage is applied to remove the majority of the unwanted beating interference introduced by the single-stage linearization filter. Unlike the other digital linearization approaches, this technique avoids the requirement for multiple iterations or symbol decision-based SSBI reconstruction. Hence, it requires relatively low DSP complexity in contrast to the other approaches. This technique offers a good tradeoff between compensation performance and digital hardware complexity. In the experimental evaluations, the results have shown that the two-stage linearization filter achieves better transmission performance than the single-stage linearization filter and the SSBI E&C scheme.

The recently proposed receiver-based digital Kramer-Kronig (KK) scheme was experimentally demonstrated, as described in Chapter 7. The digital KK scheme offers the possibility of fully reconstructing the transmitted signal from the detected signal's amplitude, and thus can provide superior linearization effectiveness in comparison to the other digital linearization techniques. Since the KK scheme introduces signal bandwidth broadening in the DSP algorithm, it is necessary to utilize a relatively high oversampling rate not required in the other digital linearization techniques, which may lead to increased hardware complexity. Experimental results indicated that good compensation performance is achieved at 4 Sa/symbol, with optimum performance at ≥ 6 Sa/symbol.

Chapter 8 presented a study on the effectiveness of performing electronic dispersion compensation (EDC) either at the transmitter (Tx-EDC) or at the receiver (Rx-EDC) in SSB SCM DD transceivers combined with different receiver linearization techniques. The four different digital linearization techniques introduced in the previous chapters, including the single-stage linearization filter, the two-stage linearization filter, the non-iterative SSBI E&C technique and the Kramers-Kronig scheme were assessed. The experimental results showed that differences in the performance of Tx and Rx-EDC depend on the effectiveness of the utilized linearization scheme, and that they can achieve similar performance if the beating interference is effectively suppressed. Hence, it becomes possible to perform the EDC at the receiver rather than at the transmitter, which simplifies the system operation. Due to the reduction in complexity, the proposed solution further increases the suitability of WDM DD SSB SCM signalling for short- and medium-reach transmission systems.

In Chapter 9, a theoretical assessment of different 112 Gb/s per channel system designs was presented, performed through ideal numerical simulations (neglecting transceiver noise and non-ideal optical filtering). The transceivers studied included the coherent (homodyne and heterodyne) and direct detection systems without and with different optical or digital linearization approaches. The simulation results indicated that the single-ended photodiode based 16-QAM DD transceiver can achieve a required OSNR at the HD-FEC threshold (BER = 3.8×10^{-3}) only 5.4 dB higher than the homodyne coherent system if a sufficiently wide spectral guard-band is utilized between the signal and the optical carrier to avoid SSBI penalty. However, the use of a guard-band leads to a halving in the spectral efficiency. The recently-proposed digital linearization schemes avoid the requirement for the spectral guard-band, and achieve a required OSNR only 6.2 dB above that of the homodyne coherent system. Some further developments of this work were also presented. By utilizing effective digital linearization techniques (two-stage linearization filter and the KK scheme) and applying Rx-EDC, the optical ISD limits of the SSB SCM DD transceiver were explored through experiments with higher-order QAM modulation formats and narrow channel spacing. 35 GHz-spaced WDM 168 Gb/s per channel SSB 64-QAM Nyquist-SCM signal was successfully transmitted over 80 km of uncompensated SSMF, a record net optical ISD of 4.54 b/s/Hz for this distance with single polarisation direct detection.

10.2 Key Technical Achievements

To sum up, the key achievements presented in this thesis are:

1. It was experimentally confirmed that the performance of SSB SCM DD transceivers is severely degraded by SSBI penalty introduced by square-law photodetection.
2. A number of novel and effective digital linearization techniques were proposed for the first time, including the non-iterative SSBI E&C, two-stage linearization filter. The first experimentally demonstrated digital Kramers-Kronig receiver was described, and its superior performance was confirmed.
3. By implementing the digital linearization approaches, we experimentally achieved the transmission of dispersion pre-compensated 112 Gb/s per channel spectrally-efficient WDM SSB 16-QAM Nyquist-SCM signals over a 240 km uncompensated SSMF link, at a record optical net optical ISD of 3.18 b/s/Hz, a record at this distance at the time of publication. The demonstrated techniques allow to triple the achievable transmission distance at this bit rate.
4. We also showed that, with the use of digital linearization, further simplification of the DD transceivers can be realized by moving electronic dispersion compensation from the transmitter to the receiver without sacrificing performance.
5. The optical ISD limit of DD transceiver was further explored through experiments with higher-order modulation formats and narrow channel spacing. 168 Gb/s per channel WDM 64-QAM signals were successfully transmitted over 80 km, achieving a record net optical ISD of 4.54 b/s/Hz over this distance.

Although the above-mentioned studies throughout this thesis can still be improved, the techniques demonstrated may be potential solutions for future links operating at 400 G (4 × 100 G) and higher over metropolitan distances.

10.3 Future Work

Despite all the work presented in this thesis, there remain a number of research and development milestones that need to be reached before the technology is ready for commercialisation:

10.3.1 Real-time Digital Circuit Designs for Receiver Linearization

As described in this thesis, a number of effective digital linearization techniques have been proposed and demonstrated, and techniques such as the single-stage linearization filter [1], the two-stage linearization filter [2, 3] and the Kramers-Kronig scheme [4-7] have demonstrable advantages concerning either the hardware structure or the SSBI compensation effectiveness. However, the key questions concern how to implement these linearization techniques in real-time and the corresponding complexity of these circuit designs.

In the next stage of this research work, the viability of the proposed DSP schemes in practical applications could be tested through the use of real-time circuits implemented with field programmable gate arrays (FPGAs). Either overlap-and-add or overlap-and-save method [8, 9] frequency domain filters would be utilized in the real-time circuit design. The power consumption and DSP complexity could be both calculated. After performing the real-time circuit design, the compensation performance of such digital linearization approaches could be compared and the technique which offers the optimum tradeoff between the compensation effectiveness and digital hardware complexity chosen for DD transceivers in metro applications.

10.3.2 Beyond 200 Gb/s/λ DD Transceiver Designs for Metropolitan Scenarios

In this thesis, DD transceivers supporting 100 Gb/s per channel WDM transmission have been demonstrated to cover the typical transmission reach of metropolitan area networks. However, it is still very challenging to achieve transmission rate of beyond 200 Gb/s per channel using SSB SCM DD transceivers. Another potential research area following the work described in this thesis is to explore whether SSB SCM DD transceivers are capable to support WDM transmission with ≥ 200 Gb/s per channel. This research goal may be achieved by using new digital signal processing techniques to improve the SSB SCM DD system's robustness to linear or nonlinear penalties or develop other novel DD transceiver designs which can provide potentially better performance than the SSB SCM DD system. At the same time, the ongoing development in the speed and power of CMOS technology will enable data converters and digital signal processing to achieve further increases in channel data rates.

References

[1] S. Randel, D. Pilori, S. Chandrasekhar, G. Raybon, and P. Winzer, "100-Gb/s discrete-multitone transmission over 80-km SSMF using single-sideband modulation with novel interference-cancellation scheme," in *European Conference and Exhibition on Optical Communication* (OFC 2015), paper Mo.4.5.2.

[2] Z. Li, M. S. Erkilinc, R. Maher, L. Galdino, K. Shi, B. C. Thomsen, P. Bayvel, and R. I. Killey, "Two-stage linearization filter for direct-detection subcarrier modulation", IEEE Photon. Technol. Lett. 28(24), 2838-2841 (2016).

[3] Z. Li, M.S. Erkılınç, K. Shi, E. Sillekens, L. Galdino, B.C. Thomsen, P. Bayvel, and R.I. Killey, "112 Gb/s/λ WDM direct-detection Nyquist-SCM transmission at 3.15 (b/s)/Hz over 240 km SSMF enabled by novel beating interference compensation", in *Optical Fiber Communication Conference*, OSA Technical Digest Series (CD) (Optical Society of America, 2017), paper Tu3I.4.

[4] A. Mecozzi, C. Antonelli, and M. Shtaif, "Kramers-Kronig coherent receiver," Optica, 3(11), 1220-1227 (2016).

[5] C. Antonelli, A. Mecozzi, and M. Shtaif, "Kramers-Kronig PAM transceiver," in *Optical Fiber Communication Conference*, OSA Technical Digest Series (CD) (Optical Society of America, 2017), paper Tu3I.5 (2017).

[6] Z. Li, M.S. Erkılınç, K. Shi, E. Sillekens, L. Galdino, B.C. Thomsen, P. Bayvel, and R.I. Killey, "SSBI mitigation and Kramer-Kronig scheme in single-sideband direct-detection transmission with receiver-based electronic dispersion compensation," J. Lightw. Technol., 35(10), 1887-1893 (2017).

[7] X. Chen, C. Antonelli, S. Chandrasekhar, G. Raybon, J. Sinsky, A. Mecozzi, M. Shtaif, and P. Winzer, "218-Gb/s single-wavelength, single-polarization, single-photodiode transmission over 125-km of standard single-mode fiber using Kramers-Kronig detection", in *Optical Fiber Communication Conference*, OSA Technical Digest Series (CD) (Optical Society of America, 2017), paper Th5B.6 (2017).

[8] J.G. Proakis, and D.G. Manolakis, "Digital signal processing, principles, algorithms, and applications," fourth edition, Pearson International Edition.

[9] S. Haykin, "Digital communication systems," Wiley.

ACRONYMS

DSF	dispersion-shifted fibres
EDFA	erbium-doped fibre amplifier
WDM	wavelength-division multiplexing
DSP	digital signal processing
FEC	forward error correction
ISD	information spectral density
VOD	video-on-demand
Wi-Fi	wireless fidelity
POP	point of presence
QAM	quadrature amplitude modulation
SoP	state of polarization
CMOS	complementary metal oxide silicon
ADC	analogue-to-digital converter
DD	direct-detection
IM/DD	intensity modulation/direct detection
DML	direct modulated laser
SSB	single-sideband
SCM	subcarrier modulation
OFDM	orthogonal frequency division multiplexing
Nyquist-SCM	Nyquist pulse-shaped subcarrier modulation
SSBI	signal-signal beat interference
EDC	electronic dispersion compensation
Tx-EDC	transmitter-based electronic dispersion compensation
Rx-EDC	receiver-based electronic dispersion compensation
SSMF	standard single mode fibre
CD	chromatic dispersion
ASE	amplified spontaneous emission
HT	Hilbert transform
SPM	self-phase modulation

XPM	cross-phase modulation
FWM	four-wave mixing
ITU	International Telecommunication Union
GVD	group-velocity dispersion
ISI	inter-symbol interference
SNR	signal-to-noise power ratio
I	in-phase
Q	quadrature
LSE	linear Schrödinger equation
NLSE	nonlinear Schrödinger equation
OBPF	optical bandpass filter
PD	photodiode
DSB	double-sideband
DD MZM	dual-drive Mach-Zehnder modulator
OOK	on-off keying
PAM	pulse amplitude modulation
CSBP	Carrier-Subcarrier beating product
CABI	Carrier-ASE beating interference
SABI	Subcarrier-ASE beating interference
AABI	ASE-ASE beating interference
CSPR	carrier-to-signal power ratio
BER	bit-error-ratio
OSNR	optical signal-to-noise power ratio
FT	Fourier transform
FBG	fibre Bragg grating
DCF	dispersion compensating fibre
FIR	finite impulse response
LMS	least mean squares
CMA	constant modulus algorithm
RDE	radius directed equalizer
DLI	delay-line interferometer
M-PSK	M-ary phase-shift keying

M-QAM	M-ary quadrature amplitude modulation
M-PAM	M-ary pulse amplitude modulation
DPSK	differential phase-shift keying
BPD	balanced photodetector
DAC	digital-to-analogue converter
CW	continuous wave
RZ	return-to-zero
NRZ	non-return-to-zero
MZM	Mach-Zehnder modulator
CS-	carrier-suppressed
PSD	power spectral density
VSB	Vestigial sideband
PMD	polarization mode dispersion
PSBT	phase-shaped binary transmission
BLPF	Bessel low-pass filter
DWDM	dense wavelength-division-multiplexing
DB	duobinary
PRBS	pseudo-random binary sequence
ASK	amplitude-shift keying
DPSK	differential phase-shift keying
QASK	quaternary ASK
PM	phase modulator
ODC	optical dispersion compensation
IFFT	inverse fast Fourier transform
FFT	fast Fourier transform
DMT	discrete multitone
MSM	multiple carrier modulation
ICI	inter-channel interference
CP	cyclic prefix
RRC	root-raised-cosine
BICBR	beat interference cancellation balanced receiver
CSF	carrier suppression filter

E&C	estimation and cancellation
VSSB-OOFDM	virtual SSB optical OFDM
SF	sideband filter
KK	Kramers-Kronig
cSSB	compatible SSB
MOD DSP	modulation DSP
DEMOD DSP	demodulation DSP
AWG	arbitrary-waveform generator
ECL	external cavity laser
OSA	optical spectrum analyser
VOA	variable optical attenuator
EVM	error-vector-magnitude
HD-FEC	hard-decision forward-error-correction
DC	direct current
FPGA	field programmable gate array
RAM	random access memory
VCSEL	vertical-cavity surface-emitting laser
PAPR	peak-to-average power ratio
LO	local oscillator
CAP	carrierless amplitude/phase modulation
MLSE	maximum likelihood sequence estimation